Submitted at the

Faculty of Mathematics and Science - Institute of Physics

Carl von Ossietzky University Oldenburg

-

Prepared at the

Theory Department

Fritz-Haber-Institute of the Max-Planck-Society

Diploma Thesis

Stability Of Bulk And Surface Ruthenium Nitrogen And Hydrogen Structures: A First-Principles Atomistic Thermodynamics Study

Submitted by: Nils Ohmer

First supervisor: Prof. Dr. Alexander K. Hartmann

Second Supervisor: Prof. Dr. Thorsten Klüner

Oldenburg, 23.03.2010

Contents

Kurzfassung

Im Rahmen dieser Arbeit werden verschiedene Volumenphasen und Oberflächenstrukturen von Ruthenium-Stickstoff- (Ru/N) und Ruthenium-Wasserstoff-Verbindungen (Ru/H) mit *ab initio* Methoden hinsichtlich ihrer thermodynamischen Stabilität untersucht. Hierzu wird die Dichtefunktionalmethode, wie sie im "Fritz Haber Institute - *ab initio* molecular simulation" (FHI-aims) Programmpaket implementiert ist, benutzt [1]. Mit Hilfe der Dichtefunktionaltheorie (siehe Abschnitt 2) wird zuerst die Gesamtenergie der jeweiligen Atomgeometrie berechnet. Diese dient dann als Freie Energie der entsprechenden Struktur dazu thermodynamische Größen wie Bildungsenthalpien oder Adsorptionsenergien zu berechnen. Unter Formulierung der Stabilitätsbedingung der Ru/N und Ru/H Verbindungen in Abhängigkeit vom chemischen Potential einer umgebenen Stickstoff/Wasserstoff-Atmosphäre, lässt sich der Verlauf der thermodynamischen Stabilität als Funktion von Druck und Temperatur untersuchen (siehe Abschnitt 3). Hierbei sind insbesondere die Bedingungen, die während der Ruthenium-katalysierten Ammoniaksynthese herrschen, von Interesse.
Die untersuchten Volumenphasen wurden so ausgewählt, dass eine Aussage über die bevorzugte Koordination, sowie Symmetrie des Gitters getroffen werden kann. Außerdem wurden die Ru/N Verbindungen hinsichtlich einer Änderung ihrer Bildungsenthalpien in Abhängigkeit von der Stickstoffkonzentration analysiert. Die Basis zur Untersuchung von Oberflächenstrukturen ist die Ruthenium (0001) Oberfläche. Es wurde die Adsorptionsenergie von Stickstoff und Wasserstoff auf dieser Oberfläche, sowie im Zwischenraum zwischen der ersten und zweiten Atomlage, hinsichtlich der Adsorptionsposition und dem Bedeckungsgrad näher studiert. Des Weiteren wurde die kombinierte Adsorption von Stickstoff auf der (0001) Oberfläche und in dem ersten Zwischenraum, sowie in einer Oberflächendefektstruktur untersucht. Da die stabilste Ru/N und Ru/H Volumenphase eine kubische Symmetrie aufweist, wurde die Oberfläche außerdem für einige Rechnungen so verändert, dass die obersten Atomlagen keine hexagonale, sondern eine kubisch dichte Kugelpackung aufweisen.

Abstract

In the framework of this thesis different bulk and surface structures of ruthenium nitrogen (Ru/N) and ruthenium hydrogen compounds (Ru/H) are studied by *ab initio* methods regarding their thermodynamic stability. For this purpose, the density functional method, as it is implemented in the "Fritz Haber Institute - *ab initio* molecular simulation" (FHI-aims) program package, is applied [1]. First the total energy of each atomic geometry is calculated using density functional theory (see section 2). This serves then as the free energy of the corresponding structure to calculate thermodynamic quantities, such as formation enthalpies or adsorption energies. Under the formulation of the stability condition of Ru/N and Ru/H compounds as a function of the chemical potential of a surrounding nitrogen/hydrogen atmosphere, the developing of the thermodynamic stability can be studied as a function of temperature and pressure (see section 3). In particular, the conditions that prevail during the ruthenium-catalyzed synthesis of ammonia are of interest.

The investigated bulk phases are chosen so that a statement about the preferred coordination and symmetry of the lattice can be made. In addition, the heat of formation of the Ru/N compounds is analyzed with respect to the nitrogen concentration. The ruthenium (0001) surface is chosen as the basis for investigating surface structures and the adsorption energies of nitrogen and hydrogen at on-surface and subsurface positions at this surface are studied as a function of adsorption site and coverage. Furthermore, the combined adsorption of nitrogen at the (0001) surface at on-surface and subsurface sites, as well as in a surface defect structure, is examined. Since the most stable bulk Ru/N and Ru/H compound has a cubic symmetry, the surface is changed moreover for some calculations so that the topmost atomic layers do not exhibit a hexagonal, but a cubic close-packed form.

Chapter 1

Introduction

Almost every second nitrogen atom in our daily food and every nitrogen atom built into any industrial produced chemical compound has first been activated via the Haber-Bosch-Process. The underlying chemical reaction of this process is the catalytic hydrogenation of nitrogen to ammonia.

$$N_2 + 3H_2 \xrightarrow[T,\ p]{Catalyst} 2NH_3 \tag{1.1}$$

It is one of the most important and most studied chemical reactions and represents a well explored model system for heterogeneous catalysis itself. Together with iron, ruthenium and osmium are the most active elements for catalyzing this reaction. In industrial Haber-Bosch reactors either Fe- or Ru-based catalysts are routinely used, where systems utilizing ruthenium benefit from lower operation temperatures and pressure (Fe: 400-700 °C, 100-350 bar [2, 3], Ru: 320-440 °C, 100 bar [4]). In both cases, the formation of a catalytically active surface is thought to be induced via dissolution of nitrogen into the bulk [5]. However, the geometry and energetics of bulk and surface ruthenium nitrogen compounds remain essentially unknown. One of the main reasons for this is, that most experimental studies are performed in vacuum, while under reaction conditions pressure of around 100 bar are predominant. Additionally to this so-called "pressure gap", a "material gap" exists, since the real structure of the catalysts is very complex, whereas single crystals are used for the low pressure experiments. This work tries to overcome the pressure gap by using first-principles *ab initio* atomistic thermodynamics to calculate formation energies under varying temper-

atures and partial pressure of N_2 and H_2. The motivation for this is, that it is not resolved yet, if under high pressure a ruthenium nitrogen or hydrogen compound is formed, which may also influence the catalytic process. Besides such an inside into what happens under reaction conditions, this thesis also helps to understand the Ru/N and Ru/H systems in general and contributes to the understanding of some experimentally produced ruthenium nitrogen compounds via sputtering techniques [6, 7, 8].

Part I

Theoretical Background

Chapter 2

Density Functional Theory

2.1 The Many-Body Problem

To predict the physical and chemical properties of a system from *ab initio* calculations, one has to solve the corresponding Schrödinger equation (SE). This equation can be reduced to an eigenvalue problem of the system's Hamiltonian $\hat{H}$ with the total energy E of the system in a particular state as the eigenvalue and the corresponding wave function ψ as the eigenfunction. In general the time-independent, non-relativistic SE for a system containing electrons and nuclei is given by

$$\hat{H}\psi(\mathbf{x}_i, \mathbf{R}_I) = E\psi(\mathbf{x}_i, \mathbf{R}_I) \quad , \tag{2.1}$$

where $\hat{H}$ containes the complete physical information about the system. The wave function $\psi(\mathbf{x}_i, \mathbf{R}_I)$ depends on the combined local coordinates and spin states of the electrons $\mathbf{x}_i = (\mathbf{r}_i, \sigma_i)$ and the local coordinates of the nuclei $\mathbf{R}_I$. If magnetic interactions are neglected, the Hamiltonian contains only the kinetic energies of and interaction potentials between the particles. For a system containing N electrons and M nuclei the Hamiltonian is given by

$$\begin{aligned} \hat{H} = &\sum_{i=1}^{N} \frac{\hbar^2}{2m_i}\Delta_{\mathbf{r}_i} - \sum_{i=1}^{N}\sum_{I=1}^{M} \frac{Z_I e^2}{4\pi\epsilon_0 r_{iI}} + \frac{1}{2}\sum_{i,j=1,i\neq j}^{N} \frac{e^2}{4\pi\epsilon_0 r_{ij}} \\ &- \sum_{I=1}^{M} \frac{\hbar^2}{2M_I}\Delta_{\mathbf{R}_I} + \frac{1}{2}\sum_{I,J=1,I\neq J}^{M} \frac{Z_I Z_J e^2}{4\pi\epsilon_0 R_{IJ}} \quad . \end{aligned} \tag{2.2}$$

Here $m_{i(I)}$ is the mass of the electron i (nucleus I), Z_I the charge of nucleus I, and $r_{iI} = |\mathbf{r}_i - \mathbf{R}_I|$, $r_{ij} = |\mathbf{r}_i - \mathbf{r}_j|$, and $R_{IJ} = |\mathbf{R}_I - \mathbf{R}_J|$ the distances between the corresponding particles. A closed-form solution of equation (2.1) with a Hamiltonian as defined in (2.2) can only be found for systems containing not more than two particles (e.g. the H-atom). Therefore the main challenge is not to write down the full Hamiltonian for a system, but to diagonalise it.

To simplify this problem a first step can be the so called Born-Oppenheimer approximation [9]. Within this approximation it is assumed, that the electrons respond much faster to an external perturbation than a nucleus, because the mass of a nucleus being 3-5 orders of magnitude bigger than that of an electron. Therefore the electrons can follow the movement of the nuclei quasi instantaneously, thus they can be treated as moving in a constant field generated by fixed nuclei. This enables a separation of the Hamiltonian into a nuclear and an electronic part $\hat{H} = \hat{H}_n + \hat{H}_e$, as well as a splitting of the total wave function into a nuclear and an electronic one $\psi(\mathbf{r}_i, \mathbf{R}_I) = \psi_n(\mathbf{R}_I)\psi_e(\mathbf{r}_i)$, where $\psi_e(\mathbf{r}_i) = \psi_e(\mathbf{r}_i; \mathbf{R}_I)$ is the electronic wave function for the current nuclear positions $\mathbf{R}_I$, and $\psi_n(\mathbf{R}_I)$ is the nuclear wave function calculated assuming instantaneous response of electrons to a change in nuclear positions. The eigenvalue problem is then reduced to two "simpler" eigenvalue problems: the electronic one

$$\hat{H}_e(\mathbf{R}_I)\psi_e(\mathbf{r}_i; \mathbf{R}_I) = E_e\psi_e(\mathbf{r}_i; \mathbf{R}_I) \quad , \tag{2.3}$$

where $\hat{H}_e(\mathbf{R}_I)$ contains the first three terms and, usually, also the last term of equation (2.2), and the nuclear one

$$\hat{H}_n\psi_n(\mathbf{R}_I) = E_n\psi_n(\mathbf{R}_I) \quad , \tag{2.4}$$

where $\hat{H}_n$ includes the nuclear kinetic energy operator plus the potential energy which depends only on the nuclear coordinates $\mathbf{R}_I$. The Born-Oppenheimer approximation reduces therefore the degrees of freedom of the whole system (3N + 3M) to two subsystems with smaller numbers of degrees of freedom (3N and 3M). But still the electronic Schrödinger equation cannot be solved for real problems in molecular and solid-state physics without additional (severe) approximations.

Two main approaches exist to solve the electronic SE. One is the Hartree-

Fock (HF) approximation [10, 11], transferring the many-body problem into an effective single particle problem by approximating $\psi_e(\mathbf{r}_i)$ by a Slater-determinant of single particle wave functions. The Slater-determinant ensures the antisymmetry of the wave function, which is needed to fulfill the so-called Pauli exclusion principle. The HF method is based on two main approximations: (i) the electronic wave function can be approximated by a single Slater determinant, and (ii) each electron moves in an average potential of all other electrons (mean-field approximation). The difference between the exact total energy E_{tot} and the HF energy E_{HF} is called correlation energy $E_c = E_{tot} - E_{HF}$. In order to improve the HF approximation and to account for the missing correlation energy more advanced wave-function-based approaches have been developed, namely second (and higher) order perturbation theory by Møller and Plesset (MP2), configuration interaction (CI), and coupled cluster (CC) methods [12, 13]. The second main approach to the many-electron problem is density functional theory (DFT) [12, 13, 14, 15]. It is based on the Hohenberg-Kohn Theorems proving that all measurable properties of a system can be derived solely from the electron density $n(\mathbf{r})$, without knowing the N-electron wave function $\Psi_e(\mathbf{r}_1, \mathbf{r}_2, \ldots, \mathbf{r}_N)$.

2.2 The Hohenberg-Kohn Theorems

To justify the use of the electron density $n(\mathbf{r})$ to determine physical properties of a system, one first needs to prove that $n(\mathbf{r})$ uniquely defines a given arrangement of nuclei. In 1964 Hohenberg and Kohn proved, that for a non-degenerate ground state of a system of interacting electrons in an external potential V_{ext}, there exists a one to one mapping between the electron density $n_0(\mathbf{r})$, the wave function $\psi_e(\mathbf{r}_i)$ and V_{ext}, within an additive constant [16]. Therefore any observable of this system can be expressed as a functional of the electron density. The electronic energy E_e is than given by

$$E_e[n(\mathbf{r})] = \int n(\mathbf{r}) V_{ext} d\mathbf{r} + F_{HK}[n(\mathbf{r})] \quad , \tag{2.5}$$

where the Hohenberg-Kohn functional $F_{HK}[n(\mathbf{r})]$ does not depend on the external potential, i.e. generated by the atom-cores, and is therefore universal. It contains

the kinetic energy of the electrons $T_e[n(\mathbf{r})]$ and the electron-electron interactions $E_{ee}[n(\mathbf{r})]$, both as functionals of the electron density. An exact form of these funcionals would lead to an exact solution of the Schrödinger equation, but is not known for either of them.

A second theorem by Hohenberg and Kohn justifies that the variational principle can be used to determine the ground state energy E_0 of a system for a trial density with $n(\mathbf{r}) \geq 0$ and $\int n(\mathbf{r})d\mathbf{r} = N$, so that

$$E_0 = E[n_0(\mathbf{r})] \leq E[n(\mathbf{r})] \quad . \tag{2.6}$$

Because $F_{HK}[n(\mathbf{r})]$ is not known explicitly, the variational principle with an approximated Hohenberg-Kohn functional does not necessarily result in an upper bound for the ground state energy of the system.

2.3 The Kohn-Sham Equations

To make DFT a practically useful theory an approximation of $F_{HK}[n(\mathbf{r})]$ is needed. In 1965 Kohn and Sham (KS) presented an approach, which is based on the separation of $T_e[n(\mathbf{r})]$ into a part T_s, that can be exactly computed, and a small correction, which needs to be handled separately [17]. T_s is the kinetic energy of a system of non-interacting electrons and it is therefore calculated by using one-particle wave functions, the Kohn-Sham orbitals ϕ. It is given by

$$T_s[n(\mathbf{r})] = \sum_{i=1}^{N} \langle \phi_i(\mathbf{r})| -\frac{\hbar^2}{2m}\Delta_i|\phi_i(\mathbf{r})\rangle \quad . \tag{2.7}$$

Separating the classical coulomb repulsion between pairs of electrons $V_c[n(\mathbf{r})] = \frac{1}{2}\frac{e^2}{4\pi\epsilon}\int\int \frac{n(\mathbf{r}_1)n(\mathbf{r}_2)}{r_{12}} d\mathbf{r}_1 d\mathbf{r}_2$ from the electron-electron interactions $E_{ee}[n(\mathbf{r})]$, the Hohenberg-Kohn functional can be rewritten as

$$F_{HK}[n(\mathbf{r})] = T_s[n(\mathbf{r})] + V_c[n(\mathbf{r})] + E_{xc}[n(\mathbf{r})] \quad . \tag{2.8}$$

Here, the exchange correlation functional E_{xc} contains now all unknown terms, namely the difference in kinetic energy between the real and the non-interacting system, as well as the non-classical part of $E_{ee}[n(\mathbf{r})]$, and is defined as

$$E_{xc}[n(\mathbf{r})] = T_e[n(\mathbf{r})] - T_s[n(\mathbf{r})] + E_{ee}[n(\mathbf{r})] - V_c[n(\mathbf{r})] \quad . \tag{2.9}$$

Because of the second Hohenberg-Kohn theorem the necessary condition for minimizing $E_e[n(\mathbf{r})]$ can be written as

$$\delta\{E_e[n] - \mu[\int n(\mathbf{r})d\mathbf{r} - N]\} = 0 \tag{2.10}$$

with the Lagrange multiplier μ (the chemical potential of the electrons), leading to the Euler-Lagrange equation

$$\mu = \frac{\delta E_e[n]}{\delta n(\mathbf{r})} = V_{ext}(\mathbf{r}) - \frac{\delta F_{HK}[n]}{\delta n(\mathbf{r})} = V_{eff}(\mathbf{r}) + \frac{\delta T_s[n]}{\delta n(\mathbf{r})} \quad . \tag{2.11}$$

This leads to the three so-called Kohn-Sham equations (2.12)-(2.14). The first describes the effective potential $V_{eff}([n], \mathbf{r})$ as a sum of the external potential $V_{ext}(\mathbf{r})$, the Hartree potential $V_H(\mathbf{r}) = \frac{\delta V_c[n(\mathbf{r})]}{\delta n(\mathbf{r})}$ and the exchange-correlation potential $V_{xc}([n], \mathbf{r}) = \frac{\delta E_{xc}([n], \mathbf{r})}{\delta n(\mathbf{r})}$, which corrects e.g. the self-interaction of the electrons included in $V_H(\mathbf{r})$:

$$V_{eff}([n], \mathbf{r}) = V_{ext}(\mathbf{r}) + \frac{1}{2}\frac{e^2}{4\pi\epsilon_0}\int \frac{n(\mathbf{r})}{r_{12}}d\mathbf{r} + V_{xc}([n], \mathbf{r}) \quad . \tag{2.12}$$

The effective potential is used to determine the KS orbitals out of effective one-particle equations

$$\left\{-\frac{\hbar^2}{2m}\Delta + V_{eff}([n], \mathbf{r})\right\}\phi_i = \epsilon_i\phi_i \tag{2.13}$$

leading to an electron density that satisfies equation (2.11) and being expressed in terms of the KS orbitals via

$$n(\mathbf{r}) = \sum_i^N |\phi_i(\mathbf{r})|^2 \quad . \tag{2.14}$$

Because $V_{eff}([n], \mathbf{r})$ depends on the electron density itself, the KS equations have to be solved self-consistently. Starting from an initial guess $n(\mathbf{r})$ (e.g. a superposition of atomic densities), $V_{eff}([n], \mathbf{r})$ can be constructed out of equation (2.12), leading to single-particle wave functions ϕ via equation (2.13), which can be used to calculate a new electron density out of equation (2.14). The new density is used to update the initial density and to repeat this procedure until $n(\mathbf{r})$ is converged within a predefined limit.

The key element in DFT is the exchange correlation functional E_{xc}. The next section gives therefore a short introduction to the main concepts.

2.4 Exchange-Correlation Functionals

The simplest approximation for E_{xc}, is the local density approximation (LDA). It uses the known exchange-correlation energy of a homogeneous electron gas, having a uniform positive background charge, to determine the xc energy of the inhomogeneous system locally at each point. The exchange-correlation energy in the LDA approximation has therefore the form

$$E_{xc}^{LDA}[n] = \int n(\mathbf{r})\epsilon_{xc}^{LDA}[n(\mathbf{r})]d\mathbf{r} \tag{2.15}$$

with ϵ_{xc}^{LDA} as the xc energy per particle of the homogeneous electron gas. Per construction this approximation is good for systems with a nearly uniform electron density, but has a lack of accuracy for inhomogeneous structures like atoms and molecules. But also for bulk and transition metal systems another approximation, called generalized gradient approximation (GGA), provides in most cases better results than LDA [18, 19] and is therefore used in this thesis without exception. GGA is an extension of LDA considering not only the electron density but also its gradient to approximate the xc energy

$$E_{xc}^{GGA}[n] = \int n(\mathbf{r})\epsilon_{xc}^{GGA}[n(\mathbf{r}), \nabla n(\mathbf{r})]d\mathbf{r} \quad . \tag{2.16}$$

While binding and cohesive energies are usually too large within LDA (overbinding), cohesive energies are underestimated in GGA. This results also in bond lengths and lattice constants which are to small when calculated with LDA and overestimated using GGA, compared to experimental values. In this thesis GGA is used in the form presented by Perdew, Burke and Ernzerhof in [20], the so-called PBE functional.

2.5 Program Package FHI-aims

For all calculations the "Fritz Haber Institute *ab initio* molecular simulation" (FHI-aims) program package was used. It allows to compute the electronic structure and total energies, including relaxations and molecular dynamics, of both finite and periodic systems [1]. Furthermore it also allows, for instance, to calculate core-level shifts and to simulate STM images.

FHI-aims is an all-electron, full-potential code using numerically tabulated atom-centered basis functions, which allows high accuracy for the calculated total energies by using predefined hierarchical basis sets for each chemical element calculated on atom-centered grids of points. Parallelization of grid-based numerical integrations results in an efficiency comparable to state of the art plane-wave pseudopotential schemes [21]. The strictly localized orbitals guarantee a nearly linear scaling of the grid-based operations, since different spatial regions are separated from one another. For a test system of Polyalanine this enables a nearly O(N) scaling with system size N for chaines with up to several hundred atoms. For bigger systems solving the single-particle eigenvalue problem (equation (2.13)), which formally scales as $O(N^3)$ with system size, becomes the limiting part in scalability [21, 22, 23]. The implemented scalar-relativistic scheme allows the treatment of systems including also heavier elements, like it was done in this thesis.

Besides DFT applications the program can also be used to perform wave-function based calculations based on Hartree-Fock and many-body perturbation theory, like MP2 or the random phase approximation (RPA). Also electronic single-quasiparticle excitations can be investigated using GW or MP2 self-energies.

Chapter 3

Ab Initio Atomistic Thermodynamics

The results of electronic structure calculations correspond to $T = 0$ K. Although *ab initio* calculations do not directly contain information about the thermodynamic behaviour of systems under real conditions, DFT results can still be used as input data for further thermodynamic analysis that allows to take into account the energy and entropy contributions to the free energy in the presence of a gas or liquid reservoir at finite temperature T and pressure p.

3.1 Constrained Thermodynamic Equilibrium

The total energy E^{tot} of a system, obtained from a DFT calculation, contributes to the internal energy U of the system. Neglecting the vibrational energy (which can be justified in some cases, especially when considering energy *differences*, but by no means should be taken for granted), the Gibbs free energy can be written as

$$G(T, p) = E^{tot} - TS + pV \quad , \tag{3.1}$$

where the leading term E^{tot} is the total energy and directly obtained from the calculations, T is the temperature, S the entropy, p the pressure, and V the volume. Within the framework of first-principles atomistic thermodynamics [24, 25, 26], this thermodynamic potential is used to identify the atomic structure with the

lowest energy under real temperature and pressure conditions of a surrounding gas phase. This gas phase works as a reservoir and is assumed to be in equilibrium with the bulk or a surface, while all components of the system are characterized by their chemical potentials $\mu_i(T, p_i)$.

Considering a fully equilibrated gas phase composed of H_2 and N_2 would result in NH_3 as the energetically most stable molecule over a wide range of temperatures and pressure. Because of the high reaction barrier for this gas phase reaction, the formation of NH_3 in the gas phase is ignored in all further considerations. This means that two independent gas phase reservoirs, N_2 and H_2, are not assumed to be in equilibrium with each other, but individually with the ruthenium surface or bulk. The thermodynamic stability of several surface and bulk Ru/N and Ru/H systems in this 'constrained equilibrium', with the gas phase reservoir containing molecular nitrogen and hydrogen as a function of temperature and partial pressure, can be investigated. The chemical potentials of the corresponding species are calculated using the ideal gas model and experimental thermodynamic data.

3.2 Bulk Nitride Stability

In a pure nitrogen environment, the stability condition of a bulk ruthenium nitrogen compound is

$$\begin{aligned} g^{bulk}_{Ru_xN_y} &< x g^{bulk}_{Ru} + \frac{y}{2}\mu_{N_2} \quad \Leftrightarrow \\ \Delta\mu_N &> \frac{1}{y}\{g^{bulk}_{Ru_xN_y} - x g^{bulk}_{Ru} - \frac{y}{2}E^{tot}_{N_2}\} \quad , \end{aligned} \tag{3.2}$$

where g_X is the gibbs free energy of phase X and $\Delta\mu_N$ is the chemical potential of nitrogen referenced to the total energy of a N_2 molecule $\Delta\mu_N = \mu_N - \frac{1}{2}E^{tot}_{N_2}$, which can also be written as $\Delta\mu_N = \frac{1}{2}\Delta\mu_{N_2} = \frac{1}{2}\mu_{N_2} - \frac{1}{2}E^{tot}_{N_2}$. Because the (T, p) dependence of the Gibbs free energy of bulk phases is rather small, the bracket on the right hand side in equation (3.2) can be substituted by $H_f^{Ru_xN_y}(T = 0\ \mathrm{K}, p = 0\ \mathrm{bar})$, the heat of formation of the nitrogen compound at $T = 0$ K and $p_{N_2} = 0$ bar. This results in a stability condition where the whole (T, p)

dependence is represented through the nitrogen chemical potential

$$\Delta\mu_N \gtrsim \frac{1}{y} H_f^{Ru_xN_y}(T = 0\ K) \quad . \tag{3.3}$$

Since under any conditions of interest nitrogen stays gaseous, an estimate for the upper limit of the nitrogen chemical potential can be defined as the point when nitrogen starts to condense on the surface, i.e. $\Delta\mu_N < 0$. Neglecting the pV contribution, the heat of formation can be calculated directly from the DFT total energies, and it is

$$\Delta\mu_N \gtrsim \frac{1}{y} H_f^{Ru_xN_y}(T = 0\ K) = \frac{1}{y}\{E_{Ru_xN_y}^{tot,bulk} - xE_{Ru}^{tot,bulk} - \frac{y}{2}E_{N_2}^{tot}\} \quad . \tag{3.4}$$

Similarly, in a pure hydrogen environment, the stability condition of ruthenium nitride can be approximately expressed as

$$\begin{aligned} g_{Ru_xN_y}^{bulk} + \frac{3y}{2}\mu_{H_2} &< xg_{Ru}^{bulk} + y\mu_{NH_3} \quad \Leftrightarrow \\ H_f^{Ru_xN_y}(0K) + 3y\Delta\mu_H &< y(\mu_{NH_3} - E_{NH3}^{tot}) + 3y\Delta E^{mol} \quad . \end{aligned} \tag{3.5}$$

Here is $\Delta\mu_H = \mu_H - \frac{1}{2}E_{H_2}^{tot}$ and $\Delta E^{mol} = \frac{1}{3}E_{NH_3}^{tot} - \frac{1}{2}E_{H_2}^{tot} - \frac{1}{6}E_{N_2}^{tot}$. If the system is assumed to be situated in a flow reactor, the continuous formation of NH_3 is counteracted by the continuous removal of this reaction product. Therefore the probability of a readsorption of a NH_3 molecule is low in comparison to the adsorption of N_2 and H_2 molecules so that the surface will not equilibrate with the surrounding NH_3 gas phase. A simple approximation for the chemical potential of NH_3 is therefore the internal energy of a free NH_3 molecule, so that $\mu_{NH_3} = E_{NH3}^{tot}$ at all temperatures and pressure. For the stability condition of ruthenium nitride in a pure hydrogen atmosphere it follows

$$\Delta\mu_H \lesssim -\frac{1}{3y} H_f^{Ru_xN_y} + \Delta E^{mol} \quad , \tag{3.6}$$

with $\Delta E^{mol} = \frac{1}{3}E_{NH_3}^{tot} - \frac{1}{2}E_{H_2}^{tot} - \frac{1}{6}E_{N_2}^{tot}$.

In the gaseous environment containing both hydrogen and nitrogen in a 'constrained equilibrium', the general stability condition for ruthenium nitride is obtained by combining equations (3.3) and (3.6):

$$\Delta\mu_H - \Delta\mu_N \lesssim -\frac{4}{3y} H_f^{Ru_xN_y} + \Delta E^{mol} \quad . \tag{3.7}$$

For low hydrogen concentrations equation (3.3) still applies, so that these two conditions (3.3, 3.7) form the basis for the examination of the stabilities of bulk ruthenium nitrogen compounds.

For the formation of bulk ruthenium hydrides the corresponding equations are

$$\Delta\mu_H \gtrsim \frac{1}{y} H_f^{Ru_xH_y}(T = 0\ K) \tag{3.8}$$

and

$$\Delta\mu_N - \Delta\mu_H \lesssim -\frac{4}{y} H_f^{Ru_xH_y} + 3\Delta E^{mol} \quad . \tag{3.9}$$

3.3 Surface Free Energy

If a homogeneous crystal is cleaved into two parts, the internal energy of the system is no longer represented by the internal energy of the bulk $E^{bulk} = TS - pV + N\mu$, where N is the number of particles in the system, and μ the chemical potential, but is increased by a value proportional to the created surface area A. Therefore the internal energy of a cleaved solid material is given by

$$E^{surf} = TS - pV + N\mu + \gamma A \quad . \tag{3.10}$$

The proportionality factor γ is called the surface energy [27], which is naturally a positive quantity, since the bulk is not exfoliating. It is defined as the surface excess free energy per unit area of the considered plane in a crystal at $T = 0\ K$, so that the most stable surface is minimizing γ. Using equation (3.1) and (3.10) the surface free energy of a multi-component system being in equilibrium with different reservoirs, expressed in terms of their chemical potentials μ_i, can be written as

$$\gamma(T, p_i) = \frac{1}{A}\left\{G^{surf} - \sum_i N_i\mu_i(T, p_i)\right\} \quad , \tag{3.11}$$

where G^{surf} is the Gibbs free energy of the cleaved solid.

3.4 Gas Phase Chemical Potential

After describing the stability conditions of bulk ruthenium nitrides and the surface free energy as a function of the chemical potentials of the nitrogen and hydrogen gas phase reservoirs, the remaining task is to express the latter in terms of temperature and pressure. Assuming the gas phases as ideal-gas-like reservoirs, the nitrogen (hydrogen) chemical potential can be expressed by

$$\frac{1}{2}\Delta\mu_{N_2}(T,p) = \Delta\mu_N(T,p) = \mu_N(T,p^0) + \frac{1}{2}kTln(\frac{p}{p^0}) \tag{3.12}$$

and

$$\frac{1}{2}\Delta\mu_{H_2}(T,p) = \Delta\mu_H(T,p) = \mu_H(T,p^0) + \frac{1}{2}kTln(\frac{p}{p^0}) \quad . \tag{3.13}$$

These equations provide the complete (T,p) dependence of the chemical potentials, if the temperature dependence of $\mu_X(T,p^0)$ (X=H, N) is known for a single pressure p^0. We can use the following connection

$$\begin{aligned} \mu_X(T,p^0) &= \frac{1}{2}\{H(T,p^0,X_2) - H(0\ K,p^0,X_2)\} \\ &- \frac{1}{2}T\{S(T,p^0,X_2) - S(0\ K,p^0,X_2)\} \end{aligned} \tag{3.14}$$

to obtain the temperature dependence from the differences in the enthalpy and entropy of a X_2 molecule. For standard pressure $p^0 = 1$ atm the required data is tabulated in thermochemical tables, so that the temperature dependence of $\mu_X(T,p^0)$ can be calculated. It is listed for some chosen temperatures in table 3.1. Combining this data with equations (3.12) and (3.13), the whole (T,p) dependence of the chemical potentials is accessable. Therefore the results from DFT calculations, obtained as a function of the chemical potentials, can be plotted in a μ_{N_2}-μ_{H_2}-plot where the scales can be converted into different pressure and temperature ranges.

T / K	$\mu_N(T, p^0)$ [eV]	$\mu_H(T, p^0)$ [eV]
100	-0.067	-0.036
200	-0.156	-0.094
298	-0.250	-0.157
300	-0.252	-0.159
400	-0.354	-0.229
500	-0.459	-0.302
600	-0.568	-0.379
700	-0.679	-0.459
800	-0.792	-0.540
900	-0.908	-0.624
1000	-1.025	-0.709
1100	-1.144	-0.796
1200	-1.265	-0.884
1500	-1.635	-1.157
2000	-2.275	-1.633

Table 3.1: $\mu_X(T,\ p = 1$ atm) for X=H, N at some temperatures of interest. The thermochemical data is taken from [28].

Part II

Calculations

Chapter 4

Convergence Tests

The total energy of a system calculated using DFT, as well as the time needed to perform this calculation, depends on several parameters, such as atomic structure model, basis sets, and k-points. To obtain trustful and reproducible results in a reasonable time, the influence of these parameters is studied as a first step for a few structures. The converged parameters are then kept fixed for all bulk and surface calculations, respectively, so that for all structures the accuracy of the results is comparable.

The parameters for bulk, surface, and molecular systems need to be converged separately, because each of these structural classes has different optimal settings. Since DFT formation energies, corresponding to the heat of formation at $T = 0$ K, are calculated as the difference of total energies (see equation (3.4)), they converge faster than the total energies themselves due to systematic error cancellation, as long as the same accuracy settings are used within one class. This is the reason why settings that do not provide converged total energies for bulk and surface calculations still provide accurate results, but in a shorter time.

4.1 Atoms And Molecules

To determine e.g. the formation energy of ruthenium nitrides and hydrides and to perform *ab initio* atomistic thermodynamic studies, the energies of H_2 and N_2, as well as the total energies of the hydrogen, nitrogen and ruthenium atom are

needed. This section presents some of the conducted convergence tests to obtain this data, as well as the results themselves.

In figure 4.1 the dependence of the calculated energy on the basis set is shown for the three atoms Ru, N, and H as well as for the nitrogen and hydrogen molecule. Each basis set stands for a pre-defined set of additional basis functions

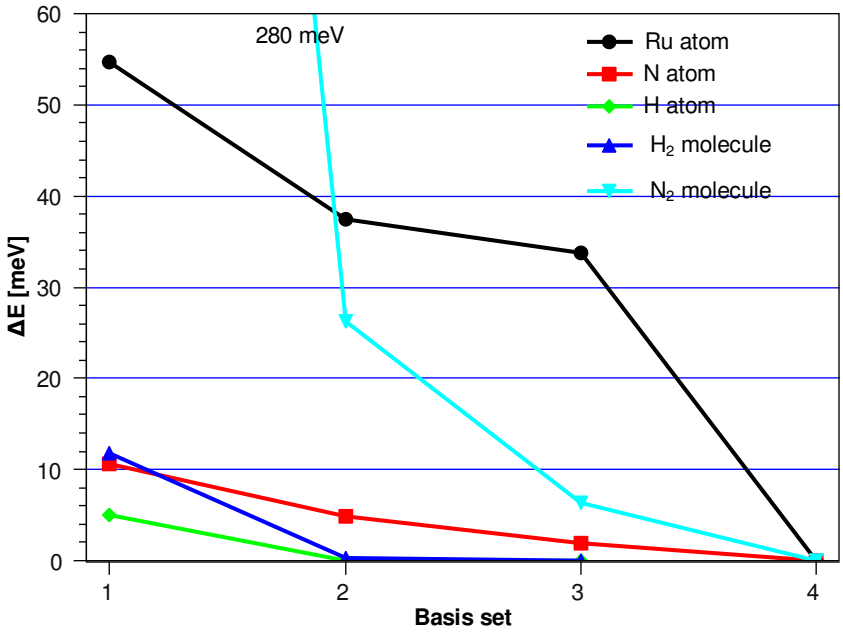

Figure 4.1: Relative energy of a Ru, N, and H atom and of the H_2 and N_2 molecule with respect to the lowest energy of each atom (molecule) as a function of the used basis set. The connecting lines are just added to guide the eye.

to the minimal basis of the corresponding element, which is given by the core and valence functions of the spherically symmetric free atom. The sequence of additional basis functions is determined by the following iterative construction strategy, which ensures a hierarchical construction of the basis and is described in more detail in [21]: First a large pool of possible additional radial basis functions with different shapes (hydrogen-like, ionic, ...) is defined. Then the total energy of a test system is calculated for all combinations of the minimal basis with one additional function out of the pool. The additional radial basis function that gives the best improvement to the total energy, is the one which is added first to the minimal basis. For the new set of basis functions again all combinations with

a function out of the pool are tested and the one with the best improvement to the total energy is included to the list of basis functions. This is repeated several times until a list of additional basis functions for each element is obtained, which systematically allows to improve the calculated energy. Within this list, the additional basis functions are organized in groups by their different angular momenta. For example the additional basis sets, or levels of accuracy (named as *tiers*), of nitrogen consist of the following additional radial basis functions, each having $(2l+1)$ angular momentum functions: spd (*tier1*), spdfg (*tier2*), spdf (*tier3*), spdfg (*tier4*). Each set contains also all basis functions of the set before. Such an appearance of "naturally ordered" *tiers* is found for nearly all elements and the exact pre-defined sets of additional radial basis functions are included in the FHI-aims program package. The obtained level of accuracy with a *tier1* basis set corresponds to a so-called "double-numeric plus polarization" (dnp) [29] or "double-zeta plus polarization" (dzp) [30] level, whereas in that cases the grouping of additional basis functions is based on intuition, while it is here a consequence of the presented construction strategy. For heavier elements *tier1* consists of more than just s, p, and d functions; e.g. for ruthenium also the first f and g basis function occurs in the list before the s, p, d group is completed. All relative energies in figure 4.1 are given with respect to the lowest calculated energy of each atom and molecule, respectively, which is in all cases obtained for the biggest basis set, as expected. For hydrogen only three basis sets are provided with the program package, but in this case the energy difference between a basis set of 2 and 3 is already less than 1 meV for both the atom and the molecule. By contrast, the calculated energy of a ruthenium atom with its 44 electrons is still changing by more than 30 meV when expanding the basis set 3 by the additional functions of the basis set 4. Of particular importance is the basis set when calculating the total energy of the nitrogen molecule, where the energy changes by around 280 meV when expanding basis set 1 to basis set 4, while the binding length is changing by only 0.008 $\AA$. Due to the fact that the description of the system becomes more accurate with increasing basis, the biggest basis set is used in all cases to calculate the final energies.

In FHI-aims different approaches are implemented to ensure a stable self-consistency [21]. For example, if calculating metallic systems, where many states exist close to the Fermi level, occupying the states by a slightly broadened distribution provides an additional stability leading to a faster and general convergence of the total energy, respectively. The selected occupation type defines the Fermi level and also the fractional occupation of the Kohn-Sham orbitals as described in [1]. The FHI-aims output provides an extrapolated total energy of the system for such calculations, which is an estimation of the total energy for a zero broadening. However, if calculating atoms or any other system with a comparable big HOMO-LUMO gap, the extrapolated total energy should be equal to the uncorrected energy, whereas the broadening should still be non-zero to guarantee the existence of a Fermi level and small enough to evoke no fractional occupation. Plotting the energy of the ruthenium atom as a function of the width of the used gaussian broadening distribution for occupying the Kohn-Sham states, shows that a broadening of 0.1 eV, which is used for bulk calculations, is not suitable to describe the Ru atom correctly. The energy is by 450 meV higher than for a smaller broadening, which is due to the distribution of the electrons over all d states. Therefore a broadening of 0.001 eV is used for all atoms and molecules.

4.1.1 Results

Besides the total energies, one also gets the electron configurations of the atoms by evaluating the energies of the different occupations of the spin-up and spin-down eigenvalues, given in the FHI-aims output. This provides a possibility to check the results especially for the Ru atom, where the expected $[Kr]4d^7 5s^1$ configuration has been obtained. All results for the atoms are listed in table (4.1). The bond lengths, total energies, and binding energies of the H_2 and N_2 molecule can be found in table (4.2). The binding energies $E_{X_2}^{bind}$ are calculated out of the total energies of the atoms E_X^{tot} and molecules $E_{X_2}^{tot}$ via

$$E_{X_2}^{bind} = -(E_{X_2}^{tot} - 2E_X^{tot}) \quad , \tag{4.1}$$

where X=H, N. While the binding energy of the H_2 molecule is only some tenth of

Atom	Total Energy [eV]	Electron Configuration
H	-13.600, 13.595[1)]	$1s^1$
N	-1484.851	$[He]2s^22p^3$
Ru	-123285.217	$[Kr]4d^75s^1$

Table 4.1: Calculated total energies and electron configurations of the H, N, and Ru atom. [1)] Reference [31].

Molecule	Bond length [$\AA$]	Total Energy [eV]	Binding Energy [eV]
H_2	0.750 0.741[2)]	-31.748	4.547 [4.478, 4.523][2)]
N_2	1.103 1.104[1)]	-2980.276	10.572 10.24[1)], [9.760, 9.807][2)]

Table 4.2: Calculated bond length, total energy and binding energy of the H_2 and N_2 molecule. [1)] Theoretical values from Reference [32] obtained with the PW91 functional, [2)] Experimental results from Reference [33, 34] and therein.

an eV higher than experimentally determined binding energies, the value obtained for the N_2 molecule differs by up to 800 meV from the experimental results. This big discrepancy is indeed already known for the N_2 molecule, and so is the referenced theoretical value determined with the PW91 functional "only" around 300 meV smaller than the one, calculated in this thesis. Such a big inaccuracy has of course an impact on the calculated formation energies and also on the performed thermodynamical studies. Using the experimental binding energy for the N_2 molecule $E_{N_2}^{bind,exp}$ and the calculated energy of a nitrogen atom E_N^{tot}, the "experimentally" expected total energy of a nitrogen molecule $E_{N_2}^{tot,exp}$ can be calculated according to equation (4.1). This energy $E_{N_2}^{tot,exp}$ can then be used to calculate out of the total energies of an atom in the ruthenium lattice $E_{Ru}^{tot,bulk}$ and of a ruthenium nitrogen compound $E_{Ru_xN_y}^{tot,bulk}$ the heat of formation of the Ru/N structure, according to equation (3.4). Doing this, a value which is by around 300 meV lower in energy than the one obtained with the calculated energy $E_{N_2}^{tot}$ is determined. This peculiarity should be kept in mind when in the following part

the results are only discussed with respect to the calculated energies.

4.2 Bulk And Surface Structures

While for the studied atoms and molecules only the accuracy of the final results is of importants, also the time needed to perform a calculation has to be taken into account for bulk and surface structures. The DFT-calculations of the atoms and small molecules can be performed in the order of seconds, whereas the same computing system needs calculation times in the order of hours or even days for bulk and especially surface structures, in particular when a structural relaxation is needed.

First the optimal basis set is determined. This is done by calculating the total energy of a bulk ruthenium fcc lattice for different numbers of additional radial basis functions and for various lattice constants, and then finding for each of the basis sets the lattice constant with the smallest total energy by fitting the data with a polynomial fit of 2nd order. Finally, for these lattice parameters of equilibrium the total energies are calculated and plotted together with the needed calculation times against the number of additional radial basis functions in figure 4.2. Here the additional radial basis functions are always chosen as in the pre-defined way, specified within the FHI-aims program package. The ruthenium fcc lattice is used as the reference system instead of the ruthenium hcp lattice, which is the crystallographic structure in which ruthenium can be found in nature, because the unit cell of the fcc system containes only 1 atom and the lattice is characterized by only one variable, while the hcp lattice has a two atomic basis and the description of the lattice needs two variables. Therefore the calculation time for optimizing the fcc lattice is much shorter, whereas the qualitative results are expected to correspond to each other. This is also the reason why the basis set and all other settings are only converged once for a single structure and are then used for all other systems.

The plateau-like behaviour of the computing time of the bulk ruthenium at bigger basis sets in figure 4.2 evolves due to a different number of needed scf-cycles (Self

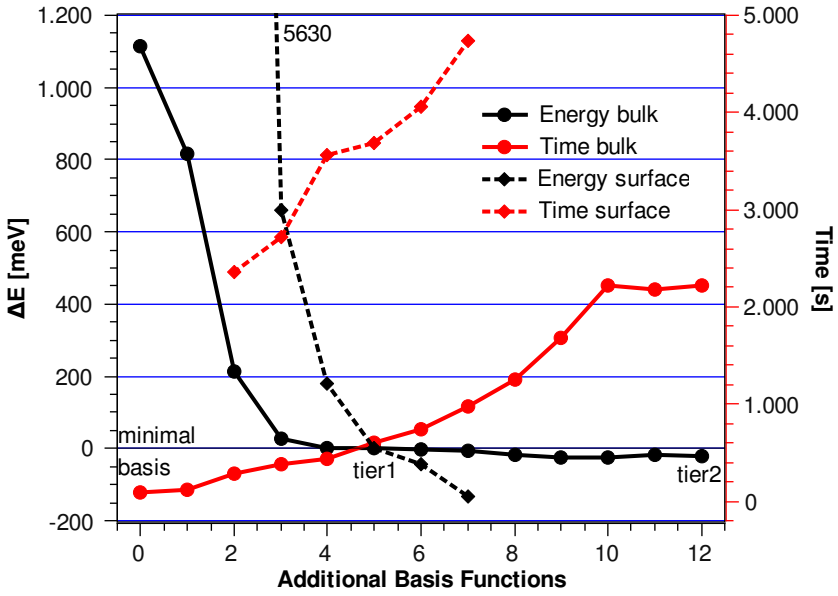

Figure 4.2: Total energies with respect to the energy calculated with the basis set *tier1* and calculation times as functions of the basis set.

Consistent Field) for convergence of the electron density. This is not a systematic characteristic and plotting the time per scf-cycle against the number of additional radial basis functions leads to a more linear behaviour as can be seen in figure 4.3. This figure also shows how the lattice parameter of equilibrium a depends on the basis set. The total energy is converged within some 24 meV and the lattice parameter of equilibrium is converged within 0.5 pm when comparring the results for the basis set *tier1* and *tier2*. The more accurate description with *tier2* would cost in this case 2200 seconds instead of the 600 seconds which are needed for the calculation with the basis set *tier1*. Therefore *tier1* is used for all calculations. While the energy for bulk calculations is already well converged for the basis set *tier1*, the total energy for the ruthenium surface, where a (2x2x5) unit cell with 2 fixed and 3 relaxing layers is used, changes by around 200 meV when using just one additional basis function less than is included in *tier1*. Due to the fact that all interesting physical quantities like the heat of formation or adsorption energies are always calculated as differences of total energies, not the convergence of the total energy but of the difference of the total energies of two structures is of

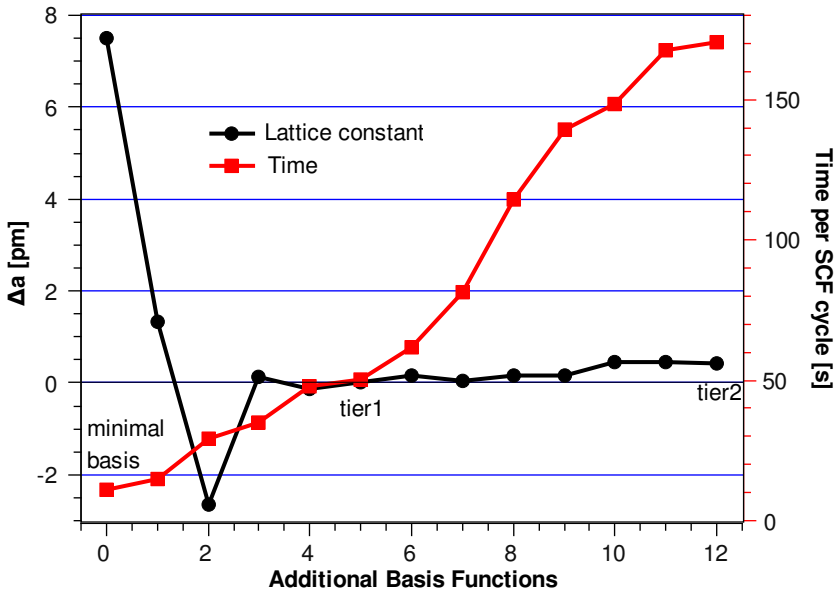

Figure 4.3: Lattice parameter of equilibrium and calculation times per scf-cycle as functions of the basis set.

physical interest. This difference is normally converging much faster. Figure 4.4 shows the heat of formation of a nitrogen subsurface interstitial in the mentioned ruthenium slab at a coverage of $\Theta = 0.25$ as a function of the used basis set for the ruthenium slab. As it is common practice in surface science, the coverage Θ is always defined as the ratio of adsorbate species to surface substrate atoms. As can be seen, the formation energy is converging more than 10 times faster than the total energy, so that the basis set *tier1* is used as a compromise between accuracy and calculation time.

Since the argument of energy differences only holds for the ruthenium slab itself and not for the interstitial nitrogen or hydrogen atoms, because these only appear in one of the two structures, they have to be described with a relatively bigger basis to get accurate results. This is also tested and a the basis sets *tier2* and *tier3* are determined to serve best for nitrogen and hydrogen, respectively.

Another important input parameter besides the basis set is the used integration grid in the reciprocal space for periodical calculations. The k-grid spacing is defined over three values, which evenly split the grid along the three reciprocal

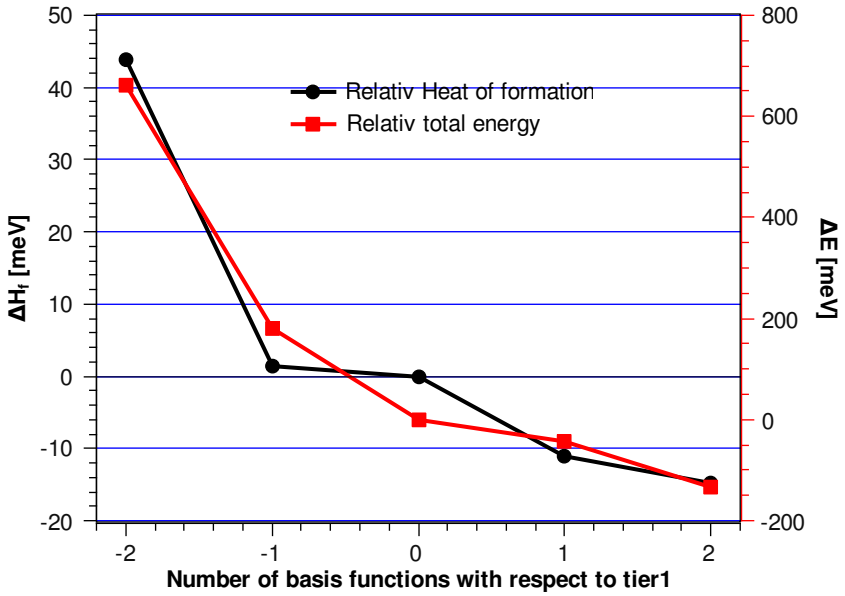

Figure 4.4: Formation energy of a subsurface nitrogen interstitial and total energy of the ruthenium slab as a function of the used basis set.

lattice vectors of the first Brillouin zone up, centering the grid around the Γ-point. In metals the Brillouin zone can be divided into areas that are occupied and unoccupied by electrons, respectively. A non-zero smearing factor (compare section 4.1) guarantees, that the functions that need to be integrated, don't change discontinuously from zero to non-zero values at the Fermi surface, which separates the two types of regions. In spite of smearing out the occupation of states at the Fermi level, an accurate description of metals still needs a relatively high number of k-points. Figure 4.5 shows relative energies and calculation times as a function of the number of k-points for ruthenium in a hexagonal closed packed form (hcp). Because the relation between the two lattice parameters of the ruthenium hcp lattice is given by $c/a = 1.58$ (see table 5.1), the chosen k-point triples guarantee a nearly equally spacing in all three directions of the Brillouin zone. Because of the minimum in calculation time and the energy convergence within 10 meV, a reference k-grid of 12x12x8 is chosen for all bulk and surface calculations. This means that for structures with different volumes the k-grid is adjusted in a way, that the k point density and spacing is comparable to that of the hcp ruthenium

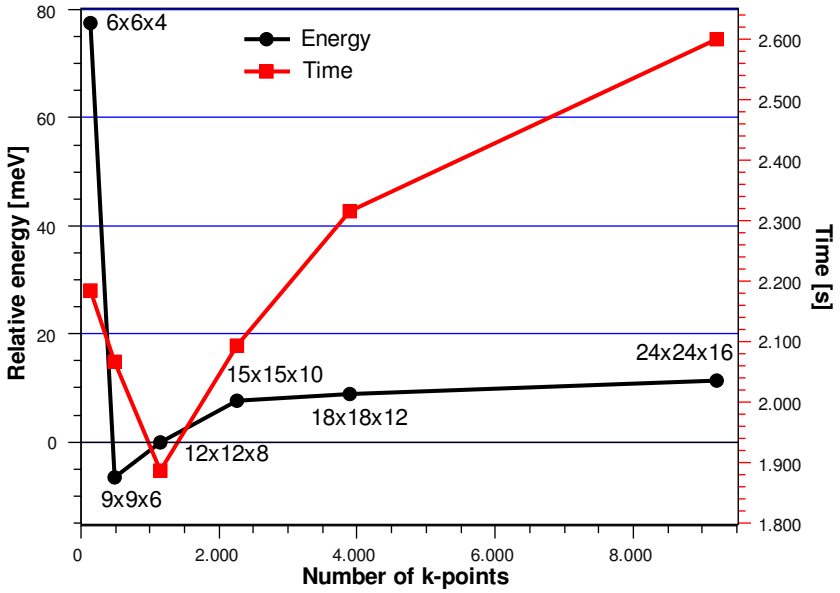

Figure 4.5: Relative energy and calculation time as a function of the used k-point grid.

lattice. Therefore the z-direction is in surface calculations represented by a single k point, while the number of k points along the lateral lattice vectors depends on the size of the unit cell, so that for a (2x2) surface unit cell the k-grid is given by 6x6x1.

Chapter 5

Ruthenium

Ruthenium is a 4d element with a [Kr]$4d^7 5s^1$ electron configuration. In nature it appears in the hcp structure and is used in various catalytical applications such as the Haber-Bosch process for synthesizing ammonia out of nitrogen and hydrogen [5, 35]. In this chapter, the structure and electronic properties of bulk ruthenium, as well as the clean ruthenium (0001) surface are studied.

5.1 Properties Of The Bulk

5.1.1 Geometry And Energetics

A hexagonal lattice with all atoms of the same type corresponds to a close-packing of spheres, where the layers of spheres are packed in an ABA form where every other layer is the same. To describe such a lattice a two atomic basis with atoms at $(0|0|0)$ and $(\frac{a}{2}|\frac{a}{2\cdot\sqrt{3}}|\frac{c}{2})$ and two lattice constants a and c, defining the lattice vectors $(a|0|0)$, (a·sin30|a·cos30|0), and (0|0|c), are needed. The volume of the two atoms containing unit cell is then given by

$$Vol = \frac{\sqrt{3}}{2}a^2 c \quad . \tag{5.1}$$

To optimize a structure with two lattice parameters by minimizing the corresponding energy $E(a, c)$, a couple of ways exist. In this work the following steps are used: First a fixed volume close to the experimental volume of the unit cell is chosen. Then several lattice parameters a around the experimental parameter

are selected, and for each of the pairs (a, c), corresponding to the fixed volume, the energy of the structure is calculated. Afterwards the energy is plotted over a, the lattice parameter with the lowest energy is determined by a polynomial fit and the energy of the corresponding structure is calculated. A quadratical fit and a cubic spline are tested for fitting these data points, giving results which vary in 0.001 $\mathring{A}$ for the equilibrium lattice constant and less than 1 meV in energy. Therefore the error of the fitting procedure is below the accuracy of the chosen convergence settings. This is repeated for several volumes around the experimental one, for each having several lattice parameter pairs (a, c). The energies of the final structures for each of the volumes are then plotted against the volume. Using the Murnaghan equation of state [36, 37], the volume with the lowest energy, as well as the bulk modulus B_0 of the structure, defined as

$$B_0 = V_0 \frac{d^2E}{dV^2}|_{V_0} \quad , \tag{5.2}$$

is subsequently determined out of this binding curve. Here V_0 is the unit cell volume calculated out of the equilibrium lattice constants. The corresponding pair of lattice parameters (a, c) is then identified by the above procedure for a fixed volume. This proceeding of finding the equilibrium lattice constant and total energy of the structure is also used for the ruthenium bulk nitrides and hydrides. It is simplified for systems defined by only one lattice parameter, because for each volume only one calculation, instead of several ones for different pairs of (a, c), has to be performed. For most of the studied structures no reference lattice parameter is known, so that initially more volumes have to be analyzed to find the energetical minimum.

Because the hcp structure is highly symmetric and no structural change is expected, there is no need for an atomic relaxation within the unit cell. Nevertheless, for the ruthenium nitrogen and hydrogen structures an atomic relaxation is performed, to ensure that the energetical minimum is found. The significance of this shows e.g. the relaxation of the [ZnO] structure, where a second slightly more stable structure is found (see section 6.1). Furthermore it was tested in a single run that for ruthenium no spin polarization needs to be taken into account, which corresponds to its non-magnetic properties.

	Calculated	Literature
Lattice parameter [$\AA$]: a	2.718	2.678-2.754[1], 2.703-2.706[2]
c	4.295	4.159-4.371[1], 4.273-4.283[2]
c/a	1.580	1.553-1.587[1], 1.581-1.584[2]
Unit cell volume per atom [$\AA^3$]	13.748	12.915-14.354[1], 13.520-13.573[2]
Bulk modulus [Mbar]	3.137	3.1-3.4[1], 3.208[2]
Total energy per atom [eV]	-123291.924	-
Cohesive energy per atom [eV]	6.707	6.74[2]

Table 5.1: Characteristics of the ruthenium hcp lattice. [1)] Calculated DFT results from [38, 39, 40, 41, 42, 43, 44], [2)] Experimental results from [31, 45, 46, 47].

All results are brought together in table 5.1. The ideal c/a ratio for a hcp structure is $\sqrt{8/3} \approx 1.633$ and therefore around 3 % above the ratio for the ruthenium lattice. Comparing this value to other elements with a hcp structure shows, that ruthenium has still a medium c/a ratio [48]. The calculated lattice constants differ by not more than 0.5 % from the experimental parameters, and show an excellent agreement with the theoretical ones from [40], where they calculated them to be $a = 2.718$ and $c/a = 1.580$, using a plane-wave basis set with pseudopotentials and the LDA functional. The GGA results from the same paper are increased by around 1.7 % compared to their own LDA lattice parameters, and are therefore further away from the GGA results from this work than from their own LDA output. The bulk modulus is by around 2.2 % smaller than the experimentally determined value of B_0, while the cohesive energy E_{coh} of ruthenium corresponds to the experimental data within a fault tolerance of 0.5 % and is calculated as the difference in total energies of a free and a bulk ruthenium atom:

$$E_{coh} = -(E_{bulk} - E_{atom}) \quad . \tag{5.3}$$

Therefore the physical parameters used for the calculations together with the GGA functional seem to describe the ruthenium hcp lattice quite well.

5.1.2 Bandstructure And Density Of States

The electronic band structure of a material is one of its central characteristics. It represents the dispersion relation of the electrons under the influence of the potential energy of the lattice. The band structure therefore describes, along specific lines in the crystal, the energy ranges in which an electron can exist. These lines are connecting high symmetry points within the Brillouin zone and are representable for the dispersion relation within the whole lattice. The first Brillouin zone, together with the symmetry points of the hcp lattice and the connecting symmetry lines, is shown in figure 5.1. The band structure helps to

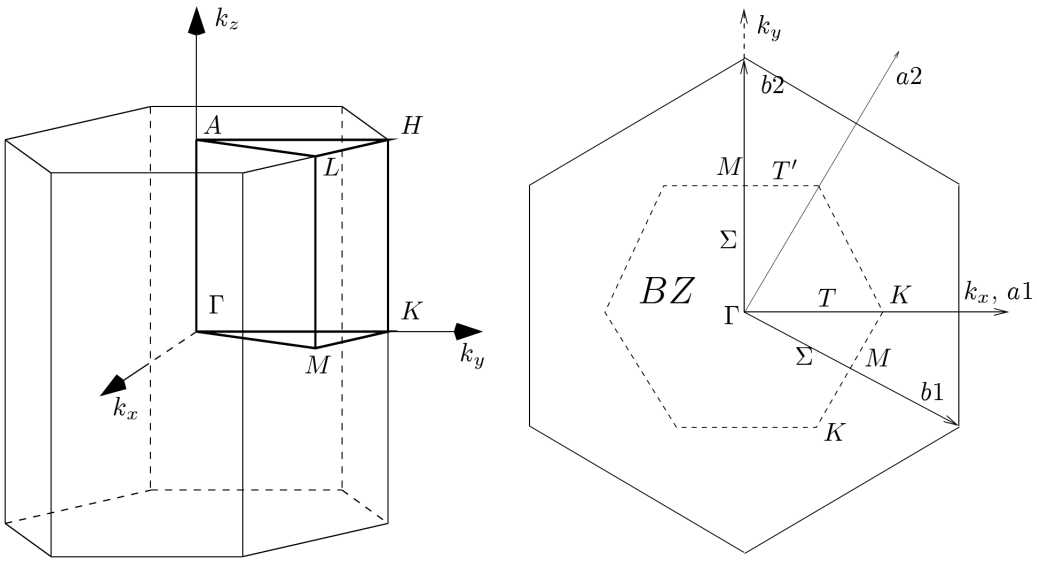

Figure 5.1: First Brillouin zone of the hcp lattice. Γ, K, M, A, H, and L are the symmetry points, and $k_{x,y,z}$ the cartesian coordinates. $a_{1,2}$ are the lattice vectors, $b_{1,2}$ the corresponding lattice vectors in the reciprocal space, and Σ, T, and T′ are the symmetry lines. Figure taken from [38].

understand electrical, thermal, and optical properties, as well as the density of states (DOS), giving the number of accessible states at a certain energy level that can be occupied by electrons. The band structure and the DOS are calculated for the final geometry of the hcp ruthenium lattice, using the converged electron density. They are shown in figure 5.2. Comparing the band structure with the one calculated in [38] using a plane wave code with pseudopotentials shows a

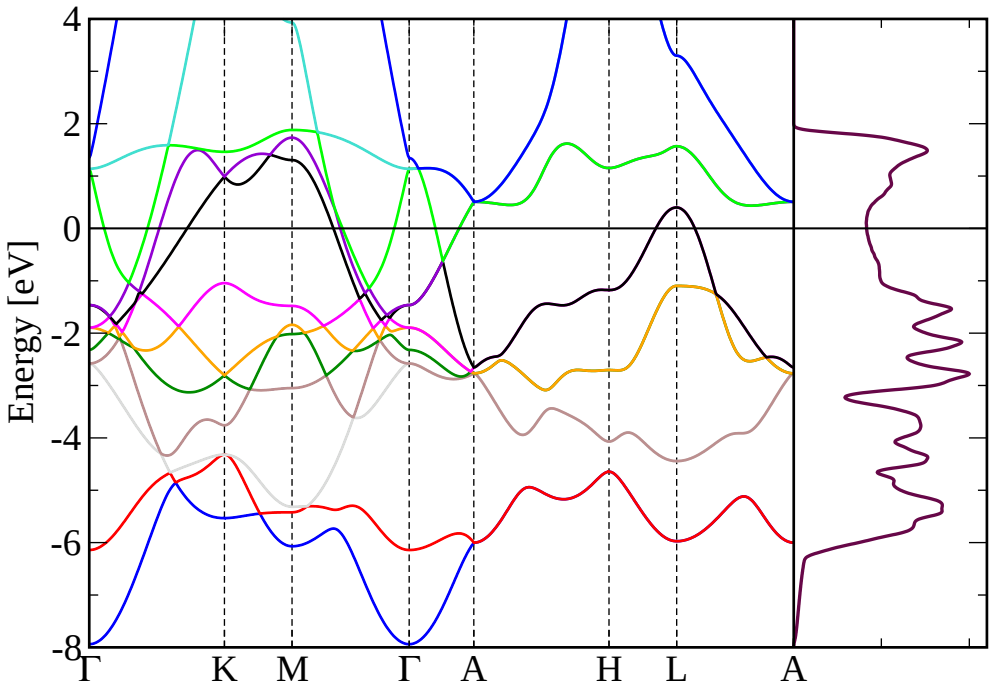

Figure 5.2: Bandstructure of hcp Ru (left) together with the DOS (right).

one-to-one agreement. Also the DOS exhibits all characteristic features, which are elaborately discussed in [38].

5.2 Properties Of The Clean Surface

Before structures with on-surface and subsurface adsorbed hydrogen and nitrogen atoms are modeled, the properties of the clean Ru(0001) surface, shown in figure 5.3, are studied. The results are then compared to literature to affirm the chosen physical parameters in the input files.

5.2.1 Surface (Formation) Energy

The surface energy γ is one of the basic quantities in surface science and determines, among other things, the equilibrium shape of a crystals surface. Most experimental data results from surface tension measurements in the liquid phase extrapolated to zero temperature [49, 50]. This procedure yields a rather high degree of uncertainty, and delivers results which are not specific for the surface

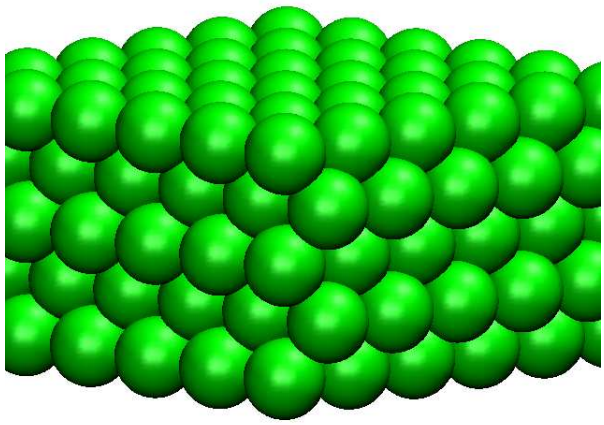

Figure 5.3: 5-layer ruthenium slab with a (0001) surface.

energy of particular surface facets.

According to equation (3.11), the specific surface energy at 0 K can be calculated via

$$\gamma = \frac{1}{2A}(E_{slab}^{tot} - N_s E_{bulk}^{tot}) \quad , \tag{5.4}$$

when fixing the ruthenium chemical potential to the energy of the bulk and neglecting the pV term of the Gibbs free energy. N_s is the number of atoms in the slab and E_{slab}^{tot} and E_{bulk}^{tot} the total energy of the slab and of a bulk ruthenium atom, respectively. The factor $\frac{1}{2}$ takes into account that the slab has an upper and a lower surface with each having a surface area A. The so calculated surface energy depends on the number of layers in the slab and converges with increasing thickness to the surface energy in terms of the energy per unit area required to form the surface from bulk material.

Because in equation (5.4) total energies of three-dimensional bulk and two-dimensional surface systems are used, problems concerning comparable accuracy may appear. Therefore, to cross check the result, the surface energy is also calculated by means of

$$\gamma_n = \frac{E(n) - n[E(n) - E(n-1)]}{2A} \quad . \tag{5.5}$$

Here n is the number of layers in the slab, and $E(n)$ the corresponding energy of the n-layer slab. Hence, the bulk energy is substituted by $E(n) - E(n-1)$ and is

therefore determined from a series of slab calculations [51, 52]. Both definitions are used in the following to calculate the surface energies of slabs containing different numbers of layers. The ruthenium surfaces are modeled by periodic arrays of symmetric slabs, having a vacuum region between the repeated slabs of 20 $\AA$. First the relaxation of the surface atomic positions is neglected and instead all atoms of the slab are kept fix at their bulk positions.

Fixed Bulk Positions

The number of layers in the slab is varied in-between two and eight. The surface area per surface atom is given by $A = a^2 = 7.390\ \AA^2$, so that with the known total energy per bulk ruthenium atom (see section 5.1) and with the total energies of the slabs, both equations (5.4) and (5.5) can be applied to calculate the surface energies. The dependence of the surface energies on the number of layers is summarized in table 5.2 and shown in figure 5.4.

n	2	3	4	5	6	7	8
γ	1.116	1.067	1.113	1.117	1.110	1.113	1.118
γ_n	-	1.214	0.930	1.096	1.156	1.089	1.074

Table 5.2: Surface energies of a Ru(0001) surface for different numbers of ruthenium layers n within the slab and fixed atomic positions. The surface energies are given in [eV/surface atom].

While γ, calculated by (5.4), seems already well converged for a four-layer slab with a value of 1.11 eV/surface atom, γ_n is still changing quite a lot between a slab containing 6 and 8 layers.

Due to a reduction of symmetry at the surface, the surface atoms are influenced by forces, different from those in the bulk, and would relax to an energetically more stable structure, if allowed. Although the surface atoms are not allowed to relax in these calculations, so that the determined surface energy should be higher than the real surface energy of the Ru(0001) surface, the apparently converged value of 1.11 eV/surface atom is already by 10 % smaller than the experimental reference value of 1.22 eV/surface atom [53]. This might be due to the above mentioned

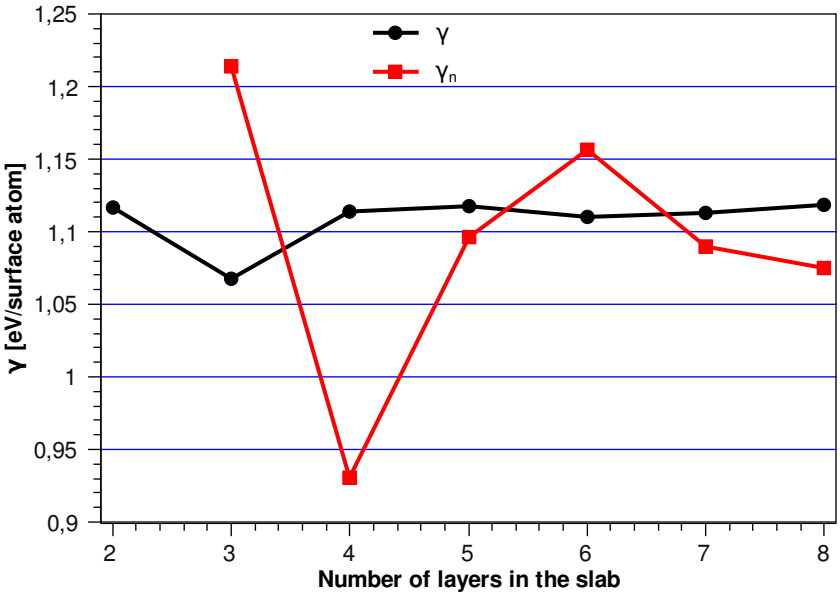

Figure 5.4: Surface energies calculated by equations (5.4) and (5.5) as a function of the number of ruthenium layers in the slab.

experimental inaccuracies. However, another DFT calculation in [54] using a pseudopotential method within the local density approximation reveals a value of 1.7 and 1.2 eV/surface atom, respectively. Here the value of 1.2 eV/surface atom is received by using supplemental orbitals outside the used 4-layer slab to handle the electron density of the metallic slab outside the surface more accurate.

In the following the topmost ruthenium layers on both sides of the slabs are allowed to relax, whereby the surface energy of the ruthenium (0001) surface is minimized during the geometrical relaxations.

Relaxed Surfaces

To determine an accurate surface energy via equation (5.4), which is exclusively used in this section, symmetric slabs are needed, so that both surfaces of the slabs are the same. In the following calculations either the central, or the three central layers of the slabs are fixed, while the number of relaxing layers per side is varied in-between one and five. Again a vacuum region of 20 $\AA$ between the repeated slabs is used and the atoms are relaxed until the forces are less than $5 \cdot 10^{-4}$ eV/$\AA$.

# of layers	fixed - relaxed	γ	Δ_{12}	Δ_{23}	Δ_{34}	Δ_{45}	Δ_{56}
3	1 - 1	1.030	-3.56	-	-	-	-
5	1 - 2	1.092	-3.74	0.66	-	-	-
7	1 - 3	1.080	-3.82	0.01	0.57	-	-
5	3 - 1	1.092	-3.46	-	-	-	-
7	3 - 2	1.081	-3.73	0.06	-	-	-
9	3 - 3	1.094	-3.81	0.09	0.75	-	-
11	3 - 4	1.091	-3.71	-0.00	0.67	-0.02	-
13	3 - 5	1.094	-3.79	0.03	0.74	-0.11	-0.14

Table 5.3: Surface energies and percentaged interlayer relaxations of a ruthenium (0001) surface for different number of ruthenium layers within the slab. The fixed layers are in the middle of the slab and fixed to their bulk positions, while on both sides between one and five layers are allowed to relax. The surface energies are given in eV/surface atom and are calculated by equation (5.4).

The calculated surface energies can be found in table 5.3 and figure 5.5, together with the results for the interlayer relaxations, discussed in the next section.
The presented results show, that the obtained surface energies are rather dominated by the number of layers in the slab than by the number of relaxing layers at each side of the slab. So the values for the two 5- and 7-layer slabs are nearly identical. Comparing these surface energies with the ones of the slabs where all atoms are fixed to their bulk positions, but having the same number of layers in the slab, reveals a decrease in surface energy of 25 to 37 meV per surface atom due to the relaxation. The apparently converged value of 1.09 eV/surface atom differs from the experimental value of 1.22 eV/surface atom [53] by around 12 %. In [41] the surface energy of a ruthenium (0001) slab, containing 5 layers of which 2 layers are allowed to relax, was calculated within the local density approximation to be 1.17 eV/surface atom. This seems to indicate, that LDA is superior to GGA for calculating surface energies, as it is also mentioned in [18]. Nevertheless, because of the experimental inaccuracies it is hard to say, wether LDA is performing better than GGA or if the LDA results are just as bad as the

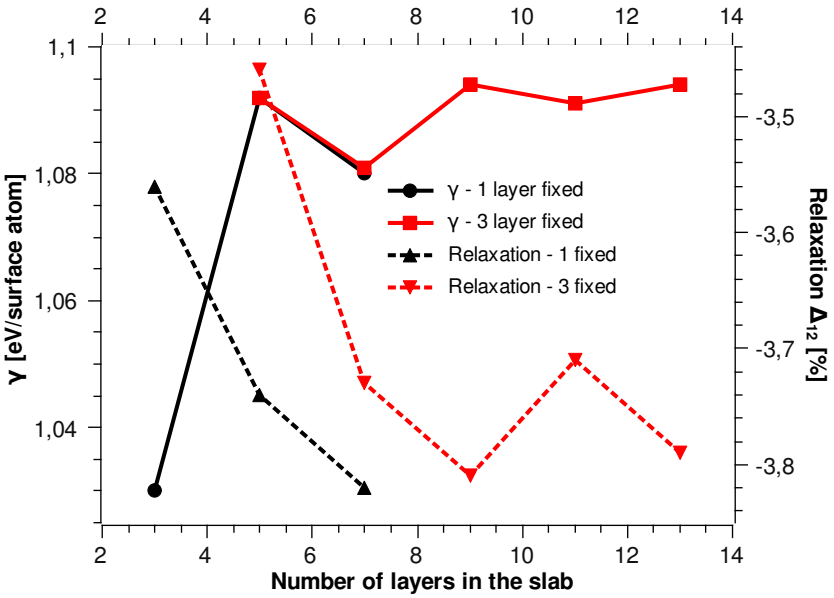

Figure 5.5: Surface energies calculated by equation (5.4), and the contraction of the topmost ruthenium layer as a function of the number of layers in the slab.

experimental values, which are not specific for the surface energy of a particular surface facet.

5.2.2 Interlayer Relaxation

In this section the structural change during the surface relaxations is quantified. Because the inner layers of the close-packed symmetric slabs are kept fix at their bulk positions, the structural change of the relaxing atoms manifests in the change of their z-coordinates. It can be described by the relation of the atomic positions before and after the relaxation. For the clean surface the percentaged interlayer relaxation between layer i and j with respect to the bulk spacing $d = c/2 = 2.147$, where c is the length of the lattice vector in z-direction of the hcp lattice, is given by

$$\Delta_{ij} = \frac{d_{ij} - d}{d} \cdot 100\% \quad , \tag{5.6}$$

where d_{ij} is the spacing between the relaxed layers.

It is well known that the distance between the two topmost layers of the ruthe-

nium (0001) surface is decreasing during relaxation, and it is also known that there is a discrepancy between theoretical and experimental results concerning the strength of this contraction. Such a disagreement is also found for other d-like metals [55], and for the ruthenium (0001) surface it is detected to be an effect of steps on the surface, over which the experiments are averaging [56]. The experimental values for the contraction of the topmost layer, calculated out of low energy electron diffraction patterns, reveal a contraction of 2 %, measured in [57] and references therein, which is increased by analyzing a single terrace to 3.5 % [56]. Theoretical calculations give first layer contractions between 3 and 4.3 %, depending on the method and the model of the slab, as found in [57] and references therein. In this context, all results obtained in this work for the relaxation of the topmost layer Δ_{12}, which are in-between -3.46 and -3.82 %, are in close agreement to the experimental results on single terraces of 3.5 % and to most of the calculated reference values, which are around a 4 % contraction. As expected, in figure 5.5 it can be seen that not the total number of layers in the slab, but the number of relaxing layers, is decisive for the magnitude of the contraction, by shifting the black dotted line to the right. Only in the case of just one relaxing layer per side, the slab thickness seems to have an influence on the contraction, which leads to a difference in relaxation of 0.1 % when comparing the three layer slab with the five layer slab. For two and more relaxing layers per side, the final geometrical structures reveal contractions of around 3.7 to 3.8 %. Another distinctive feature is, that the second-layer relaxations are normally pretty small, whereas the third-layer relaxations show again relatively big values of 0.57 to 0.75 %, which corresponds to an expansion of the spacing between the third and fourth layer of the relaxed structures (see table 5.3). This expansion seems to be a consequence of the slab model with an odd number of layers, because for a symmetric 10 layer slab with two fixed layers in the middle, relaxations of $\Delta_{12} = -4$ %, $\Delta_{23} = -0.16$ %, and $\Delta_{34} = 0.14$ % are found with a full potential augmented plane waves plus local orbitals method using the PBE functional [57].

5.2.3 Defect Formation

A 5-layer slab with a vacuum layer of 20 $\mathring{A}$, where the two bottom layers are fixed to their bulk positions and the other three layers are allowed to relax until the forces are less than $5 \cdot 10^{-4}$ eV/$\mathring{A}$, is used for the following calculations. Removing one atom from the top layer of a (2x2) unit cell of the Ru(0001) surface, creates a surface defect structure where every fourth surface atom is missing. The heat of formation of the defect is calculated as

$$H_f^{defect} = E_{slab,defect}^{tot} - E_{slab,clean}^{tot} - E_{Ru,bulk}^{tot} \quad . \tag{5.7}$$

Here $E_{slab,defect}^{tot}$ and $E_{slab,clean}^{tot}$ are the total energies of the slab with and without the surface defect, respectively, and $E_{Ru,bulk}^{tot}$ is the total energy of a bulk ruthenium atom. The heat of formation of this defect structure is found to be $H_f^{defect} = 1.687$ eV. This high value already shows the low willingness of defect formations at the ruthenium surface. It can further be used to calculate the concentration of surface defects c_{defect} at different temperatures via

$$c_{defect} = \frac{Z_d}{Z_0} \cdot exp[-\frac{\Delta G}{kT}] \quad . \tag{5.8}$$

Z_d and Z_0 are the partition functions of the system with and without defects, so that this quotient accounts for the contribution of the configurational entropy to the defect concentration. For the used (2x2x5) unit cell, the quotient has a value of 4. Neglecting the formation entropy of a single vacancy, the Gibbs energy ΔG is just represented by the heat of formation, so that the defect concentration at 600 K is found to be around $3 \cdot 10^{-14}$ per surface atom. This low defect concentration reflects the high heat of formation of a surface defect.

Chapter 6

Ruthenium Nitrogen Compounds

The literature of Ru/N compounds is scarce. The interactions and properties of the molecular RuN-system were analysed by Ram et al. [58] and Steimle et al. [59], while Colmenares et al. present a theoretical analysis of the RuN_2 molecule in [60]. In 2005 Chou et al. [6] reported on a polycrystalline pH sensing membrane, based on ruthenium and grown by radio frequency sputtering, which should contain bulk ruthenium nitrides, when the ruthenium is sputtered with nitrogen. The analysis of the composition is based on energy dispersive X-ray spectroscopy (EDS), which is element-specific, but does not contain information about the chemical environment. Therefore it is questionable if really ruthenium nitrides have been formed or if the interpretation of the data should not rather follow the suggestions made by Damayanti et al. in [7]. In this publication from 2006 they report on dissolved nitrogen and N grain boundary stuffing in ruthenium films, as well as possible formation of metastable ruthenium nitride clusters, when sputtering ruthenium in a nitrogen atmosphere. Annealing the films causes effusion of nitrogen and a crystallization of ruthenium. In 2007 Moreno-Armenta et al. [8] also report on an insertion of nitrogen into the ruthenium surface, this time by reactive pulsed laser ablation. In all three publications [6, 7, 8] the Ru/N compounds are formed out of atomic ruthenium and nitrogen molecules, leading to metastable structures, starting to decompose into metallic ruthenium and gaseous nitrogen at temperatures above 100 °C. The methods have in common that the species are quickly thermalized when arriving at the substrate and no

additional energy sources exist to decompose the originating structure. Therefore these methods are also useful to prepare metastable materials.

Up to date there is no evidence of a stable bulk or surface ruthenium nitride or any other solid and thermodynamically stable ruthenium nitrogen compound. This is not very particular, since to the author's knowledge, in the whole platinum group exists strictly speaking no known nitride and only a few nitrogen compounds. Here should only be mentioned the published synthesis of the platinum nitride PtN [61], which turns out to yield the same structure as the PtN_2 synthesized later by Crowhurst et al. [62], which is isostructural with pyrite and therefore rather a diazenide than a nitride.

In this chapter the DFT results of various bulk and surface Ru/N structures are presented. The structures are analyzed according to their relative stabilities and a thermodynamic analysis is performed to investigate stability conditions and to calculate concentrations of interstitial nitrogen atoms in the ruthenium lattice.

6.1 Bulk Structures

This section provides an overview on the calculated bulk Ru/N structures, followed by a summary of the results concerning their lattice parameters, DFT formation energies, relative stabilities and others. In the last subsection further investigations related to thermodynamic stabilities under varying temperature and pressure conditions are presented.

6.1.1 Calculated Structures

In a first approach mononitrides of ruthenium are studied in the five most prominent AB-structures: zinc sulfide (zincblende) [ZnS], zinc oxide (wurtzite) [ZnO], sodium chloride [NaCl], nickel arsenide [NiAs], and caesium chloride [CsCl]. This allows us a comprehensive investigation of the preferred coordination in ruthenium mononitrides, since the five structures represent three different atomic coordinations in the two most common crystal systems, cubic and hexagonal. In zincblende and wurtzite the atoms have a fourfold coordination, in the sodium

chloride and nickel arsenide structure a sixfold, and in the caesium chloride structure the atoms have a cubic coordination. The zincblende, sodium chloride and caesium chloride lattices belong to the cubic crystal system, while the wurtzite and nickel arsenide structure are representatives of the hexagonal system. Further information about these structures can be found in any inorganic chemical textbook like [63, 64].

All structures are optimized according to the procedure for the ruthenium lattice described in section 5.1. During optimizing the [ZnO] structure, the predefined lattice was relaxing at bigger unit cell volumes to a new geometry. In this structure the N atoms are rather forming a distorted face centered orthorhombic sublattice than a hcp one, while the Ru atoms are shifted in a way that their sublattice has now a distorted symmetry, which lies inbetween the hcp and the simple hexagonal system. Surprisingly, this new structure [ZnO-2] is lower in energy than the original [ZnO] structure with its equilibrium lattice constant. Additionally to these five AB-structures, another one is analyzed where the positions of the Ru and N atoms in the [NiAs] structure have been interchanged. It is called anti-[NiAs] or [AsNi] structure. This leads to a hcp lattice of Ru atoms where the octahedral interstitial sites are occupied by N atoms, now forming a trigonal prism, like the Ru atoms are doing in the original [NiAs] structure. By comparing these results with the ones for the [ZnO] structure it is possible to make a statement which interstitial sites are prefered by nitrogen atoms within a ruthenium hcp lattice.

Besides these AB-structures RuN_2 is studied in the pyrite structure [FeS_2] and in the [CaF_2] structure, where the ruthenium atoms form a fcc lattice with N atoms in all tetrahedral interstitial sites. The [FeS_2] structure is of interest, because in [62] the existence of a platinum group metal nitrogen compound, namely PtN_2, with such a symmetry is reported, as already mentioned before. It is build up by a fcc lattice of Ru atoms where the octahedral holes are occupied by N_2 barbells. Here two different supercells, containing each 4 unit cells, are used to find out how the orientation of the N_2 barbells influences the formation energy.

For a lower nitrogen content in a ruthenium lattice the [Fe_4N] structure is op-

timized. It consists of a fcc lattice of Ru atoms, where every fourth octahedral interstitial site is occupied by N atoms in a way that all octahedrals are corner shared. Therefore the structure has two symmetry types of Ru atoms: one type forms the octahedron around the N atoms and has two nitrogen atoms as nearest neighbours and the other one has no N atoms in its first coordination sphere. Because such an arrangement of N atoms in a fcc iron lattice is by around 240 meV more stable than an arrangement, where the iron atoms are surrounded by either one or two N atoms [65], it can be assumed that also for a ruthenium lattice this constitution of nitrogen atoms will be more stable. To compare again, at this lower nitrogen concentration, the formation energy of N atoms in the octahedral interstitials with the one of N atoms in the tetrahedral interstitial sites of a ruthenium lattice, also a fcc lattice of Ru atoms is studied where 1/8 of the tetrahedral holes is occupied by nitrogen atoms. In this structure, referred to as [Ru_4N], the N atoms are distributed in a way that the tetrahedrons are not connected to each other and all ruthenium atoms possess the same symmetry.

6.1.2 Results

To analyze the preferred coordination in ruthenium mononitrides, the theoretical heat of formation ΔH_f^0 of the seven optimized structures is plotted in figure 6.1. According to equation (3.4) they are calculated via

$$\Delta H_f^0 = E_{RuN}^{tot,bulk} - E_{Ru}^{tot,bulk} - \frac{1}{2} E_{N_2}^{tot} \tag{6.1}$$

and are therefore also referred to as DFT formation energies. The black dots in this figure represent the formation energies of the stated structures, while the red dot below the [ZnO] structure gives the formation energy of the [ZnO-2] structure, which appeared during geometry relaxation of the wurtzite lattice, and the red dot above the [NiAs] belongs to the [AsNi] structure. The lines connecting the black dots are just added to guide the eye.

Although all structures have a positive formation energy and are therefore endothermic, a tendency of stabilisation to lower coordination numbers (CN) can be found. The [CsCl] structure with its cubic coordination is the most unstable

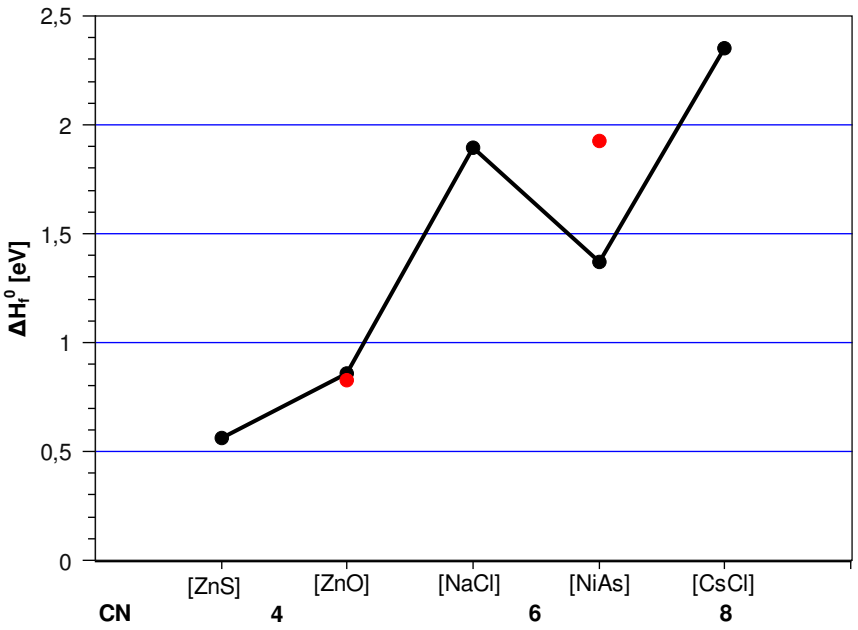

Figure 6.1: DFT formation energies of some RuN structures. The red dots belong to the heat of formation of the [ZnO-2] and [AsNi] structure, respectively.

geometry. All three structures with a sixfold coordination are lower in energy, but still more endothermic than the structures with fourfold coordinated atoms. Within the sixfold coordination the hexagonal [NiAs] structure is more stable than the cubic [NaCl] lattice, while in the most stable fourfold coordination the cubic geometry is favoured over the hexagonal one, so that [ZnS] turns out to be the relatively most stable structure. It is predicted to be metallic (see figure 6.4) and non-magnetic. The ruthenium mononitrides behave with this sequence of stability like the iron mononitride, which is known to crystallize in the [ZnS] structure [66], and confirm the general trend of the transition metal nitrides to lower CN for increasing number of d-electrons. The same ranking was also found by von Appen [67] who studied mononitrides of platinum group metals with the Vienna *Ab initio* Simulation Package (VASP) [68] using a plane wave basis set, ultrasoft pseudopotentials, and the PW91 functional. His DFT formation energies of the five most prominent AB-structures show a largely systematic deviation from the results obtained in this work. They are each around 200 meV lower in energy, except for the [ZnS] structure which exhibit an energy difference of just

140 meV. Accordingly, the difference between the formation energies of two structures calculated by von Appen is nearly the same like in this work and deviate by not more than 20 meV, except when the [ZnS] structure is used to calculate a difference. This clearly shows, that the results can only be seen as a qualitative description, since the choice of the method and functional has a big influence on the absolute formation energies, but do hardly influence the relative stabilities. All results, like the lattice parameters, unit cell volumes, bulk moduli, and heat of formations can be found in table 7.2 in the appendix. For the [ZnO] and [ZnO-2] structure, the energy-volume diagram and a contour plot are shown in figure 6.2.

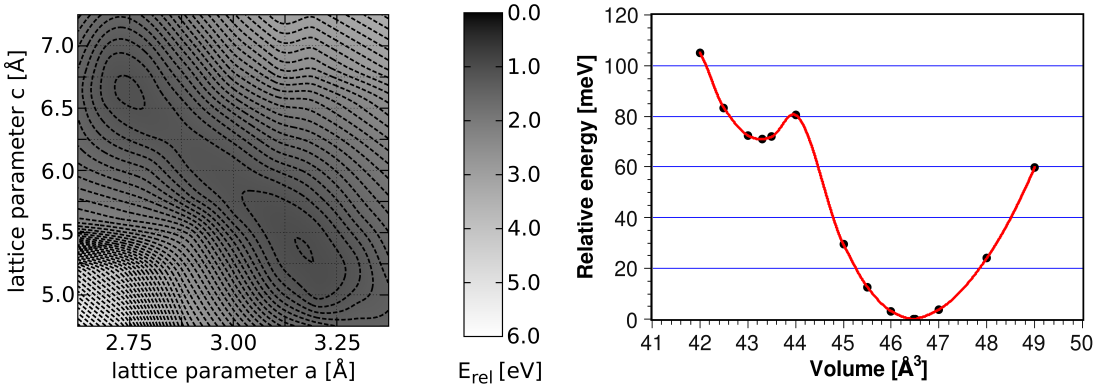

Figure 6.2: Contour plot and E-V-diagram of the [ZnO] and [ZnO-2] structure, respectively. Here the volume and relative energies are given for the conventional unit cell, with each two ruthenium and nitrogen atoms.

The contour plot shows the potential energy surfaces of the structure as a function of the lattice parameters a and c. It is calculated via the interpolation of the energies of 68 points in the interval $a = 2.625 - 3.375$ $\mathring{A}$ and $c = 4.75 - 7.25$ $\mathring{A}$, whereas most of the points have been around the imaginary line connecting the two minima in the contour plot. Along this line, the unit cell volume is increasing from the left to the right, whereas the energetical minimum for each volume is not located on this line, but is rather close to either one of the minima. Therefore no continuous change in the lattice parameters and structures takes place, but an abrupt change in the symmetry of the unit cell. The red curve in the E-V-

diagram is an akima spline connecting the energies of the optimized volumes, and is just added to guide the eye. It can be seen that the [ZnO] structure is up to a conventional unit cell volume of around 44 $\mathring{A}^3$ more stable than the [ZnO-2] structure. At higher unit cell volumes the symmetry is changing to the [ZnO-2] structure. Without further calculations the relatively higher bulk modulus of the [ZnO] structure can already be read off the curvature of the connecting red line in the E-V-diagram. The value is with 2.67 Mbar around 50 % higher than the one for the [ZnO-2] structure.

To study the influence of higher and lower nitrogen concentrations in a ruthenium lattice as a function of the occupied interstitial site, a fcc instead of a hcp lattice of ruthenium atoms is used. This is done for two main reasons: First, the most stable ruthenium mononitride, the [ZnS] structure, exhibits a fcc symmetry. Furthermore, also in the sixfold coordinated structures a fcc lattice of ruthenium atoms ([NaCl] structure) is slidely more favorable than a hcp one ([AsNi] structure). Secondly, optimizing a fcc lattice costs much less calculation time, since only one lattice parameter has to be optimized, and it should be sufficient for a qualitative description. In figure 6.3 the DFT formation energies of ruthenium nitrogen compounds with a ratio of Ru:N of 4:1, 1:1, and 1:2 are shown. The N atoms are either situated in the tetrahedral or octahedral interstitial sites of a fcc ruthenium lattice.

In case of the [FeS_2] structure, N_2-dumbbells are situated in each octahedral interstitial site. To ascertain the influence of the relative adjustment of these dumbbells to each other on the formation energy, two geometries with a different arrangement of the nitrogen are studied. The difference in formation energy between these two structures is less than 50 meV, so that it can be concluded that another possible energy gain due to another arrangement of the nitrogen dumbbells is for the purpose of this work negligible small.

For ruthenium to nitrogen ratios of 4:1 and 1:1, fourfold coordinated nitrogen atoms are preferred, while for the highest nitrogen concentration in the ruthenium lattice, N_2-dumbbells in octahedral interstitials are favoured over occupying each

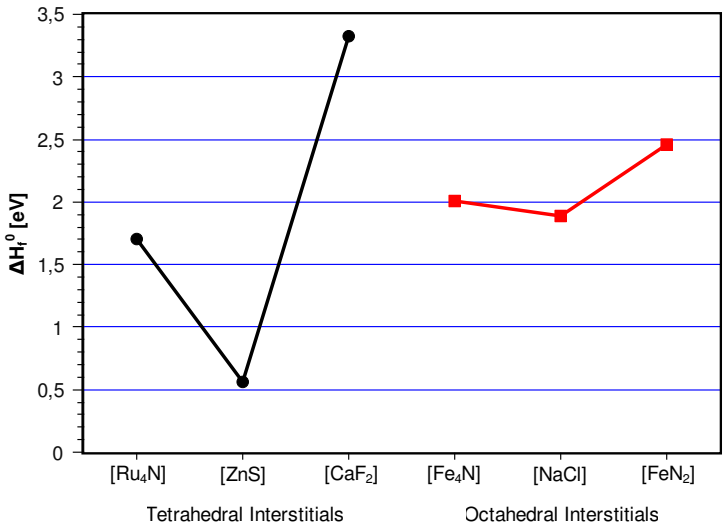

Figure 6.3: DFT formation energies of ruthenium nitrogen compounds with different concentrations of nitrogen atoms in the tetrahedral (left) and octahedral (right) interstitial sites of a fcc ruthenium lattice. The solid lines connecting the calculated energies are just used to guide the eye.

tetrahedral site of the ruthenium fcc lattice with a nitrogen atom. The behaviour at high nitrogen concentrations might be comprehensible when reminding, that only compounds with the small fluoride ions are known to form a [CaF_2] structure, except when big cations of the lanthanoids are involved. Furthermore e.g. PtN_2 is found to crystallize in the [FeS_2] structure [62], as already mentioned before. For both interstitial sites a concentration of ruthenium to nitrogen of 1:1 gives the smallest DFT formation energy. Therefore it seems as if a "clustering" of nitrogen atoms in the ruthenium lattice stabilizes the resulting structure. Nevertheless, to validate a general trend, further geometries with even smaller nitrogen contents would be needed. In this context, one has to remember, that the DFT formation energy is calculated with respect to metallic ruthenium in the hcp structure. Because all phases here have a ruthenium fcc sublattice and the energy difference between a fcc and hcp ruthenium lattice is calculated to be 105 meV per atom, the smaller the nitrogen content, the bigger the unit cell to describe the structure, and the bigger the influence of the general energy difference between ruthenium in the fcc and hcp structure on the formation energy.

To analyze therefore a possible clustering effect of nitrogen in a fcc ruthenium lattice, the formation energy of the resulting structures should be calculated with respect to fcc ruthenium. Taking this energy difference of 105 meV per ruthenium atom into account when comparring the structures with a ruthenium to nitrogen ratio of 4:1 and 1:1, the picture of a stabilization by clustering nitrogen atoms is still valid for fourfold coordinated nitrogen, but changes for the sixfold coordination. While here the [NaCl] structure is by 118 meV more stable than the [Fe_4N] structure when calculating the formation energies with respect to hcp ruthenium, the [Fe_4N] structure is by around 200 meV lower in energy than the [NaCl] one when comparing the energies with respect to fcc ruthenium.

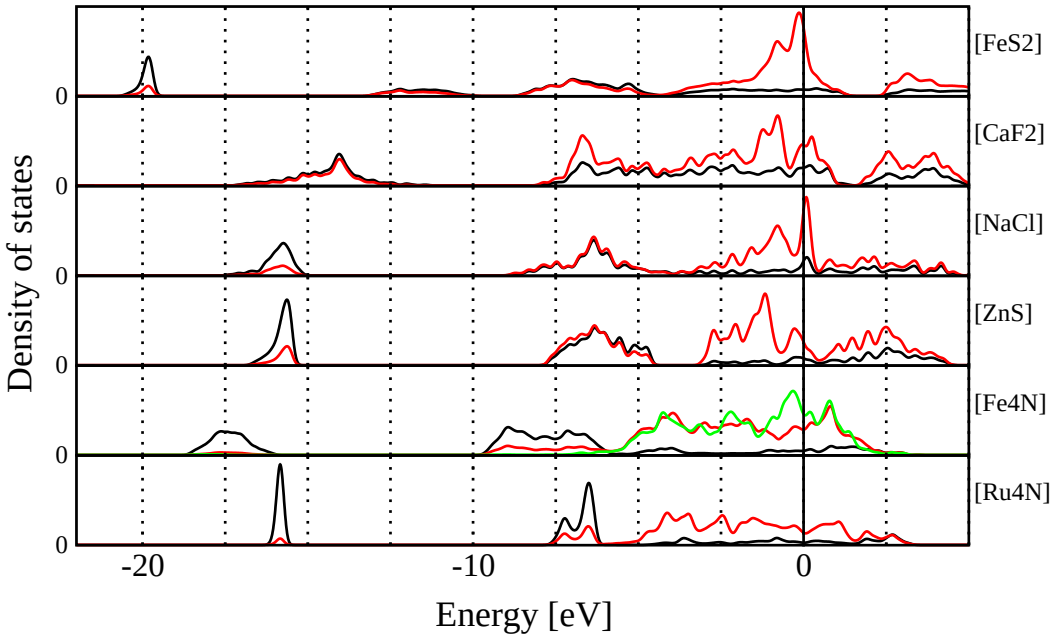

Figure 6.4: Atom projected density of states for some Ru/N compounds. The black lines give the DOS of the N atoms and the red lines of the Ru atoms. In the [Fe_4N] structure two symmetrical different Ru atoms exist, so that an additional green line is included for the Ru atom without N atoms as nearest neighbours.

Besides the energetics, the DOS are calculated for the six structures to get an insight into their electronic nature. They are plotted in figure 6.4. All structures

have a separated band in common which lies between -20 and -13 eV, depending on the geometry. It is mainly formed by N 2s electrons, whereas for the ruthenium nitrogen compounds with fourfold coordinated nitrogen atoms an increase of the ruthenium contribution to this band can be found for increasing nitrogen content from [Ru_4N] over [ZnS] to [CaF_2]. For none of the geometries a band gap around the fermi level can be observed in the DOS, so that all theoretical phases are predicted to have metallic character. The valence bands are in all cases formed out of N 2p and Ru 4d 5s hybrids, and similarities between the different structures, especially for the ruthenium to nitrogen ratios of 2:1 and 1:1, are pronounced.

6.1.3 Thermodynamic Analysis

The formation energies of all calculated bulk ruthenium nitrogen structures are positiv, with the lowest value of $\Delta H_f^0 = 0.564$ eV for the [ZnS] structure. Considering equation (3.3) and (3.12) from chapter 3, it is already clear that high pressure are needed to stabilize these structures. Following the procedure described in section 3.2 to analyze the stability regions of the calculated phases in a mixed atmosphere of N_2 and H_2, figure 6.5 is obtained.

On the x-achses the chemical potential of nitrogen and on the y-achses the chemical potential of hydrogen is plotted. The stability region for each structure is the area right below the corresponding line. This means that for a thermodynamical stable ruthenium nitride in the [ZnS] structure at a temperature of 600 K, which corresponds to the reaction temperature during the ruthenium catalyzed Haber-Bosch process [4], a pressure of around 10^{20} bar would be needed. This value is unbelievable high. Even if we take into account, that the calculations may reveal a too high formation energy, since in [67] they are by around 200 meV lower, the needed pressure are still very high. A drop of the formation energy by 100 meV corresponds to a drop of the necessary pressure to stabilize the structure at 600 K by a factor of around 50. Therefore the concentration of nitrogen atoms in the ruthenium lattice under reaction conditions of the ruthenium catalyzed ammonia synthesis ($T = 600$ K, $p = 100$ bar [4]) is negligible small. Using equation (5.8)

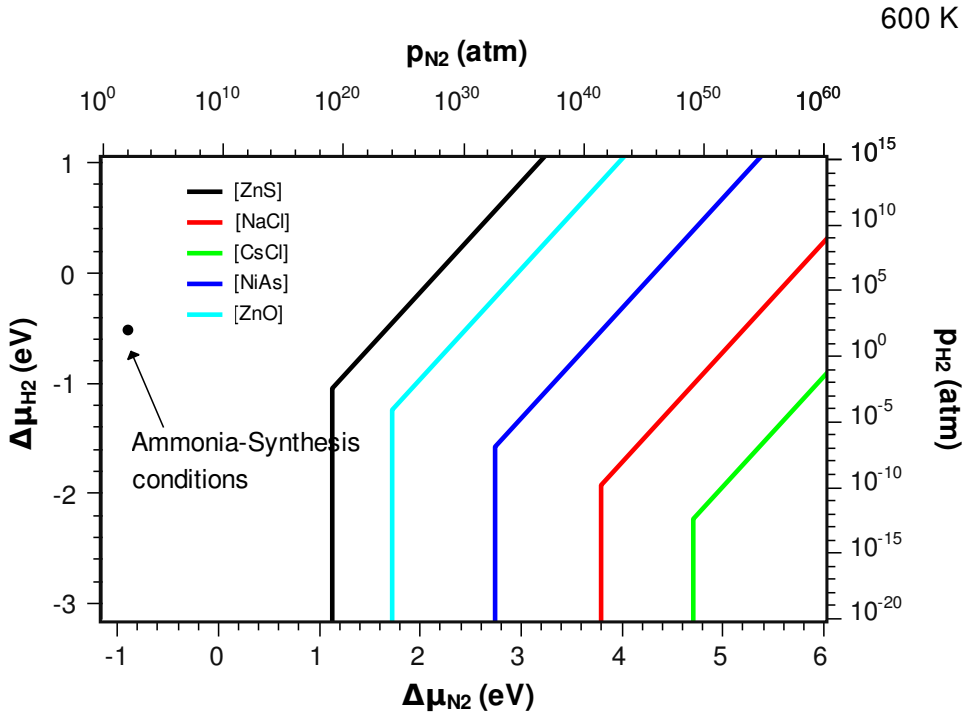

Figure 6.5: Stability regions of ruthenium bulk nitrides as a function of the chemical potentials $\Delta\mu_{N_2}$ and $\Delta\mu_{H_2}$. The pressure scales correspond to a temperature of $T = 600$ K.

from section 5.2.3, a nitrogen concentration of $n = 3 \cdot 10^{-9}$ per ruthenium atom is obtained under reaction conditions. Here the Gibbs free energy ΔG is used, calculated via

$$\Delta G = N_N \cdot (\Delta H_f^0 - \Delta\mu_N(p,T)) \quad , \tag{6.2}$$

where $N_N = 1$ is the number of nitrogen atoms in the unit cell.

Although no thermodynamical stable ruthenium nitride is found, the ability of experimental groups to synthesize such structures [6, 7, 8, 69] can still be understood. In all publications, mentioned already at the beginning of this chapter, the Ru/N compounds are formed out of atomic ruthenium and nitrogen molecules via different sputtering methods of a ruthenium target. Therefore the ruthenium reservoir in these experiments is not represented by bulk, but by atomic ruthenium. So it is justified to calculate the formation energies with respect to the energy of a ruthenium atom to analyze which compounds can in principle be syn-

thesized by these methods. The cohesive energy of ruthenium is calculated to be 6.707 eV (see section 5.1), so that the formation energies are formal reduced by this value. The heat of formation of ruthenium nitride in the zincblende structure, with respect to atomic ruthenium, is therefore -6.143 eV. In [6, 69] the reaction conditions for synthesizing the ruthenium nitride film are given by the substrate temperature $T = 298$ K and a nitrogen pressure of $p = 9 \cdot 10^{-6}$ bar. With equation $\Delta\mu_N(T,p) = \mu_N(T,p^0) + \frac{1}{2}kTln(\frac{p}{p^0})$, and the corresponding value for $\mu_N(T,p^0)$ from table 3.1, the nitrogen chemical potential under this condition is calculated to be $\Delta\mu_N = -0.399$ eV. With this value and the formation energy of the nitride -6.143 eV, the stability condition in equation (3.3) is fulfilled, so that a formation of metastable ruthenium nitrogen compounds can in principle be understood. The synthesized structures decompose into metallic ruthenium and nitrogen at temperatures above 500 K [7] and a pressure of around $p = 10^{-8}$ bar. This corresponds to a nitrogen chemical potential of $\Delta\mu_N = -0.856$ eV. Although the stability condition is still fulfilled when calculating the formation energy with respect to ruthenium atoms, the metastable structure is evolving to its thermodynamically more stable constituents. Therefore equation (3.3) with respect to atomic ruthenium can be considered as a necessary, but not as a sufficient condition, when studying the formation of Ru/N compounds by sputtering techniques.

6.2 Surface Structures

After analyzing some bulk ruthenium nitrogen compounds in the previous section, the properties of the ruthenium (0001) surface with on-surface and subsurface adsorbed nitrogen atoms should be discussed here. First an overview is given on the calculated structures, followed by a summary of the results like DFT formation energies, relative stabilities, and others. The third part of this section contains again some thermodynamic considerations of the results.

6.2.1 Calculated Structures

First the adsorption energies of nitrogen atoms at the fcc and hcp sites on the ruthenium (0001) surface are calculated for various coverages. The hcp site is expected to give the highest adsorption energies for nitrogen atoms on the surface, since there exist already some published literature on these structures [32, 70, 71, 72]. Nevertheless the energetics of these geometries are calculated again, to be able to compare the results from this work with some literature values and to test thereby also the surface model and physical parameters in comparison to the published results. It should also give an idea of how the energies change with the used functional and how big therefore an error bar for the adsorption energies might be. Furthermore structures with a combined on-surface and subsurface adsorption of nitrogen atoms are studied later on, so that these calculations are also used to distinguish between the different contributions to the overall formation energy. The nomenclature of the different on-surface and subsurface sites is shown in figure 6.6.

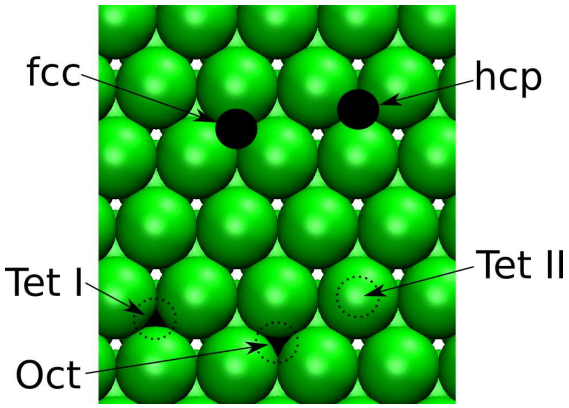

Figure 6.6: Surface sites on Ru(0001). Illustrated are the on-surface hcp and fcc site, as well as the subsurface sites Tet-I, Tet-II, and Oct.

Secondly, structures with subsurface adsorbed nitrogen atoms are studied. Here we have three different subsurface interstitial sites (see figure 6.6) for which again the energetics are analyzed as a function of the nitrogen coverage. Furthermore different arrangements of the subsurface nitrogen atoms for one and the same coverage, as well as combinations of nitrogen atoms in different subsurface in-

terstitial sites, are taken into account to study clustering effects. In addition, for some calculations the topmost ruthenium layer is shifted in a way, that a fcc packing of the top ruthenium layers results. This is done, because the most stable bulk ruthenium nitrogen geometry is found to be the [ZnS] structure with its fcc lattice of ruthenium atoms, where every second tetrahedral interstitial site is occupied by a nitrogen atom. Finally a surface defect structure (see section 5.2.3) with nitrogen atoms in the defect and some structures with combined on-surface and subsurface adsorbed nitrogen atoms are studied.

The ruthenium surface is modeled by a periodic array of slabs with a vacuum region between the repeated slabs of 20 $\mathring{A}$. For the structures with subsurface adsorbed nitrogen atoms, each slab contains 5 ruthenium layers, from which the two bottom layers are kept fixed at their bulk positions, whereas the top layers, on which the nitrogen atoms are sitting, are allowed to relax. Geometries containing only on-surface adsorbed nitrogen are modeled by a slab with two fixed and two, instead of three, relaxing layers. All structures are relaxed until the forces are less than $5 \cdot 10^{-4}$ eV/$\mathring{A}$. A (2x2) surface unit cell is used for calculations with a nitrogen coverage of 0.25 or higher, while the coverage of 0.125 is realized by a (2x4) surface unit cell. When analyzing structures with combined nitrogen adsorption on different subsurface sites usually a (2x4) unit cell ist used. Exceptions are explicitly mentioned in the text or in the tables 7.3-7.7 in the appendix.

6.2.2 Results

The calculated adsorption energies of on-surface adsorbed nitrogen in the fcc and hcp position for different coverages are presented in figure 6.7 and listet in table 7.3 in the appendix. The average adsorption energy per nitrogen atom is calculated via

$$E_a^N = \frac{1}{N_N}(E_{Ru/N}^{slab} - E_{Ru}^{slab} - \Delta N_{Ru} E_{Ru}^{bulk} - \frac{1}{2} N_N E_{N_2}) \tag{6.3}$$

where $E_{Ru/N}^{slab}$ and E_{Ru}^{slab} are the total energies of the slab with and without adsorbed nitrogen, E_{Ru}^{bulk} the total energy of a ruthenium atom in the bulk and E_{N_2} the

energy of a N_2 molecule. N_N is the number of nitrogen atoms in the surface unit cell and ΔN_{Ru} the difference in the number of ruthenium atoms between the two slabs, and therefore only for the defect structure with a value of -1 nonzero. An exothermic adsorption is characterized by a negative adsorption energy, so that a nitrogen compound becomes more stable with a decrease of E_a^N.

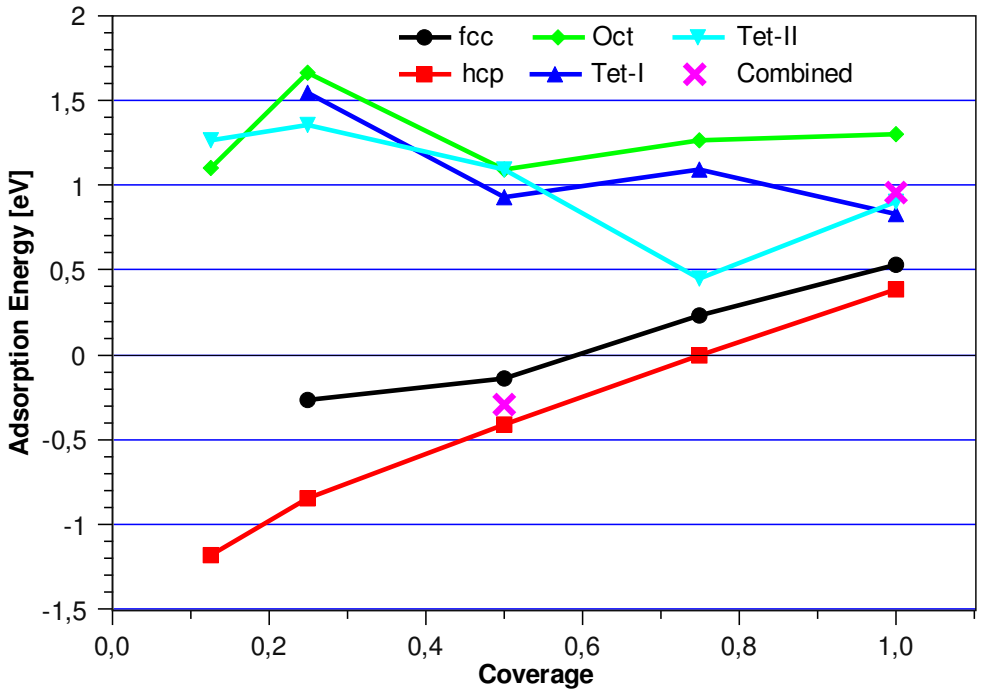

Figure 6.7: Calculated adsorption energies of nitrogen on ruthenium (0001) in different on-surface and subsurface sites as a function of the coverage. Also shown are two structures with both on-surface and subsurface adsorbed nitrogen. The lines connecting the calculated energies are just added to guide the eye.

As can be seen for nitrogen adsorbed in fcc and hcp sites, the adsorption energy per nitrogen atom is decreasing nearly linearly with increasing coverage. This behaviour was already described before in literature and is attributed to strong indirect repulsive interactions between the adsorbates due to the need to share the limited d-band electrons of ruthenium at higher coverages [70, 71]. While the general trend is already reproduced with different functionals, the quantified adsorption energies vary quite a lot in literature. The results from this work reveal

an exothermic adsorption up to a coverage of around 0.6 at the fcc, and 0.75 at the hcp site, respectively. For a coverage of 0.25 at the hcp site, an adsorption energy of nearly -0.85 eV per nitrogen atom is found. For the same site and coverage values of -0.29 [72], -0.65 [71], -0.7 [32], and -0.77 eV/atom [70] can be found in literature. While in [72] the RPBE functional [73] is used for a two-layer slab where all ruthenium atoms are kept fixed at their bulk positions, in [32] and [70] the PW91 functional [74] is used for a five- and six-layer slab where one and two layers are allowed to relax, respectively. The results from this thesis for on-surface adsorbed nitrogen are therefore close to the ones, determined with the PW91 functional. Although in [73] it is argued that the RPBE functional should give in general better results for adsorption energies on transition metals than the PBE or PW91 functional, the PBE functional is still exclusively used in this thesis, to give comparable results for bulk and surface calculations. Furthermore the big difference of around 0.56 eV between [72] and the calculated value from this work of -0.85 eV/atom might not only be due to the different functional, but also due to the model of the slab.

The percentage change Δ_{12}^{s} in the first metal interlayer distance of the Ru/N surfaces with respect to the clean ruthenium surface is presented in figure 6.8. According to equation (5.6) in section 5.2.2 the interlayer relaxation between layer i and j is calculated via

$$\Delta_{ij}^{s} = \frac{d_{ij} - d}{d} \cdot 100\% \quad . \tag{6.4}$$

For the clean four-layer slab with two relaxing layers the spacing between the first and second layer is $d = 2.077$ $\mathring{A}$, and for the five-layer slab, used when subsurface adsorbed nitrogen is involved, it is $d = 2.074$ $\mathring{A}$. To determine Δ_{12}^{s}, the center of mass of each layer is used. Therefore the interlayer relaxation is an average value and does not reflect the real surface geometries. This becomes especially important for subsurface adsorbed nitrogen, which comes along with a significant relaxation of the surface.

In [72], where the two-layer slab with fixed bulk positions is used, it is stated that a relaxation of the topmost ruthenium layer decreases the adsorption energy of nitrogen on the surface by only around 40 meV. Unfortunately it is not said

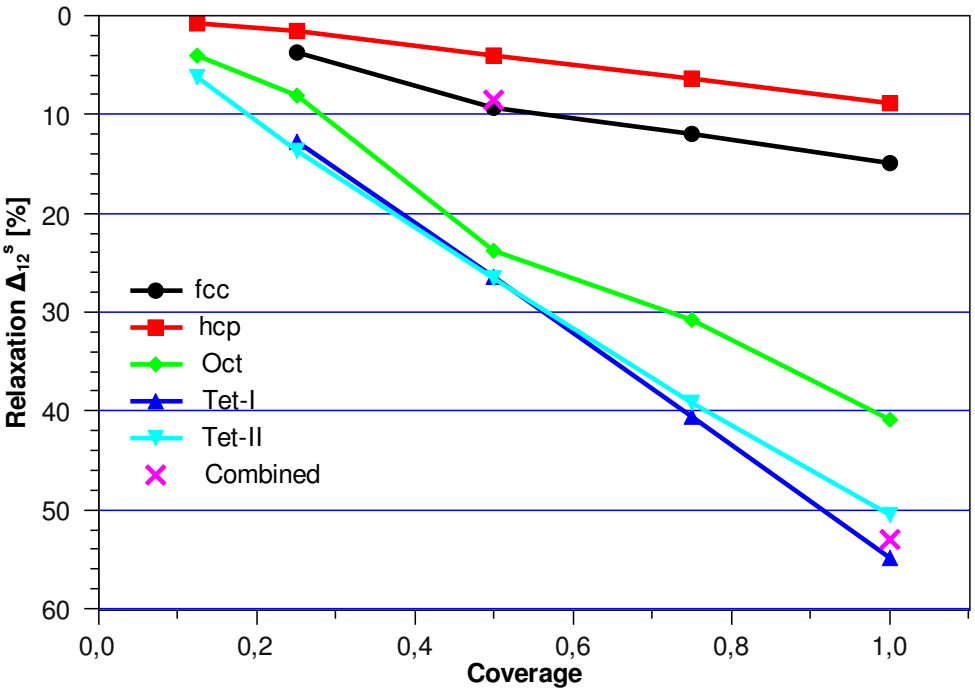

Figure 6.8: Percentage change of the first interlayer spacing for different adsorption sites compared to the clean surface, plotted as a function of the nitrogen coverage.

at which coverage this was tested. Since a nitrogen coverage between 0.25 and 0.5 in the hcp site increases the first interlayer distance for the four-layer slab by around 1.5-4 % and bringing it therefore back close to the bulk position (compare section 5.2.1), it is likely that for the two-layer slab calculated with the RPBE functional in [72] something similar happens. This moderate decrease in adsorption energy of 40 meV might therefore be just due to the fact, that the relaxing surface comes for the tested coverages again close to the original bulk geometry. For smaller and higher coverages or for adsorbed nitrogen in fcc sites, the energy gain is expected to be more significant due to the relaxation of the ruthenium layers, since e.g. for $\Theta = 1$ the spacing is increased for an adsorption in the fcc sites by nearly 15 %. Altogether it is hard to say without further testing, which part of this difference in adsorption energy between the results from [72] and this thesis is attributed to the functional and which is due to the surface model.

The calculated expansion of the first ruthenium interlayer spacing for a nitrogen coverage of 0.25 is confirmed by Low Energy Electron Diffraction measurements [32], revealing an expansion of (-2 ± 2) % with respect to the bulk layer distance and are therefore in a good agreement with the calculated value of 1.5 % (-1.8 %) with respect to the clean surface (to the bulk). Furthermore the calculated vertical distance h between the adatom and the surface is in good agreement with the measured distance of 1.05 $\AA$ [32], whereby the center of mass of each layer is used as reference.

Like for on-surface, also for subsurface adsorbed nitrogen, the interlayer spacing Δ_{12}^{s} has a nearly linearly dependence on the nitrogen coverage. While Δ_{12}^{s} has for on-surface adsorbed nitrogen a maximum value of 15 %, its maximum for subsurface adsorbed nitrogen is above 50 %. This already indicates, that relaxing the top surface layers of these slabs is crucially important to obtain good adsorption energies. Therefore the surface model with two bulk fixed and three relaxing layers of ruthenium atoms is chosen. Besides this huge structural changes, two main differences between on-surface and subsurface adsorbed nitrogen are obviously when examine figure 6.7: Unlike on-surface adsorbed nitrogen, there are no exothermic structures of subsurface adsorbed nitrogen on the ruthenium (0001) surface. Furthermore, while the adsorption energy of on-surface adsorbed nitrogen is increasing nearly linearly with coverage from -1.2 to 0.4 eV for $\Theta = 0.125$ to $\Theta = 1$ (hcp site), this is not the case for subsurface adsorption and each site has its minimum in adsorption energy at a different coverage (see figure 6.7 and table 7.4 in the appendix). This indicates that in contrast to on-surface adsorption the repulsive interactions between subsurface adsorbed nitrogen atoms are not so pronounced, which may be due to a sufficient supply with d-band electrons from the ruthenium lattice. Besides electronic effects, the geometries of the reconstructed surfaces are suspected to be crucially important for the different adsorption energies for varying nitrogen coverages.

The most stable structure with only subsurface adsorbed nitrogen appears at a coverage of $\Theta = 0.75$ for nitrogen in the Tet-II site. For all the other coverages

of 0.125, 0.25, 0.5 and 1 the adsorption energy is by at least 450 meV higher. A striking feature of the geometries with subsurface nitrogen atoms in the Tet-II sites is, that the ruthenium atom above the nitrogen is lifted by up to 0.6 $\AA$ with respect to the other ruthenium atoms in the topmost layer. While this leads for coverages of $\Theta = 0.125$ and 0.25 to isolated ruthenium atoms, which "stand out of the surface", a rough surface with a wavelike structure results for $\Theta = 0.5$. At a coverage of 0.75 these "waves" of lifted ruthenium atoms are connected to each other, which stabilizes the surface, while one out of four ruthenium atoms of the topmost layer is still located below them, closer to the other atoms of the slab. Lifting up this last ruthenium atom at $\Theta = 1$, results in the very big and disadvantageous interlayer spacing of $\Delta^s_{12} = 50$ %.

Another aspect of the geometrical influence is, that the subsurface nitrogen atoms in the Tet-I site are only stabilized at coverages above $\Theta = 0.125$. Otherwise they evolve to the on-surface adsorbed nitrogen upon geometry relaxation. This is due to the fact that they are located on a slope of the potential energy surface, and only at higher coverages they are stabilized by a steric repulsion of the ruthenium atoms, that need to be pushed in lateral directions to let a nitrogen atom out of the subsurface interstitial site. To further study these effects and possible stabilizations through clustering of subsurface nitrogen atoms, some more structures are analyzed, shown in figure 6.9 and 6.10

In these figures the starting positions of the subsurface nitrogen atoms on the ruthenium (0001) surface are sketched with the coloured circles, while the black lines mark the unit cells. All combinations of subsurface nitrogen at the red-marked sites with subsurface nitrogen at any other color-coded site within the same line has been studied. The calculations discussed before with a coverage of 0.25 and higher are all done with a (2x2) surface unit cell, which was periodically continued according to the lattice vectors used in figure 6.10. The results of all calculations with combined adsorption in different subsurface interstitial sites are listed in table 7.5 in the appendix. They strongly support the importance of the coverage and geometry on the stabilization of the Tet-I site. For all combina-

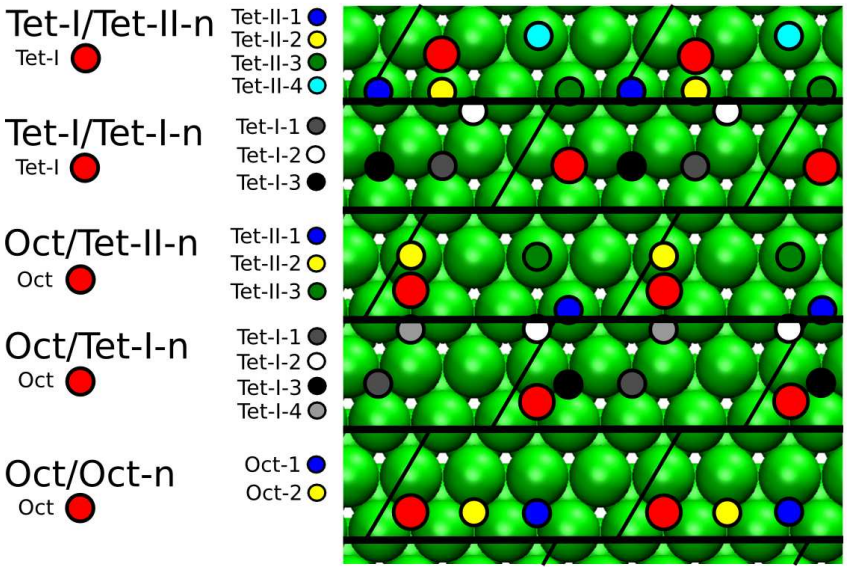

Figure 6.9: Starting positions of the subsurface nitrogen on the ruthenium (0001) surface for the calculations with combined adsorption in different subsurface interstitial sites. The black lines mark the unit cells and horizontally devide the image into five parts. The top part e.g. shows all calculated combinations of subsurface adsorbed nitrogen in the Tet-I and Tet-II sites. The Tet-I site is marked in red and it is for each calculation combined with one of the other color-coded positions.

tions, except one, the nitrogen atoms situated in the Tet-I sites, are evolving to on-surface positions during geometry relaxation, although the subsurface nitrogen coverage is always 0.25. The reason why the nitrogen atoms in the Tet-I site are not relaxing to the on-surface when the (2x2) surface unit cell is used with the same nitrogen coverage, is expected to be indeed just an effect of the chosen unit cell. While in the (2x2) unit cell the ruthenium atoms that are pushed into lateral directions to let the nitrogen atom out of the subsurface interstitial site, are pushed against each other because of the periodicity of the unit cell; this is not the case for the (2x4) unit cell. The only structure where a nitrogen atom stays in its Tet-I site at this coverage is the combination Tet-I/Tet-I-3. Here the two subsurface nitrogen atoms in the Tet-I site are as close to each other as possible. Only one of them evolves to the on-surface adsorbed nitrogen upon

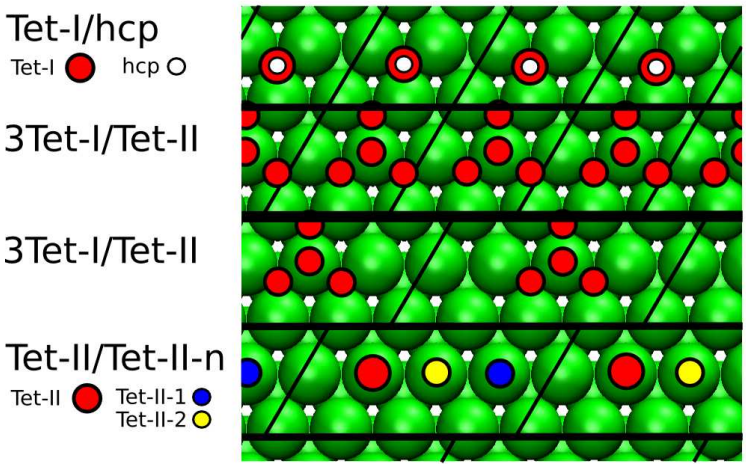

Figure 6.10: Starting positions of adsorbed nitrogen atoms on the ruthenium (0001) surface before a structural relaxation is accomplished. The black lines mark the unit cells. The two top parts of the image are geometries with a (2x2), and the two bottom parts with a (2x4) surface unit cell. The different lattice vectors used to describe the structures, can be recognized by the different continuation of the unit cells.

geometry relaxation, while the other one stays in its subsurface position. This is the first example of stabilizing subsurface nitrogen atoms in interstitial sites by on-surface adsorption in the close neighborhood.

Before more effects of on-surface/subsurface interactions are described, first another result of forming subsurface "clusters" is discussed, which can be seen when comparing the adsorption energies of nitrogen atoms in the subsurface octahedral sites for different arrangements. The closer the two subsurface nitrogen atoms are, the lower is the adsorption energy. For the (2x2) surface unit cell, where the nitrogen atoms are as far away from each other as possible, a value of $E_a^N = 1.67$ eV ist found. It is reduced to $E_a^N = 1.30$ eV and $E_a^N = 1.19$ eV for the combinations Oct/Oct-1 and Oct/Oct-2, respectively. This means, that for subsurface adsorbed nitrogen in the octahedral site with a coverage of $\Theta = 0.25$, the adsorption energy is changed by nearly 500 meV just because of the arrangement of the subsurface interstitials.

But besides stabilizing effects, also destabilizing effects of additional subsurface

nitrogen is observed. While nitrogen atoms in the octahedral site stay for all coverages between 0.125 and 1 in their subsurface position, they evolve to the surface for the calculated combination Oct/Tet-I-3. The reason for this is, that the nitrogen atom in the Tet-I position, like the one in Tet-II described before, lifts one of the ruthenium atoms of the top layer. Because of this geometrical change, it is easier for the surrounding ruthenium atoms to be pushed into lateral directions, which makes it possible for the subsurface nitrogen atom in the octahedral interstitial site to evolve to the on-surface. Afterwards also the nitrogen in the Tet-I position is relaxing to the on-surface.

Because the nitrogen atoms in the Tet-I site are usually evolving to on-surface positions during geometry relaxation, also on-surface subsurface interactions of nitrogen atoms can be studied with the initially selected geometries. First we will have a closer look at the adsorption energies E_a^N of the systems Oct/Tet-I-n (n=2-4). Because the nitrogen atoms in the Tet-I sites are relaxing to the on-surface position above their interstitial site, combinations of subsurface atoms in the octahedral site and on-surface adsorbed nitrogen atoms in the hcp site are the result. Here the adsorption energy per nitrogen atom is decreased from 346.7 over 277.9 to 230.4 meV in the order of $n = 2,\ 3,\ 4$. Again, the closer the on-surface and subsurface nitrogen atoms are, the more stable becomes the structure, whereas for $n = 3$ and $n = 4$ the distance between them is the same, and only the arrangement between neighboring "clusters" varies.

Because of these effects the structure 3Tet-I/Tet-II is studied in a (2x2) and (2x4) surface unit cell and the results are marked in figure 6.7 and 6.8 with a cross. The structure consists of a nitrogen atom in the Tet-II site and three nitrogen atoms in the adjacent Tet-I sites. For the (2x2) unit cell one of the nitrogen atoms in the Tet-I sites is evolving to its corresponding on-surface position, while in the (2x4) surface unit cell all three atoms in the Tet-I sites are relaxing to their on-surface positions above the initial Tet-I sites. The adsorption energy of the resulting structure in the (2x4) surface unit cell is $E_a^N = -296.5$ meV per nitrogen atom. Therefore the final geometry with one ruthenium atom in the subsurface Tet-II site and three ruthenium atoms at the adjacent hcp sites is exothermic.

Because in the bulk the most stable ruthenium nitrogen compounds have a fcc lattice of ruthenium atoms, the top layer of the Ru(0001) surface is transformed so that the cubic symmetry arises. This means that the ABABA close-packed form of the five-layer ruthenium (0001) slab is changed into an ABABC close-packed form. The DFT formation energy of this clean surface is 126 meV per surface atom. The adsorption energies of subsurface nitrogen on this surface at $\Theta = 0.25$ are listed in table 7.1 and 7.6 in the appendix. They are calculated with respect to two different reference surfaces to emphasize the influence of the dedicated energy to bring the ruthenium atoms into their new position. The energies E_a^N are calculated with respect to the N_2 molecule and the clean ruthenium (0001) surface, according to equation (6.3). The reference slab for the adsorption energy $E_{a,fcc}^N$ is the ABABC close-packed clean surface. While for nitrogen in

	Oct	Tet-I	Tet-II
E_a^N at ABABA	1.664	1.542	1.354
E_a^N at ABABC	1.569	1.824	1.731
$E_{a,fcc}^N$ at ABABC	1.063	1.319	1.226

Table 6.1: Adsorption energies of subsurface nitrogen at a coverage of 0.25 at the ruthenium (0001) and the ABABC close-packed surface in eV. The reference slab for the energies E_a^N and $E_{a,fcc}^N$ is the ruthenium (0001) and the ABABC close-packed surface, respectively.

the tetrahedral interstitial sites at the ABABC surface the adsorption energy E_a^N is increasing by around 280 and 380 meV with respect to the adsorption energy at the original ABABA surface, respectively, the subsurface adsorbed nitrogen in the octahedral site is stabilized by around 100 meV at the surface with the ABABC packing. So the sixfold coordinated site becomes the most stable one, when the packing of the ruthenium layers is changed to ABABC.

Because a (2x2) surface unit cell is used to model a nitrogen coverage of $\Theta = 0.25$, around 500 meV of the endothermic adsorption energies are attributed to the rearrangement of the topmost ruthenium layer. This energy, spent to build the

new ruthenium surface, is not expected to change so much for other nitrogen coverages, since both slab models consist of close-packed ruthenium atoms and are therefore very similar. Under this assumption the coverage for the different subsurface adsorption sites, where a rearrangement of the topmost ruthenium layer is advantageous to E_a^N, can be determined without further DFT calculations. It should enable us to make a rough estimate, if a subsurface nitrogen coverage with an exothermic adsorption energy exists for the ABABC packed ruthenium surface. Therefore the energies $E_{a,fcc}^N$ are calculated. For the subsurface adsorbed nitrogen in the octahedral site the adsorption energy $E_{a,fcc}^N$ is by around 600 meV smaller than E_a^N for the ruthenium (0001) surface. This means, for more than $\frac{5}{6}$ N atoms in the octahedral interstitial sites of the (2x2) surface unit cell, corresponding to $\Theta = 0.21$, the rearrangement of the topmost ruthenium layer would reduce the adsorption energy. Accordingly, for the tetrahedral interstitial sites, coverages of around 0.56 (Tet-I) and 0.98 (Tet-II) can be calculated. At the ruthenium (0001) surface the most stable geometry with only subsurface adsorbed nitrogen, is achieved by the nitrogen adsorption into the Tet-II site at a coverage of $\Theta = 0.75$ (see figure 6.7). For this site at such a coverage no stabilization through the rearrangement of the ruthenium atoms takes place, and the energy gain through such a rearrangement is for subsurface adsorbed nitrogen in the other interstitial sites and for all calculated coverages smaller than the energy difference to this structure. Therefore, under the assumption that the energy to rearrange the topmost ruthenium layer is not changing with coverage, it is not expected that subsurface adsorbed nitrogen in the ABABC packed ruthenium surface will form a more stable geometry than at the ruthenium (0001) surface; particularly not an exothermic structure.

Even the surfaces of single crystals exhibit steps and defect structures, and these morphologies are found to be especially important for the catalytic activity [75, 76]. Because these geometries are of such importance, also the nitrogen adsorption in such a surface defect is studied. The corresponding surface model is already described in section 5.2.3, whereas one, two and four nitrogen atoms

are positioned in and around the surface defect, respectively. For the geometries with one and two nitrogen atoms, the adatoms are (both) positioned in the defect, while for the defect structures with four nitrogen atoms the arrangement of the 3Tet-I/Tet-II structure is used, where the missing ruthenium atom is the one above the nitrogen interstitial in the Tet-II site. This last arrangement of nitrogen atoms is not only realized on a (2x2), but also on a (2x4) surface unit cell with corresponding nitrogen coverages of $\Theta = 1$ and 0.5, respectively. The results are listed in table 7.7 in the appendix and the adsorption energies are both calculated with respect to the clean surface with and without the ruthenium defect.

In the case of only one nitrogen atom, the adatom stays in the defect at the Tet-II position with an adsorption energy of $E_a^N = 2.7$ eV. When calculating E_a^N with respect to the surface defect structure, it is reduced by 1.687 eV, which is the formation energy of the surface defect. Also for the initial structure with two nitrogen atoms in the defect, both atoms stay within the defect during geometry relaxation. The bond length of the N_2 molecule in the defect is 1.35 $\mathring{A}$, which is around 20 % more than for an isolated molecule. The adsorption energy is with 1.3 (0.4) still endothermic. For the 3Tet-I/Tet-II adsorption structure at the (2x2) surface unit cell, two of the subsurface atoms in the Tet-I sites evolve to the adjacent on-surface fcc sites during geometry relaxation. The third nitrogen atom of a Tet-I site is relaxing into the defect, forming the same N_2 molecule with a bond length of 1.34 $\mathring{A}$ as for the geometry with only 2 nitrogen atoms in the defect. The additional two nitrogen atoms at the on-surface fcc sites contribute to a reduction of the adsorption energy to $E_a^N = 0.684$ eV. The same 3Tet-I/Tet-II adsorption structure is also studied at the bigger (2x4) surface unit cell with a surface defect concentration of $\Theta = 0.125$. In this case all three nitrogen atoms of the Tet-I sites evolve to adjacent on-surface fcc sites during geometry relaxation and the adsorption energy is with 0.09 eV per nitrogen atom (-0.33 eV neglecting the formation energy of the defect) the lowest of all studied defect structures. Since non of the geometries is exothermic, they do not promote the formation of surface defects. But still, adsorbed nitrogen atoms in an existing surface defect are stabilized by adjacent on-surface adsorbed N atoms.

6.2.3 Thermodynamic Analysis

To determine the relative stabilities of the calculated surface structures with adsorbed nitrogen atoms for different chemical potentials of nitrogen $\Delta\mu_N$, the Gibbs free energy of adsorption ΔG is calculated via equation (6.2), introduced in section 6.1.3, where vibrational contributions and the pV term are neglected. In figure 6.11 the calculated Gibbs free energies are plotted as a function of the nitrogen chemical potential. For a clear representation, only the most stable phases of on-surface and subsurface adsorbed nitrogen at the different coverages are used to create this image.

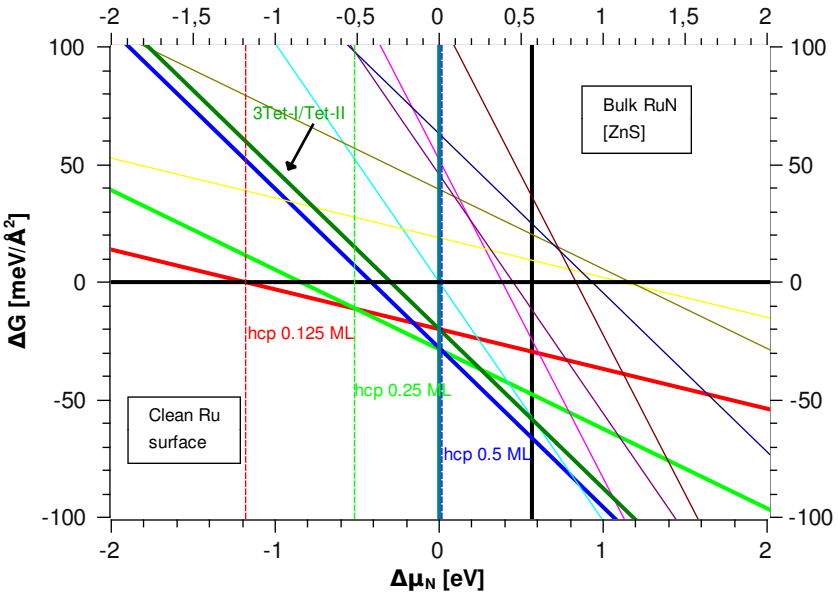

Figure 6.11: Calculated Gibbs free energy of adsorption ΔG as a function of the nitrogen chemical potential $\Delta\mu_N$. The unfavorable adsorption structures are indicated by thin lines, except for the 3Tet-I/Tet-II geometry. At $\Delta\mu_N = 0$ eV nitrogen is condensing on the surface. The rightmost vertical line is the heat of formation of bulk Ru/N in the [ZnS] structure, and the dashed vertical lines indicate the chemical potentials, where the corresponding phases become most favorable: red for 0.125 ML, green for 0.25 ML, and blue for 0.5 ML of on-surface adsorbed nitrogen in hcp site.

The structure with the lowest Gibbs free energy at a given nitrogen chemical

potential is the most stable and therefore most favorable structure. The dashed leftmost vertical line marks the nitrogen chemical potential up to where a clean ruthenium (0001) surface is the thermodynamical most stable surface structure. For higher chemical potentials an on-surface adsorption of 0.125 monolayer (ML) of nitrogen at the hcp site is most favorable, before at even higher potentials than $\Delta\mu_N = -0.514$ eV an adsorption phase of 0.25 ML of nitrogen at the hcp site becomes more favorable. At a chemical potential $\Delta\mu_N = 0$ eV nitrogen starts to condense on the surface, and the rightmost vertical line indicates the formation of bulk Ru/N in the [ZnS] structure. All the unfavorable adsorption structures are indicated by thin lines.

It can be seen that there is no nitrogen chemical potential where a geometry with subsurface adsorbed nitrogen atoms is the most stable one. Even the 3Tet-I/Tet-II structure with its negative formation energy is subordinated to a pure on-surface adsorption of 0.5 ML in the hcp site. But still the general drawback should be kept in mind, that the hole sequence of equilibrium phases can be changed if only one other, thermodynamically more stable, structure is found.

Out of figure 6.11 it is possible to construct a two-dimensional phase diagram, where the most favorable phases are shown as a function of temperature and pressure, by converting the nitrogen chemical potential into (T, p)-pairs via equation (3.12) from section 3.4. Figure 6.12 shows these stability ranges of the most favorable phases, evaluated in figure 6.11, directly plotted in the (T, p)-space.

The black dot marks the reaction conditions of the ruthenium catalyzed ammonia synthesis. Therefore a nitrogen coverage of $\Theta \leqq 0.25$ ML is found to be present under these conditions of $T = 600$ K and $p = 100$ bar. Here it should be recalled that under real synthesis conditions we do not have only a nitrogen, but also a hydrogen reservoir and that the hole system is at a steady state, which means that the local adsorption structures are expected to change with time.

Although no phase with subsurface adsorbed nitrogen atoms could be found that is most favorable at any nitrogen chemical potential, still the concentration of subsurface adsorbed nitrogen atoms can be calculated. Using equation (5.8) from section 5.2.3 with the Gibbs free energy according to equation (6.2), a

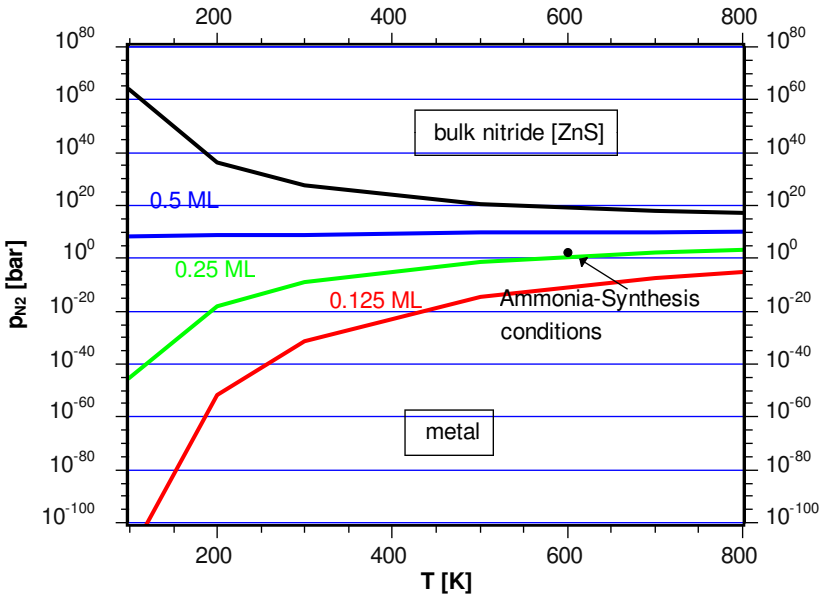

Figure 6.12: Stability range of the most favorable phases from figure 6.11, directly plotted in the (p, T)-space.

subsurface nitrogen concentration, originating from the 3Tet-I/Tet-II structure, of $n = 8 \cdot 10^{-6}$ per surface atom ($1 \cdot 10^{10}$ cm^{-2}) at $T = 600$ K and $p = 100$ bar is found. This is by three orders of magnitude more than the calculated nitrogen concentration in the bulk of the ruthenium lattice. As a comparison, the concentration of n- and p-dopants in semiconducting silicon is in the order of $10^{-6} - 10^{-7}$ for a medium doping. Therefore also such a comparatively low nitrogen concentration in the subsurface interstitial sites may already influence the properties of the catalyst.

Chapter 7

Ruthenium Hydrogen Compounds

Like in the nitrogen case, also for the Ru/H system the on-surface adsorption of hydrogen is extensively discussed in literature, since ruthenium is not only an important catalyst in the synthesis of ammonia, but also in the synthesis of hydrocarbons out of H_2 and CO (studied e.g. in [77]). Xu et al. have performed periodic DFT calculations to study not only the energetics of on-surface, but also of subsurface adsorbed hydrogen in the first and second interlayer sites for three different coverages of $\Theta = 0.33,\ 0.5,\ 1$ [78]. Unfortunately, they do not distinguish between the Tet-I and Tet-II site and have only discussed the subsurface hydrogen adsorption at the Oct and Tet-I site. Consequently, still no complete picture of subsurface adsorbed hydrogen at the ruthenium (0001) surface exists. Besides such surface studies, also experimental works on dissolution of hydrogen into bulk ruthenium under high pressure [79] or electrochemically [80] have been performed. But to the author's knowledge no stoichiometrically stable bulk ruthenium hydrogen structures are reported in literature.

The structure of this chapter about ruthenium hydrogen compounds in the bulk and at the ruthenium (0001) surface is the same as before for the Ru/N phases. First some bulk structures are discussed, starting with an overview of the calculated Ru/H geometries, followed by a summary of the results and a thermodynamic analysis. Subsequently, the ruthenium (0001) surface with on-surface and

subsurface adsorbed hydrogen is examined more closely.

7.1 Bulk Structures

7.1.1 Calculated Structures

Just as the bulk ruthenium mononitrides, the hydrides are studied in the five most prominent AB-structures: zincblende [ZnS], wurtzite [ZnO], sodium chloride [NaCl], nickel arsenide [NiAs], and caesium chloride [CsCl]. As a reminder, these five structures already allow to perform a comprehensive examination of the preferred coordination in ruthenium monohydrides, since they represent three different atomic coordinations in the two most common crystal systems, cubic and hexagonal. The fourfold coordination is represented by the zincblende and wurtzite structure, the sixfold coordination by the sodium chloride and nickel arsenide structure, and in the caesium chloride structure the atoms have a cubic coordination. The lattices of [ZnS], [NaCl] and [CsCl] belong to the cubic crystal system, while [ZnO] and [NiAs] are representatives of the hexagonal one. Here the ruthenium hydride in the [NiAs] structure is given by a hcp lattice of Ru atoms where the octahedral interstitial sites are occupied by the H atoms. Again all structures are optimized according to the procedure for the ruthenium lattice, described in section 5.1.

7.1.2 Results

The theoretical heat of formation ΔH_f^0 of the mentioned bulk ruthenium hydrogen structures is plotted in figure 7.1 to analyze the preferred coordination in ruthenium monohydrides. It is calculated according to equation (3.4) (section 6.1.2). The black dots in this figure represent the formation energies of the stated structures, while the solid lines connecting the black dots are just added to guide the eye.

As for the Ru/N compounds, also for the ruthenium hydrides all calculated structures have a positive formation energy and are therefore endothermic. The [CsCl] structure with its eightfold coordination is again the most unstable geometry. But

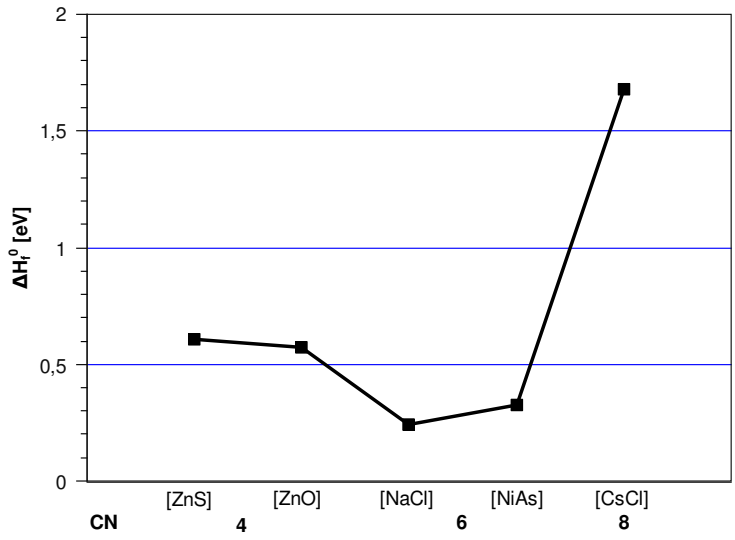

Figure 7.1: DFT formation energies of some RuH structures. The solid line is added to guide the eye.

this time no general trend of stabilisation to lower coordination numbers can be observed, since the [NaCl] and [NiAs] structures with their hexagonal coordination are more stable than the fourfold coordinated [ZnS] and [ZnO] structures. Within the fourfold coordination the hexagonal [ZnO] structure is slidely more stable than the cubic [ZnS] lattice, while in the most stable sixfold coordination the cubic geometry is favoured over the hexagonal one, so that [NaCl] turns out to be the relatively most stable structure. Like for the bulk ruthenium nitrogen phases also for the Ru/H compounds, ruthenium exhibits a cubic symmetry and a fcc packing in the most stable geometry. The same ranking was also found by Smithson et al. [81] who studied the stability and electronic structure of several metal hydrides with the Vienna *Ab initio* Simulation Package (VASP) [68], using a plane wave basis set, ultrasoft pseudopotentials, and the local density approximation. Their DFT formation energies show a largely systematic deviation of around 300 meV from the results obtained in this work. Therefore, like for the ruthenium nitrides, also for the Ru/H compounds the obtained results can only be seen as a qualitative description, since the choice of the method and functional has a big influence on the absolute formation energies. But again, they do hardly influence the relative stabilities. All results, like the lattice parameters,

unit cell volumes, bulk moduli, and heat of formations can be found in table 7.8 in the appendix. With a value of 0.24 eV the rutheniummonohydride in the [NaCl] structure is by around 320 meV lower in energy than the most stable rutheniummononitride in the [ZnS] structure. For the Ru/H compounds no further investigations concerning the hydrogen concentration within the lattice have been performed.

7.1.3 Thermodynamic Analysis

The formation energies of all calculated bulk ruthenium hydrogen structures are positiv, with the lowest value of $\Delta H_f^0 = 0.240$ eV for the [NaCl] structure. Considering again equation (3.3) and (3.12) from chapter 3, it is clear that also for the bulk hydrides high pressure are needed to stabilize these structures. Following the procedure described in section 3.2, and which is already used for the bulk nitrides to analyze the stability regions of the calculated phases in a mixed atmosphere of N_2 and H_2, figure 7.2 is obtained.

This time the chemical potential of hydrogen is plotted on the x-achses and the one of nitrogen on the y-achses. Hence an image is obtained, which looks similar to the one in figure 6.5 (section 6.1.3) for the Ru/N phases. Due to the fact, that the stability region of each phase is the area on the right side of the corresponding line, a pressure of at least 10^{10} bar would be needed to obtain a thermodynamical stable rutheniummonohydride in the [NaCl] structure at a temperature of 600 K. This is already ten orders of magnitude less than what is needed to stabilize a Ru/N compound in the [ZnS] structure, but still around eight orders of magnitude more than what is typically used as reaction pressure during the ruthenium catalyzed Haber-Bosch-Process [4]. Using equation (5.8) from section 5.2.3 and adjusting equation (6.2) from section 6.1.3 to the hydrogen case with the formation energy of the most stable ruthenium monohydride in the [NaCl] structure, a concentration of H atoms of $n = 6 \cdot 10^{-5}$ per ruthenium atom is obtained under reaction conditions of $T = 600$ K and $p = 100$ bar in the ruthenium lattice. This is by four orders of magnitude more than the calculated nitrogen concentration in the bulk, but still far away from the formation of a stoichiometric compound.

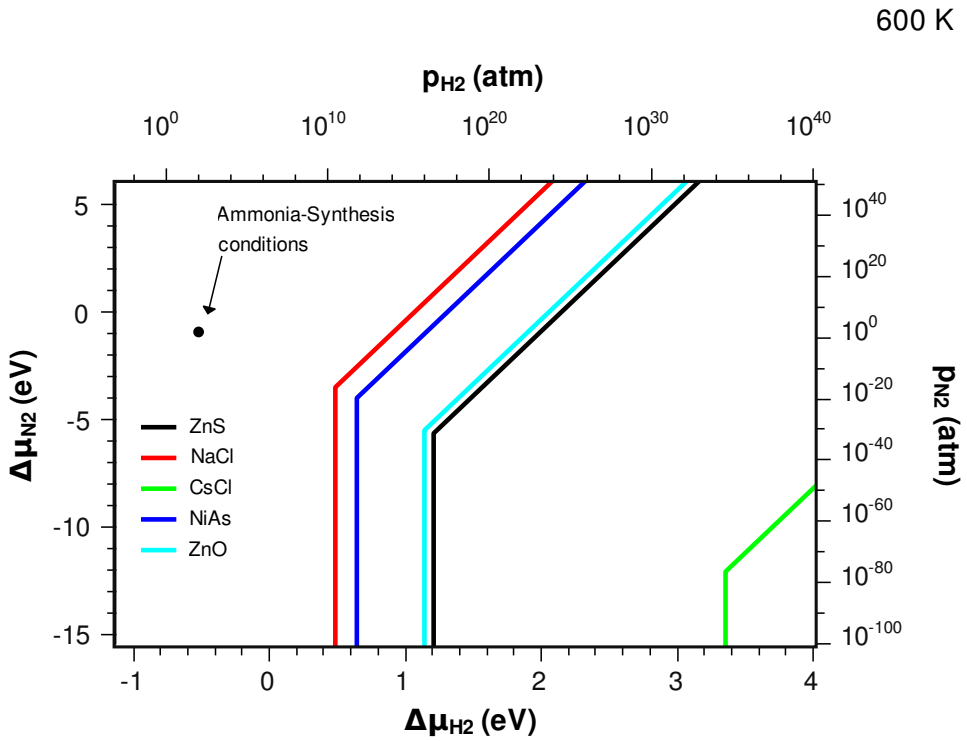

Figure 7.2: Stability regions of ruthenium bulk hydrides as a function of the chemical potentials $\Delta\mu_{H_2}$ and $\Delta\mu_{N_2}$. The pressure scales correspond to a temperature of $T = 600$ K.

Comparing this concentration again with the concentration of n- and p-dopants in semiconducting silicon of $10^{-6} - 10^{-7}$ for a medium doping, endorses a possible influence on the properties of the catalyst. Especially if we take into account, that the calculations may reveal a too high formation energy, since in [81] the DFT formation energies are found to be around 300 meV lower, the needed pressure is reduced by a factor of around $50^3 \approx 10^5$. This is because a drop of the formation energy by 100 meV corresponds to a drop of the necessary pressure to stabilize the structure at 600 K by a factor of around 50.

In [79] the hydrogen concentration in ruthenium is meassured to be $n = 0.03 \pm 0.01$ at $p = 90$ kbar and $T = 250$ °C. Using the results out of this thesis for the formation energy of a ruthenium monohydride in the [NaCl] structure, a concentration of $n = 10^{-3}$ is obtained under these conditions. In view of all the approximations and the influence of the method and functional on the formation energy, this fits

surprisingly well to the experimental results, since the predicted concentration is just by one order of magnitude lower, than the measured one. Using the formation energy $\Delta H_f^0 = -0.1$ eV, calculated by Smithson et al. [81] for ruthenium monohydride in the [NaCl] structure, a hydrogen to ruthenium ratio of $n = 2.8$ would result under the given conditions of temperature and pressure. This differs from the measured concentration by two orders of magnitude and is therefore further away from an experimental validation than the results obtained in this work.

7.2 Surface Structures

7.2.1 Calculated Structures

Like for the adsorbed nitrogen, first the coverage dependence of the on-surface adsorbed hydrogen species at the fcc and hcp site of the ruthenium (0001) surface is studied. Then the adsorption energies of subsurface adsorbed hydrogen in the Oct, Tet-I and Tet-II interstitial sites (compare figure 6.6) are calculated for different coverages, to analyze their relative stabilities and to investigate possible clustering effects, like for the subsurface adsorbed nitrogen. Because also for the bulk hydrides, the most stable structure is found to have a cubic symmetry, the topmost layer of the ruthenium slab is again rearranged, so that the ABABC close-packed surface structure occurs. Subsequently, the energetics of subsurface adsorbed hydrogen on this structure and of adsorbed H atoms on the well-known (2x2) surface defect structure are studied.

The ruthenium surface is again modeled by a periodic array of slabs with a vacuum region between the repeated slabs of 20 $\mathring{A}$. Slabs with subsurface adsorbed hydrogen consist of five ruthenium layers, out of which three are allowed to relax, while slabs with on-surface adsorbed hydrogen atoms are again modeled by two bulk fixed and two relaxing layers of ruthenium atoms. For all coverages a (2x2) surface unit cell is used and all structures are relaxed until the forces are less than $5 \cdot 10^{-4}$ eV/$\mathring{A}$.

7.2.2 Results

The calculated adsorption energies of on-surface adsorbed hydrogen in the fcc and hcp position for different coverages are presented in figure 7.3 and all results are also listed in table 7.9 in the appendix. Here the average adsorption energy per hydrogen atom is calculated according to equation (6.3) from section 6.2.2.

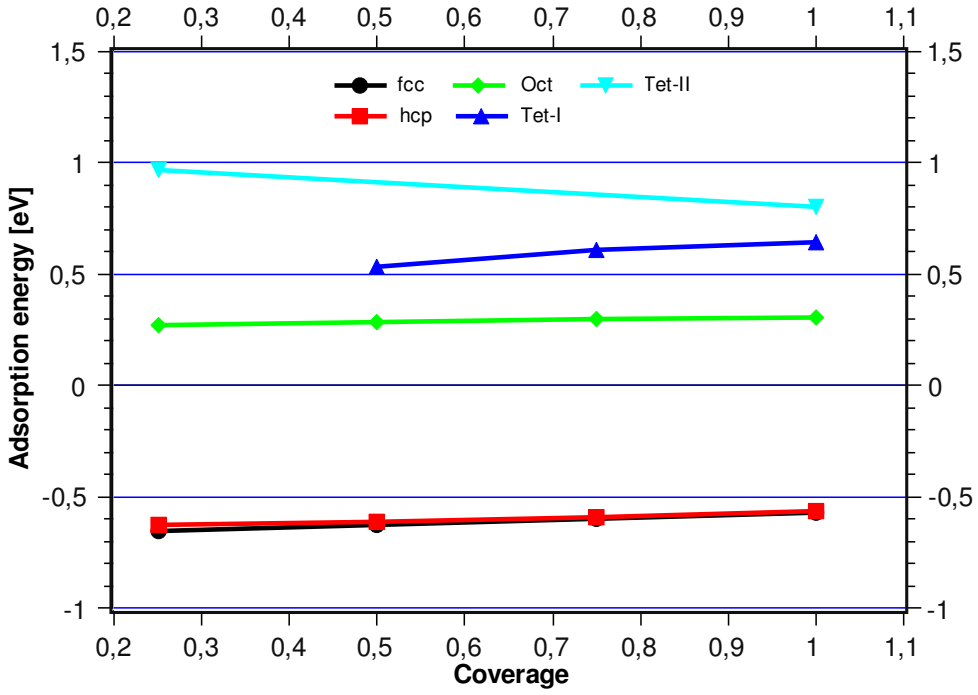

Figure 7.3: Calculated adsorption energies of hydrogen on ruthenium (0001) in different on-surface and subsurface sites as a function of the coverage. The lines connecting the calculated energies are added to guide the eye.

Like for on-surface adsorbed nitrogen, a nearly linear decrease in adsorption energy per hydrogen atom can be seen for increasing hydrogen coverage. But this time the change in adsorption energy is with -654 meV for $\Theta = 0.25$ and -572 meV for $\Theta = 1$ comparatively low. In particular the hydrogen adsorption on the ruthenium (0001) surface is also exothermic at high coverages. In contrast to the adsorption of nitrogen, the fcc site is for all studied coverages preferred over the hcp site. Such a systematic decrease in adsorption energy could not be identified in the work by Xu et al. [78], where hydrogen adsorption for three different

coverages $\Theta = 0.33,\ 0.5,\ 1$ is studied at a ruthenium slab containing six atomic layers of ruthenium atoms, using a plane-wave basis set with ultrasoft pseudopotentials, and the PW91 functional. Here the adsorption energy for $\Theta = 0.33$ is smaller than the one for $\Theta = 0.5$. Due to the fact, that in this thesis no hydrogen coverage of 0.33 at the ruthenium surface is studied, it is difficult to decide wether it is a peculiarity of this coverage or if some other effects, resulting from the different physical description of the system, may influence the results. Comparing their calculated adsorption energies of hydrogen in the fcc site of -0.603 eV at a coverage of $\Theta = 0.5$ and -0.573 eV at $\Theta = 1$ with the results received in this work shows, that both values differ by not more than 4 %. Therefore it is very likely, that also for a coverage of 0.33 a similar adsorption energy and therefore a deviation from this so far nearly linear trend of decreasing adsorption energy for increasing coverage would be obtained. In [72] an adsorption energy of -0.52 eV is found for a hydrogen adsorption at a coverage of $\Theta = 0.25$ in the fcc site of the ruthenium surface. The big difference of around 20 % to the results presented in this thesis is more or less expected, because of the chosen surface model and functional in the corresponding publication (see also discussion in section 6.2.2).

Also for adsorbed hydrogen the percentage change in the first metal interlayer distance of the Ru/H compounds Δ^s_{12}, is calculated for the different hydrogen coverages according to equation (6.4) from section 6.2.2 and presented in figure 7.4.

Again, a nearly linear relation between coverage and interlayer spacing exists, whereas on-surface adsorbed hydrogen in both fcc and hcp adsorption sites has a similar influence on Δ^s_{12}. This might be connected to their very similar adsorption energies and would be in line with the results for on-surface adsorbed nitrogen (see figures 6.7 and 6.8), where there is a bigger difference in both adsorption energy and interlayer relaxation. The adsorption height of hydrogen, namely the vertical distance from the hydrogen atom to the first layer of ruthenium atoms, is changing from 1.03 over 1.04 to 1.05 for coverages of $\Theta = 1,\ 0.5,\ 0.25$, and is therefore identical to the results in [78] and cited references therein for $\Theta = 1,\ 0.5$.

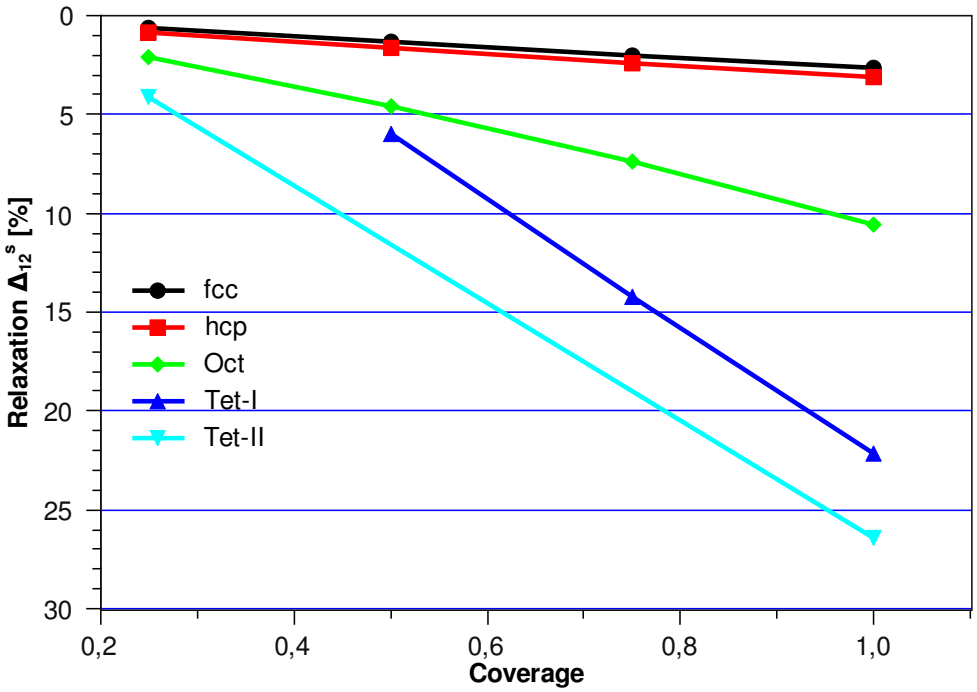

Figure 7.4: Percentage change of the first interlayer spacing for different adsorption sites compared to the clean surface, plotted as a function of the hydrogen coverage.

Like for on-surface, also for subsurface adsorbed hydrogen, the interlayer spacing Δ_{12}^s has a nearly linearly dependence on the hydrogen coverage. While Δ_{12}^s has for on-surface adsorbed hydrogen a maximum value of just 3 %, its maximum for subsurface adsorption is above 25 % for hydrogen in the Tet-II site at a coverage of $\Theta = 1$. These huge structural relaxations confirm the chosen surface model with two bulk fixed and three relaxing layers of ruthenium atoms, which is also used for surface structures with subsurface adsorbed nitrogen atoms. All geometries with subsurface adsorbed hydrogen are found to be endothermic, like their complementary structures with subsurface interstitial nitrogen atoms. While in the nitrogen case the adsorption energy per subsurface nitrogen atom strongly depends on the nitrogen coverage, a relatively flat coverage dependence not only for on-surface, but also for subsurface adsorbed hydrogen in all three subsurface adsorption sites (see figure 7.3) is predominant. For hydrogen atoms in the oc-

tahedral and tetrahedral-I site a small stabilization with decreasing coverage can be observed, whereas hydrogen in the Tet-II site at a coverage of $\Theta = 1$ is more stable than at a coverage of $\Theta = 0.25$. At coverages of 0.5 and 0.75 the H atoms in the Tet-II site are located on a slope of the potential energy surface and evolve to subsurface adsorbed hydrogen atoms in the octahedral interstitial site with an adsorption energy of around 0.3 eV per hydrogen atom. Furthermore the subsurface hydrogen atoms in the Tet-I site are only stabilized at coverages above $\Theta = 0.25$. Otherwise they evolve to the on-surface adsorbed hydrogen upon geometry relaxation. A similar behaviour was already presented for nitrogen atoms in this interstitial site in section 6.2.2.

For all hydrogen coverages the octahedral interstitial site is preferred over the Tet-I site, which again is favored over the Tet-II site. This relative stabilization of the sixfold coordination site in the subsurface reflects the stability hierarchy found for bulk ruthenium hydrids. Comparing the results for subsurface adsorbed hydrogen in the Oct and Tet-I site with some literature values, this sequence of stability as well as the flat coverage dependance and the small stabilization for decreasing hydrogen coverages is confirmed by [78]. Moreover, also the total adsorption energies at coverages of $\Theta = 0.5$ and $\Theta = 1$ differ by not more than 3.5 % from the values in [78], except for the octahedral site at a coverage of 0.5, where a deviation of around 12 % can be found. All values in [78] are calculated using a plane-wave basis set with ultrasoft pseudopotentials and the PW91 functional for a supercell model containing six layers of ruthenium atoms in the slab out of which three are allowed to relax. Because the adsorption energy of hydrogen in the subsurface octahedral site is by around 0.9 eV higher than that of on-surface adsorbed hydrogen in the fcc site, it is expected that it is difficult for the hydrogen atoms to penetrate into the subsurface.

Like for the bulk ruthenium nitrogen compounds, also for the bulk Ru/H structures the most stable geometry has a fcc lattice of ruthenium atoms; this time with occupied octahedral holes. Therefore the top layer of the ABABA close-packed Ru(0001) surface is again transformed so that an ABABC close-packing

arises with a cubic symmetry for the top layers of the slab (compare section 6.2.2). The adsorption energies of subsurface hydrogen on this surface at a coverage of $\Theta = 0.25$ are listed in table 7.1 and 7.11 in the appendix. Like for subsurface nitrogen atoms at the ABABC close-packed surface, they are calculated again with respect to two different reference surfaces, the ABABC ($E^H_{a,fcc}$) and the original ABABA (E^H_a) surface. This is done to emphasize the influence of the dedicated energy to bring the ruthenium atoms into their new position, which is around 126 meV per surface atom. Both adsorption energies E^H_a of subsurface hydrogen

	Oct	Tet-I	Tet-II
E^H_a at ABABA	267.315	relaxed to on-surface hcp	970.294
E^H_a at ABABC	705.534	840.024	1193.283
$E^H_{a,fcc}$ at ABABC	199.784	334.275	687.534

Table 7.1: Adsorption energies of subsurface adsorbed hydrogen at a coverage of 0.25 at the ruthenium (0001) and the ABABC close-packed surface in meV. The reference slab for the energies E^N_a and $E^N_{a,fcc}$ is the ruthenium (0001) and the ABABC close-packed surface, respectively.

in the Oct and Tet-II site at the ABABC surface are increased by around 440 and 220 meV, with respect to the adsorption energy at the original ABABA surface, respectively. Since E^H_a at the ABABC surface is for the Tet-I site by around 135 meV higher than for the octahedral interstitial site, the sixfold coordination is still the most preferred one when changing the arrangement of the ruthenium layers within the slab to the ABABC-packing. Here it should be mentioned, that subsurface adsorbed hydrogen in the Tet-I site at a coverage of $\Theta = 0.25$ at the ABABC surface does not evolve to the adsorbed hydrogen upon geometry relaxation, like it is the case for the ABABA surface structure. Again around 504 meV of the endothermic adsorption energies E^H_a at the ABABC-packed (2x2) surface unit cell are attributed to the rearrangement of the topmost ruthenium layer. Under the assumption that this energy is not changing so much for other hydrogen coverages, it can be predicted if a subsurface hydrogen coverage with an exothermic adsorption energy exists for the ABABC close-packed ruthenium

surface without further DFT calculations. To do so the energies $E^H_{a,fcc}$ are calculated. The difference between $E^H_{a,fcc}$ and the adsorption energy of adsorbed hydrogen on the ABABA surface E^H_a is for the octahedral site 68 meV and for the Tet-II site 283 meV. Therefore the rearrangement of the topmost ruthenium layer would reduce the adsorption energy only for hydrogen in the Tet-II site at coverages above $\Theta = 0.45$ (compare again section 6.1.2 for more details), whereas sixfold coordinated hydrogen can not promote such a rearrangement due to the relative small energy gain of 68 meV per hydrogen atom. For a hydrogen coverage of $\Theta = 1$ in the Tet-II site of the ABABC surface structure an adsorption energy of $E^H_a = (805 + 4 \cdot 126 - 4 \cdot 283)$ meV= 177 meV is predicted. It is calculated out of the adsorption energy of hydrogen on the ABABA surface at this coverage $E^H_a = 805$ meV (see table 7.10 in the appendix), the DFT formation energy of the ABABC clean surface of 126 meV per surface atom, and the energy gain per hydrogen atom in the Tet-II site of the rearranged surface structure of 283 meV. Therefore at higher coverages the prefered subsurface site at the ABABC surface should change from Oct to Tet-II and it is expected that subsurface adsorbed hydrogen in the Tet-II site of the ABABC-packed ruthenium surface will form a more stable geometry than subsurface adsorbed hydrogen at the ruthenium (0001) surface at any site or at any appropriate coverage. But still, also for the ABABC surface structure no hydrogen coverage with an exothermic adsorption energy is expected.

Like for the Ru/N system, also for the Ru/H system the adsorption on a surface defect structure, already introduced in section 5.2.3, is studied. Here structures with one and two hydrogen atoms in the defect are analyzed. The results are listed in table 7.12 in the appendix and the adsorption energies are both calculated with respect to the clean surface with and without the ruthenium defect. In the case of only one hydrogen atom, the adatom stays in the defect at the Tet-II position with an adsorption energy of $E^H_a = 1581.555$ meV. When calculating E^H_a with respect to the surface defect structure, it is reduced by the formation energy of the surface defect of 1.687 eV to -105.477 meV. For the initial structure with

two hydrogen atoms in the defect, one of the atoms evolves to the adjacent on-surface fcc position during geometry relaxation. The additional hydrogen atom at the on-surface fcc site contributes to a reduction of the adsorption energy to 542.391 meV per hydrogen atom (−301.124 meV neglecting the formation energy of the defect). Although we find negative adsorption energies when calculating them with respect to the surface defect structure, both geometries are still endothermic when taking the clean ruthenium (0001) surface as the reference state. Therefore the analyzed geometries do not promote the formation of surface defects. But still we can retain by comparing the obtained values with the results of section 6.2.2, written down in table 7.7 in the appendix, that an adsorption of hydrogen in the defect is favored over an adsorption of nitrogen.

7.2.3 Thermodynamic Analysis

Like for the different phases of ruthenium nitrogen surface structures, the relative stabilities of the calculated Ru/H surface geometries are analyzed as a function of the hydrogen chemical potential $\Delta\mu_H$. Therefore the Gibbs free energies of adsorption ΔG, calculated according to equation (6.2) from section 6.1.3, are plotted in figure 7.5 over $\Delta\mu_H$.

For a clear representation, again only the most stable phases of on-surface and subsurface adsorbed adatoms at the different coverages are used to create this image. This ends up in selecting for all coverages the geometries where hydrogen atoms are adsorbed at the fcc (on-surface) or at the Oct site (subsurface). The unfavorable adsorption structures are indicated by thin lines and the rightmost vertical line marks the formation of bulk Ru/H in the [NaCl] structure. At the chemical potential $\Delta\mu_H = 0$ hydrogen starts to condense on the surface. The dashed vertical lines indicate the hydrogen chemical potentials where a new surface structure becomes most favorable. Here the equilibrium phase is changing in a relatively narrow band between $\Delta\mu_H = -0.654$ eV and $\Delta\mu_H = -0.490$ eV from a clean ruthenium surface, over on-surface adsorbed hydrogen in the fcc site with coverages of $\Theta = 0.25,\ 0.5,\ 0.75$ to $\Theta = 1$. But out of figure 7.5 it can not be concluded, that e.g. for chemical potentials higher than $\Delta\mu_H = -0.490$ eV

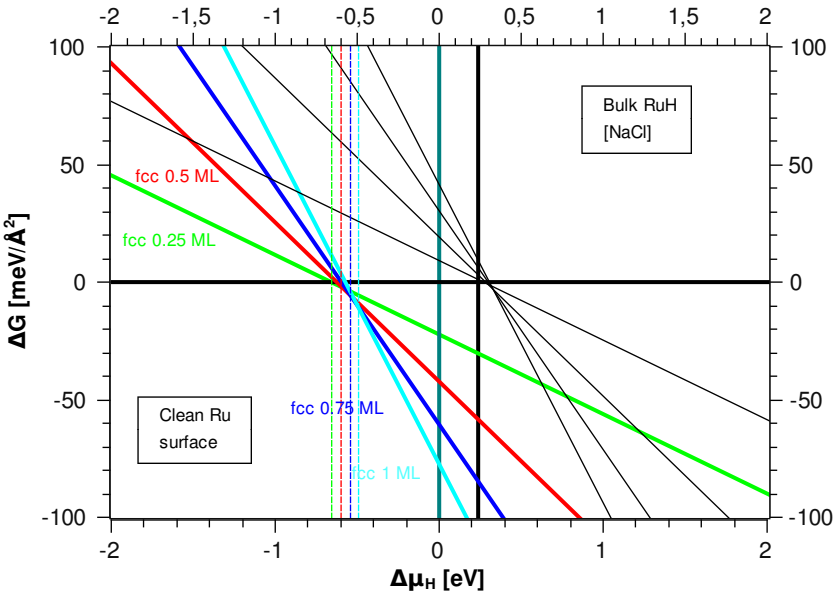

Figure 7.5: Calculated Gibbs free energy of adsorption ΔG as a function of the hydrogen chemical potential $\Delta\mu_H$. The unfavorable adsorption structures are indicated by thin lines. At $\Delta\mu_H = 0$ hydrogen starts to condense on the surface. The rightmost vertical line is the heat of formation of bulk Ru/H in the [NaCl] structure, and the dashed vertical lines indicate the chemical potentials, where the corresponding phases become most favorable: green for 0.25 ML, red for 0.5 ML, blue for 0.75 ML, and turquoise for 1.0 ML of on-surface adsorbed hydrogen at fcc site.

an on-surface hydrogen coverage of 1 is favored over a coverage of $\Theta = 2$, since no structure with a higher hydrogen coverage than $\Theta = 1$ has been taken into account. Moreover the relatively flat coverage dependence of adsorbed hydrogen on the ruthenium (0001) surface (compare figure 7.3) suggests, that for higher hydrogen chemical potentials a coverage bigger than 1 can be expected for on-surface adsorbed hydrogen atoms. The flat coverage dependence for on-surface, as well as subsurface adsorbed hydrogen is also reflected in figure 7.5, since the intersections of the lines for different surface structures lie relatively close together. Like for the Ru/N surface structures, none of the analyzed geometries with subsurface adsorbed hydrogen is the most favorable one at any chemical potential.

Out of figure 7.5 the two-dimensional phase diagram in figure 7.6 is constructed, where the most favorable phases are shown as a function of temperature and pressure. The black dot marks the reaction conditions of the ruthenium catalyzed ammonia synthesis. Based on the calculated formation energies of the different structures, figure 7.6 reveals a hydrogen coverage of $\Theta \geqq 1$ ML under these conditions of $T = 600$ K and $p = 100$ bar, neglecting the presence of a nitrogen reservoir.

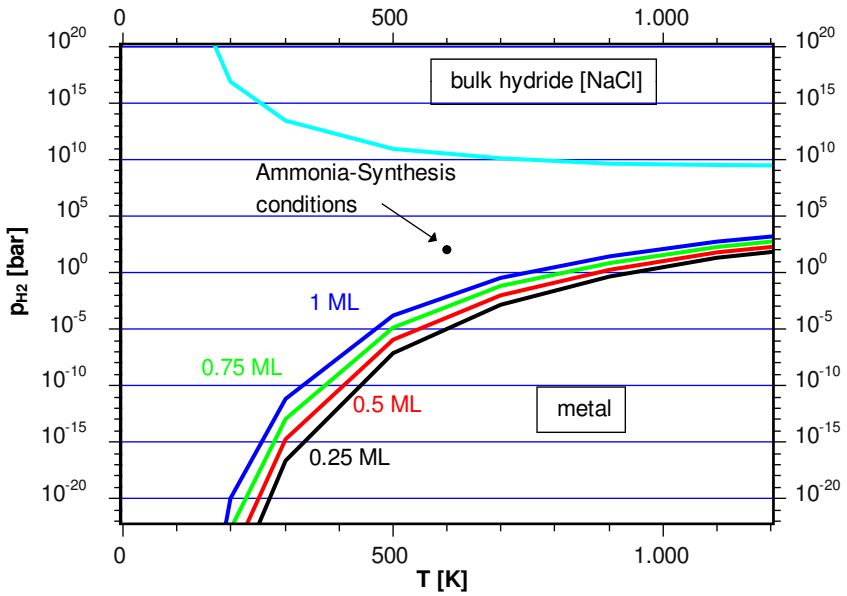

Figure 7.6: Stability range of the most favorable phases from figure 7.5, directly plotted in the (p, T)-space.

Because of this high formal hydrogen coverage under reaction conditions it might be of interest for future studies to analyze geometries with combined on-surface and subsurface adsorbed hydrogen, since for the nitrogen case on-surface adsorbed nitrogen atoms stabilize subsurface adsorbed N atoms and the stabilization effect is in general higher, the closer the on-surface and subsurface nitrogen atoms are together. If something similar also happens in the hydrogen case, it is very likely that subsurface adsorbed hydrogen atoms exist at a considerable concentration under conditions of the Haber-Bosch process, and that they may influence the performance of the catalyst.

But also without further investigations of combined adsorption structures, a concentration of subsurface adsorbed H atoms can be estimated on the basis of the studied phases with hydrogen atoms in subsurface interstitial sites. Using equation (5.8) from section 5.2.3 with the Gibbs free energy according to equation (6.2), a subsurface hydrogen concentration, originating from the surface structure with a hydrogen coverage of $\Theta = 0.25$ in the Oct site, of $n = 4 \cdot 10^{-5}$ per surface atom ($6 \cdot 10^{10}$ cm^{-2}) at $T = 600$ K and $p = 100$ bar is obtained. Based on the results for the octahedral interstitial site this concentration is of the same order of magnitude as is obtained for the hydrogen concentration in the bulk of a ruthenium lattice (section 7.1.3). This suggests, that a penetration of hydrogen atoms into the subsurface interstitial sites of a ruthenium (0001) surface is energetically not favored over a penetration into the bulk of a ruthenium lattice. But such a conclusion is due to the limited amount of studied structures very vague.

Part III

Conclusion And Outlook

7.3 General Limitations

Here the major uncertainties concerning the calculated formation and adsorption energies and the associated thermodynamic studies should be recalled. The first drawback concerning the accuracy of the obtained results is the calculated binding energy of the N_2 molecule, which is by around 800 meV higher than corresponding experimental values. This big deviation leads to a change in the formation energy of Ru/N structures of around 300 meV when calculating them with respect to the experimental binding energies (see section 4.1). Another uncertainty is connected with the choice of the functional and the used code. It is related to the first one, since the functional also affect the calculated N_2 binding energies. In [67] the results for bulk Ru/N compounds have a systematically deviation and are each around 200 meV lower in energy than the results obtained in this work (see section 6.1.2). These values are calculated with VASP using a plane wave basis set, ultrasoft pseudopotentials, and the PW91 functional. The calculated formation energies of bulk Ru/H structures differ from the values obtained by H. Smithson et al. [81] by around 300 meV (see section 7.1.2); and again, the results from the reference are lower in energy. They are calculted with VASP, using a plane wave basis set, ultrasoft pseudopotentials, and the local density approximation. Although other functionals may produce "better" results for a special type of problem, as it is argued for adsorption energies to be the RPBE functional [73], there is no functional which gives equally good results for molecules, bulk and surface structures. Therefore all energies are calculated with the same, widespread, PBE functional. The bottom line is that the calculated absolute formation and adsorption energie are arguable and have to be handled with caution, whereas the relative stabilities of the structures are much more trustworthy.

A third point that influences the analysis is especially connected to the used thermodynamic model. Here inter alia the two following and not further discussed approximations have been made: (i) neglecting the pV term. This approximation is confirmed in literature to be sufficient for a pressure up to around 10^2 bar. The amount of an additional contribution that has to be expected at higher pressure,

with which we are dealing here, is not further discussed in literature and for simplicity also not studied in this work; but its possible influence should also be kept in mind for a critical discussion of the results. (ii) neglecting zero-point energies. This contribution to the total energy might be especially important for the Ru/H phases due to the low mass of the hydrogen atom. In [82] it is reported by Miwa et al. that in a fluorite structure the contribution can be in the order of 100 meV per hydrogen atom.

7.4 Results And Outlook

Because the numerous results are already discussed in detail in the corresponding sections, only the most important of them should be recapitulated here.

For the bulk ruthenium nitrogen phases, a general trend of stabilisation to lower coordination numbers can be observed, with [ZnS] as the most stable structure, where the nitrogen atoms occupy the tetrahedral interstitial sites of an fcc ruthenium lattice. Studying the influence of different nitrogen concentrations in the bulk ruthenium lattice with nitrogen to ruthenium ratios of 1:4, 1:1, and 2:1, shows that a ratio of 1:1 is most favoured for occupied tetrahedral interstitial sites, whereas sixfold coordinated nitrogen atoms are stabilized to smaller concentrations. By thermodynamic studies the reported formation of metastable ruthenium nitrogen compounds via sputtering techniques could be reconstructed.

Of the studied bulk Ru/H systems the most stable structure is also found to have a fcc lattice of ruthenium atoms, but with hydrogen in the octahedral sites; the [NaCl] structure. Its formation energy is smaller than the one of the Ru/N in the [ZnS] structure, but still a pressure of 10^{10} bar at 600 K is needed for a thermodynamical stabilization.

On-surface adsorbed nitrogen and hydrogen atoms have in common that their adsorption energies E_a depend nearly linearly on the coverage, whereas for nitrogen the stabilization to smaller coverages is more pronounced and the hcp site is favoured over fcc, while for hydrogen it is vice versa. Hydrogen atoms in the subsurface of the ruthenium (0001) slab prefer to occupy the sixfold coordination

site, like in the bulk, and the coverage dependence of the adsorption energy is for all three sites very flat. On the contrary, the adsorption energy of subsurface adsorbed nitrogen atoms strongly depends on the coverage. Like in the bulk, the smallest value of E_a is obtained for an adsorption in the fourfold coordinated site, namely the Tet-II site, at a nitrogen coverage of $\Theta = 0.75$. The different stabilizations of the subsurface nitrogen interstitials strongly depend on the structure of the relaxed surfaces. A general trend of a stabilization of "clustering" N atoms in the subsurface, as well as a trend of stabilizing subsurface nitrogen atoms by on-surface adsorbed N atoms is found. But so far, no structure with subsurface adsorbed nitrogen or hydrogen atoms is found to be the most favourable one at any nitrogen or hydrogen chemical potential. However, the calculated concentrations of N and H atoms at 600 K and 100 bar in a pure nitrogen and hydrogen atmosphere, respectively, are already in a range where they might change the chemical composition of the ruthenium surface in a way that influences the catalytic mechanism.

Further studies may focus first on analyzing the contributions of the zero-point energies and the pV term to the formation energies and thermodynamical stabilities under varying temperatures and pressure, to make the next step to more trustfull results without an additional need of CPU time. Since a stabilization of subsurface nitrogen atoms by on-surface adsorbed N atoms is found, similar studies of a combined on-surface and subsurface adsorption of hydrogen might also be of interest, since the on-surface coverage of hydrogen atoms under reaction conditions is found to be very high. Finally studies with combined on-surface and subsurface adsorption of hydrogen and nitrogen may be of interest, because under real conditions of the ruthenium catalyzed ammonia synthesis both nitrogen and hydrogen species are adsorbed at the surface.

Part IV

Appendix

Results

Bulk Ruthenium Nitrogen Compounds

Structure	Lc [$\AA$] (hcp: a, c)	Vol [$\AA^3$]	B_0 [Mbar]	ΔH_f^0 [eV]	$\Delta H_{f,atom}^0$ [eV]
[ZnS]	4.551	23.568	2.598	0.564	-6.143
[NaCl]	4.304	19.934	3.013	1.892	-4.814
[CsCl]	2.675	19.146	3.053	2.353	-4.354
[ZnO]	2.746, 6.630	21.648	2.669	0.860	-5.846
[ZnO-2]	3.196, 5.252	23.237	1.792	0.825	-5.881
[NiAs]	2.950, 5.267	19.863	2.672	1.371	-5.335
[AsNi]	2.757, 6.013	19.804	2.965	1.927	-4.779
[FeS_2]	4.881	29.082	2.256	2.455	-4.251
[CaF_2]	4.840	28.353	2.916	3.326	-3.380
[Fe_4N]	3.985	63.305	2.941	2.010	-24.818
[Ru_4N]	4.031	65.519	2.807	1.700	-25.128

Table 7.2: The different calculated bulk Ru/N structures with their lattice parameter (Lc), volume of the primitive unit cell (Vol), bulk modulus (B_0), and heat of formation per formular unit at 0K with respect to bulk (ΔH_f^0) and atomic ruthenium ($\Delta H_{f,atom}^0$).

Adsorbed Nitrogen

Site	Θ	E_a^N [eV]	Δ_{12}^s [%]	h [$\mathring{A}$]	Comment
hcp	0.125	-1.179	0.825	1.024	relaxed from Tet-I
	0.25	-0.846	1.515	1.050	
	0.5	-0.414	4.061	1.087	
	0.75	$-5.188 \cdot 10^{-4}$	6.441	1.139	
	1	0.383	8.837	1.196	
fcc	0.25	-0.264	3.747	1.054	
	0.5	-0.140	9.394	1.056	
	0.75	0.234	11.919	1.122	
	1	0.533	14.989	1.182	

Table 7.3: Results for on-surface adsorbed nitrogen on the ruthenium (0001) surface. Adsorption site, coverage Θ, adsorption energy E_a^N, first ruthenium interlayer relaxation Δ_{12}^s, and height of adsorbed species above the topmost ruthenium layer h.

Site	Θ	E_a^N [eV]	Δ_{12}^s [%]	Comment
Oct	0.125	1.105	4.067	
	0.25	1.664	8.029	
	0.5	1.093	23.811	
	0.75	1.262	30.714	
	1	1.298	40.941	
Tet-I	0.125	-	-	relaxed to on-surface hcp
	0.25	1.542	12.713	
	0.5	0.932	26.349	

Site	Θ	E_a^N [eV]	Δ_{12}^s [%]	Comment
	0.75	1.093	40.499	
	1	0.833	54.887	
Tet-II	0.125	1.262	6.217	
	0.25	1.354	13.644	
	0.5	1.096	26.512	
	0.75	0.451	39.227	
	1	0.905	50.481	

Table 7.4: Results for subsurface adsorbed nitrogen on the ruthenium (0001) surface. Adsorption site, coverage Θ, adsorption energy E_a^N, and first ruthenium interlayer relaxation Δ_{12}^s.

Initial Sites	Differing final sites	E_a^N [meV]
Oct/Oct-1	-	1304.043
Oct/Oct-2	-	1185.837
Oct/Tet-I-1	fcc/hcp	-690.614
Oct/Tet-I-2	Oct/hcp	346.711
Oct/Tet-I-3	Oct/hcp	277.883
Oct/Tet-I-4	Oct/hcp	230.352
Oct/Tet-II-1	-	1234.740
Oct/Tet-II-2	hcp/Tet-II-2	88.691
Oct/Tet-II-3	-	1259.812
Tet-I/Tet-I-1	hcp/hcp	-1023.192
Tet-I/Tet-I-2	hcp/hcp	-901.521
Tet-I/Tet-I-3	Tet-I/hcp	86.033
Tet-I/Tet-II-1	hcp/Tet-II	51.390
Tet-I/Tet-II-2	hcp/Tet-II	69.677
Tet-I/Tet-II-3	hcp/Tet-II	88.132

Initial Sites	Differing final sites	E_a^N [meV]
Tet-I/Tet-II-4	hcp/Tet-II	95.003
Tet-II/Tet-II-1	-	1326.712
Tet-II/Tet-II-2	-	1162.764
3Tet-I/Tet-II [2)]	3hcp/Tet-II	-296.543
3Tet-I/Tet-II [1,3)]	hcp/2Tet-I/Tet-II	961.054
Tet-I/hcp [1,2)]	-	1845.875

Table 7.5: Combined adsorption of nitrogen on the ruthenium (0001) surface in different on-surface and subsurface sites. A (2x4) surface unit cell is used with a nitrogen coverage of $\Theta = 0.25$. Initial and differing final adsorption sites after structural relaxation, and adsorption energy E_a^N. [1)]: a (2x2) surface unit cell is used, [2)]: $\Theta = 0.5$, [3)]: $\Theta = 1$. The differing final adsorption site is always the on-surface site above the initial subsurface interstitial site, except for the Oct/Tet-II-2 structure.

Site	E_a^N [eV]	Δ_{12}^s [%]
Oct	1.569	8.311
Tet-I	1.824	12.875
Tet-II	1.731	12.403

Table 7.6: Results for subsurface adsorbed nitrogen on the ruthenium ABABC close-packed surface at a coverage of $\Theta = 0.25$. Adsorption site, adsorption energy E_b^N, and first ruthenium interlayer relaxation Δ_{12}^s.

Number N atoms	E_a^N [eV]	Comment
1	2.743, 1.056[1)]	
2	1.275, 0.431[1)]	bond length 1.35 $\mathring{A}$
4	0.684, 0.262[1)]	bond length 1.34 $\mathring{A}$ 2N at fcc
4	0.087, -0.334[1)]	$\Theta_{defect} = 0.125$, 3N at fcc

Table 7.7: Results for adsorbed nitrogen on a ruthenium (0001) surface with a surface defect concentration of 0.25. Number of N atoms at the defect structure, and adsorption energy E_a^N. [1)]: adsorption energy with respect to the surface defect structure.

Bulk Ruthenium Hydrogen Compounds

Structure	Lc [$\AA$] (hcp: a, c)	Vol [$\AA^3$]	B_0 [Mbar]	ΔH_f^0 [eV]
[ZnS]	4.102	17.263	2.287	0.605
[NaCl]	3.994	15.936	2.723	0.240
[CsCl]	2.597	17.527	2.238	1.677
[NiAs]	2.825, 4.631	16.010	2.718	0.323
[ZnO]	2.926, 4.675	17.334	2.288	0.572

Table 7.8: The different calculated bulk Ru/H structures with their lattice parameter (Lc), volume of the primitive unit cell (Vol), bulk modulus (B_0), and heat of formation per formular unit at 0K (ΔH_f^0).

Adsorbed Hydrogen

Site	Θ	E_a^H [meV]	Δ_{12}^s [%]	h [$\AA$]
hcp	0.25	-625.510	0.883	1.021
	0.5	-611.019	1.669	1.017
	0.75	-590.065	2.392	1.020
	1	-564.861	3.076	1.020
fcc	0.25	-653.903	0.605	1.048
	0.5	-626.560	1.309	1.035
	0.75	-599.152	2.050	1.027
	1	-571.958	2.647	1.028

Table 7.9: Results for on-surface adsorbed hydrogen on the ruthenium (0001) surface. Adsorption site, coverage Θ, adsorption energy E_a^H, first ruthenium interlayer relaxation Δ_{12}^s, and height of adsorbed species above the topmost ruthenium layer h.

Site	Θ	E_a^H [meV]	Δ_{12}^s [%]	Comment
Oct	0.25	267.315	2.124	
	0.5	282.686	4.583	
	0.75	296.995	7.383	
	1	306.340	10.538	
Tet-I	0.25	-	-	relaxed to on-surface hcp
	0.5	535.987	5.953	
	0.75	610.165	14.220	
	1	644.581	22.187	
Tet-II	0.25	970.294	4.157	
	0.5		4.632	relaxed to Oct

Site	Θ	E_a^H [meV]	Δ_{12}^s [%]	Comment
	0.75		7.398	relaxed to Oct
	1	805.197	26.445	

Table 7.10: Results for subsurface adsorbed hydrogen on the ruthenium (0001) surface. Adsorption site, coverage Θ, adsorption energy E_a^H, and first ruthenium interlayer relaxation Δ_{12}^s.

Site	E_a^H [meV]	Δ_{12}^s [%]
Oct	705.534	2.406
Tet-I	840.024	2.609
Tet-II	1193.283	4.021

Table 7.11: Results for subsurface adsorbed hydrogen on the ruthenium ABABC close-packed surface at a coverage of $\Theta = 0.25$. Adsorption site, adsorption energy E_a^H, and first ruthenium interlayer relaxation Δ_{12}^s.

Number H atoms	E_a^H [meV]	Comment
1	1581.555, -105.477[1)]	
2	542.391, -301.124[1)]	1H relaxed to fcc

Table 7.12: Results for adsorbed hydrogen on a ruthenium (0001) surface with a surface defect concentration of 0.25. Number of H atoms at the defect structure, and adsorption energy E_a^H per hydrogen atom. [1)]: adsorption energy with respect to the surface defect structure.

Bibliography

[1] V. Blum, M. Scheffler, A. Dolfen, R. Gehrke, S. Gutzeit, P. Havu, V. Havu, F. Hanke, R. Johanni, X. Ren, A. Sanfilippo, P. Rinke, and K. Reuter, FHI-aims - All-Electron Ab Initio Molecular Simulations: A Users' Guide, (2008). 4, 5, 14, 26

[2] M.E. Davis and R.J. Davis, *Fundamentals of Chemical Reaction Engineering*, 1 Ed. (2002). 6

[3] J.R. Jennings, *Catalytic ammonia synthesis: fundamentals and practice* (1991). 6

[4] K. Honkala, A. Hellman, I.N. Remediakis, A. Logadottir, A. Carlsson, S. Dahl, C.H. Christensen, and J.K. Nørskov, Science 307, 555 (2005). 6, 54, 76

[5] R. Schlögl, *Handbook of Heterogeneous Catalysis*, Bd. 5, pp 2501-2575 (2008). 6, 33

[6] J.-C. Chou, S.-I Liu, and S.-H. Chen, Jpn. J. Appl. Phys. Vol. 44, No. 3, 1403 (2005). 7, 45, 55, 56

[7] M. Damayanti, Appl. Phys. Lett. 88, 044101 (2006). 7, 45, 55, 56

[8] M.G. Moreno-Armenta, J. Diaz, A. Martinez-Ruiz, and G. Soto, J. Phys. Chem. Solids 68, 1989 (2007). 7, 45, 55

[9] M. Born and R. Oppenheimer, Annalen der Physik 389, Issue 20, 457 (1927). 10

[10] D.R. Hartree, Proc. Camb. Phil. Soc. 24, 328 (1928). 11

[11] V.A. Fock, Z. Phys. 61, 126 (1930). 11

[12] W. Koch and M.C. Holthausen, *A Chemist's Guide to Density Functional Theory*, 2nd Edition, Wiley-VCH, Weinheim, (2001). 11

[13] D.S. Sholl and J.A. Steckel, *Density Functional Theory*, Wiley & Sons, Hoboken (New Jersey), (2009). 11

[14] K. Burke, The ABC of DFT, (2003). 11

[15] K. Capelle, *A Bird's-Eye View of Density-Functional Theory*, (2006). 11

[16] P. Hohenberg and W. Kohn, Phys. Rev. B 136, 864 (1964). 11

[17] W. Kohn and L.J. Sham, Phys. Rev. A, 140, 1133 (1965). 12

[18] A.E. Mattsson, P.A. Schultz, M.P. Desjarlais, T.R. Mattsson, and K. Leung, Mod. Simul. Mater. Sci. Eng. 13, R1 (2005). 14, 41

[19] J. Rogal, *Stability, Composition and Function of Palladium Surfaces in Oxidizing Environments: A First-Principles Statistical Mechanics Approach*, Dissertation, Free University of Berlin, (2006). 14

[20] J. Perdew, K. Burke, and M. Ernzerhof, Phys. Rev. Lett. **77**, 3865 (1996). 14

[21] V. Blum, R. Gehrke, F. Hanke, P. Havu, V. Havu, X. Ren, K. Reuter, and M. Scheffler, Preprint submitted to Elsevier, (2008). 15, 24, 26

[22] V. Havu, *Making electronic structure methods scale: Large systems and (massively) parallel computing*, Presentation at the "Hands-on Tutorial on ab initio molecular simulations", Berlin (2009). 15

[23] V. Blum, *Practical Electronic Structure Theory: Overview From Abstract Concepts to Concrete Predictions*, Presentation at the "Hands-on Tutorial on ab initio molecular simulations", Berlin (2009). 15

[24] K. Reuter, C. Stampfl, and M. Scheffler, *Ab initio atomistic thermodynamics and statistical mechanics of surface properties and functions*, to appear in

Handbook of Materials Modeling, Volume 1, Fundamental Models and Methods, Springer, Berlin Heidelberg, 149 (2005). 16

[25] K.Reuter and M. Scheffler, Appl. Phys. A 78, 793 (2004). 16

[26] K. Reuter and M. Scheffler, Phys. Rev. B 65, 035406 (2001). 16

[27] A. Zangwill, *Physics at Surfaces*, Cambridge University Press, Cambridge, (2001). 19

[28] D.R.Stull, and H.Prophet, JANAF Thermochemical Tables, 2nd ed. (U.S. National Bureau of Standards, Washington DC, (1971). 21

[29] S. Kenny, A. Horsfield, and H. Fujitani, Phys. Rev. B 62, 4899 (2000). 25

[30] J. Junquera, O. Paz, D. Sanchez-Portal, and E. Artacho, Phys. Rev. B 64, 235111 (2001). 25

[31] C. Kittel, *Einführung in die Festkörperphysik*, Oldenbourg, München, (2006). 27, 35

[32] S. Schwegemann, A.P. Seitsonen, H. Dietrich, H. Bludau, H. Over, K. Jacobi, and G. Ertl, Chem. Phys. Lett. 264, 680 (1997). 27, 57, 60, 62

[33] www.webelements.com 27

[34] A. Karton, B. Ruscic, and J.M.L. Martin, J. of Mol. Struc.: THEOCHEM 811, 345 (2007). 27

[35] R. Schlögl, Angew. Chem. Int. Ed. 42, 2004 (2003). 33

[36] F.D. Murnaghan, *Proceedings of the National Academy of Sciences of the United States of America*, Vol. 30, No. 9, 244 (1944). 34

[37] U. Scherz, *Quantenmechanik*, Teubner, Stuttgart Leipzig, (1990). 34

[38] G. Bester, *Analyse der elektronischen Struktur von Metallen und intermetallischen Verbindungen im Rahmen der Dichtefunktionaltheorie*, Dissertation, University of Stuttgart, (2002). 35, 36, 37

[39] B. Wen, J. Zhao, F. Bai, and T. Li, Intermetallics 16, 333 (2008). 35

[40] C. Stampfl and M. Scheffler. Phys. Rev. B 54, 2868 (1996). 35

[41] B. Hammer, Phys. Rev. Lett. 83, 3681 (1999). 35, 41

[42] P.J. Feibelman, J.E. Houston, H.L. Davis, and D.G. O'Neill, Surf. Sci. 302, 81, (1994). 35

[43] R. Heid, L. Pintschovius, W. Reichardt, and K.-P. Bohnen. Phys. Rev. B 61, 12059, (2000). 35

[44] J.R. Chelikowski, D.T. Chan, and S.G. Louie, Phys. Rev. B 34, 6656, (1986). 35

[45] Landolt-Börnstein. group III, 23c, Springer, Berlin, (2003). 35

[46] Landolt-Börnstein. group III, 14a, Springer, Berlin, (1988). 35

[47] Landolt-Börnstein. group III, 24b, Springer, Berlin, (1994). 35

[48] N.W. Ashcroft and N.D. Mermin, *Solid State Physics*, Holt, Rinehart and Winston, New York, (1976). 35

[49] W.R. Tyson and W.A. Miller, Surf. Sci. 62, 267 (1977). 37

[50] F.R. de Boer, R. Boom, W.C.M. Mattens, A.R. Miedema, and A.K. Niessen, *Cohesion in Metals*, North-Holland, Amsterdam, (1988). 37

[51] M. Bruno, F.R. Massaro, and M. Prencipe, Surf. Sci. 602, 2774 (2008). 39

[52] R. Dovesi, B. Civalleri, R. Orlando, C. Roetti, and V.R. Saunders, in: B.K. Lipkowitz, R. Larter, T.R. Cundari (Eds.), *Reviews in Computational Chemistry*, Vol. 21, Wiley, New York, 70 (2005). 39

[53] L. Vitos, A.V. Ruban, H.L. Skriver, and J. Kollár, Surf. Sci. 411, 186 (1998). 39, 41

[54] M.Y. Chou and J.R. Chelikowsky, Phsy. Rev. B 35, 2124 (1987). 40

[55] P.J. Feibelman, Surf. Sci. 360, 297 (1996). 43

[56] J. de la Figuera, J.M. Puerta, J.I. Cerda b, F. El Gabaly, and K.F. McCarty, Surf. Sci. 600, L105, (2006). 43

[57] B.A. Hamad, Surf. Sci. 602, 3654 (2008). 43

[58] R.S. Ram and P.F. Bernath, J. of Mol. Spec. 213, 170 (2002). 45

[59] T.C. Steimle and W. Virgo, J. Chem. Phys. 119, No. 24 (2003). 45

[60] F. Colmenares and S. Meléndez, Chem. Phys. Lett. 380, 292 (2003). 45

[61] E. Gregoryanz, C. Sanloup, M. Somayazulu, J. Badro, G. Fiquet, H.-K. Mao, and R.J. Hemley, Nat. Mater. 3, 294 (2004). 46

[62] J.C. Crowhurst, A.F. Goncharov, B. Sadigh, C.L. Evans, P.G. Morrall, J.L. Ferreira, and A.J. Nelson, Science 311, 1275 (2006). 46, 47, 52

[63] E. Riedel and C. Janiak, *Anorganische Chemie*, 7. ed., de Gruyter, Berlin, (2009). 47

[64] N. Wiberg and E. Wiberg, *Lehrbuch der Anorganischen Chemie*, 102. ed., de Gruyter, Berlin, (2007). 47

[65] A.N. Timoshevskii, V.A. Timoshevskii, B.Z. Yanchitsky, and V.A. Yavna, Comp. Mat. Sci. 22, 99 (2001). 48

[66] K. Suzuki, H. Morita, T. Kaneko, H. Yoshida, and H. Fuijmori, J. Alloys and Compounds 201, 11 (1993). 49

[67] J. von Appen, *Quantenchemische Untersuchungen an Nitriden der Platingruppenmetalle*, Dissertation, University of Aachen, (2006). 49, 54, 90

[68] G. Kresse, M. Marsman, and J. Furthmüller, *VASP the guide*, (2009). 49, 75

[69] Y.-H. Liao and J.-C. Chou, Sensors 9, (2009). 55, 56

[70] J.J. Mortensen, Y. Morikawa, B. Hammer, and J.K. Nørskov, J. Catal. 169, 85 (1997). 57, 59, 60

[71] L. Diekhöner, A. Baurichter, H. Mortensen, and A.C. Luntz, J. Chem. Phys., Vol. 112, No. 5, 2507 (2000). 57, 59, 60

[72] Á. Logadóttir and J.K. Nørskov, J. Catal. 220, 273 (2003). 57, 60, 61, 80

[73] B. Hammer, L.B. Hansen, and J.K. Nørskov, Phys. Rev. B 59, 7413 (1999). 60, 90

[74] J.P. Perdew, J.A. Chevary, S.H. Vosko, K.A. Jackson, M.R. Pederson, D.J. Singh, and C. Fiolhais, Phys. Rev. B 46, 6671 (1992). 60

[75] S. Dahl, E. Törnqvist, and I. Chorkendorff, Journal of Catalysis 192, 381-390 (2000). 68

[76] S. Dahl, Á. Logadóttir, R.C. Egeberg, J.H. Larsen, I. Chorkendorff, E. Törnqvist, and J.K. Nørskov, Phys. Rev. Lett. Vol 83, No 9, 1814 (1999). 68

[77] J.G. Ekerdt and A.T. Bell, Journal of Catalysis Vol 58, Issue 2, 170 (1979). 73

[78] L. Xu, H.Y. Xiao, and X.T. Zu, Chem. Phys. 315, 155 (2005). 73, 79, 80, 82

[79] V.E. Antonov, I.T. Belash, V.Yu. Malyshev, and E.G. Ponyatovsky, Platinum Metals Rev. 28 (4), 158 (1984). 73, 77

[80] V.S. Bagotzky, A.M. Skundin, and E.K. Tuseeva, Electrochimica Acta. 21, 29 (1976). 73

[81] H. Smithson, C.A. Marianetti, D. Morgan, A. Van der Ven, A. Predith, and G. Ceder, Phys. Rev. B 66, 144107 (2002). 75, 77, 78, 90

[82] K. Miwa and A. Fukumoto, Phys. Rev. B 65, 155114 (2002). 91

Acknowledgements

First of all I want to thank Prof. Dr. Alexander K. Hartmann, Prof. Dr. Thorsten Klüner, and Prof. Dr. Matthias Scheffler for giving me the opportunity to prepare my diploma thesis at the Fritz-Haber-Institute of the Max-Planck-Society and thus working in the field of heterogeneous catalysis, using state of the art *ab initio* simulation methods.

Furthermore I want to thank those I was working with at the Fritz-Haber-Institute and without whose help this thesis wouldn't have been possible or less fun. Particularly emphasised should be Dr. Sergey Levchenko who supervised me. He is such a good supervisor as one can hope for, since he was patient, helpful and motivating at any time during my thesis.

Finally I thank the German National Academic Foundation for financial support.

Plagiarism Declaration Form

I hereby declare, that this work was written by myself and I did not use any other references and aids except for those indicated.

.....

Nils Ohmer